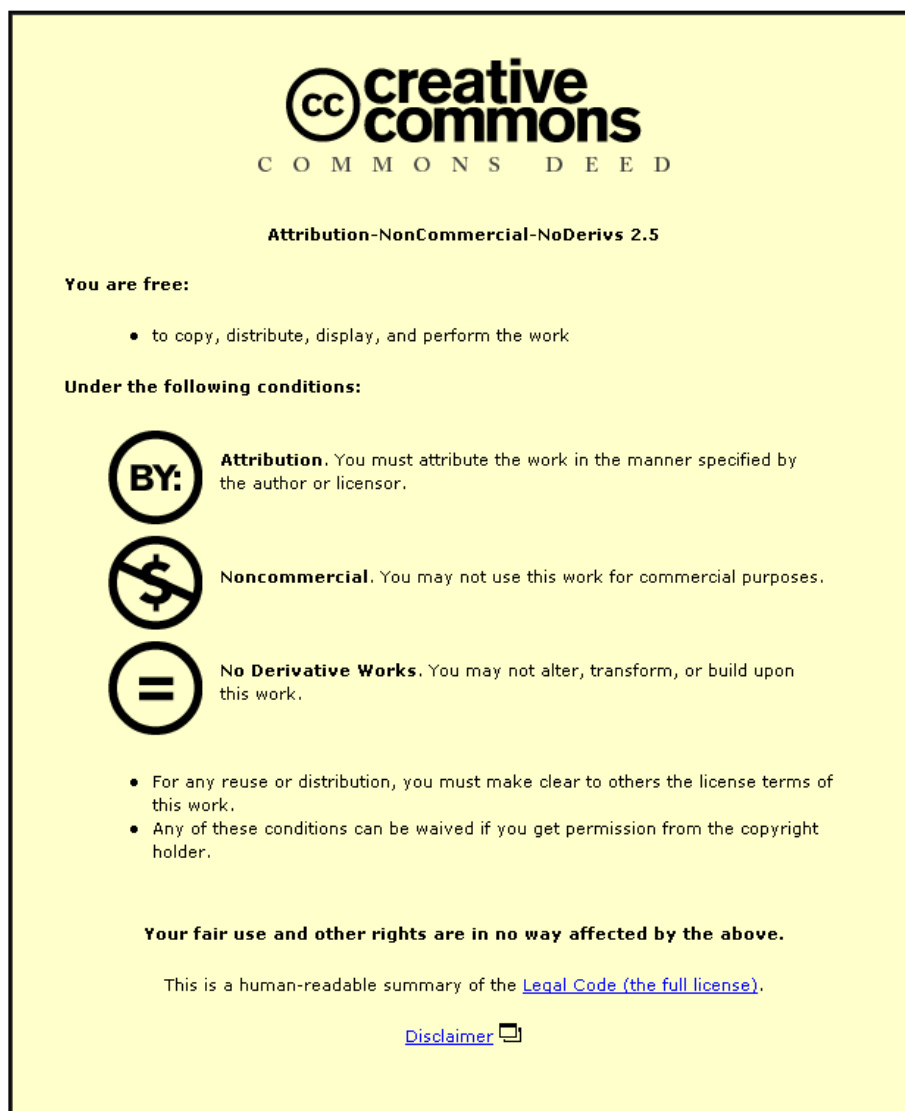


This item was submitted to Loughborough University as a PhD thesis by the author and is made available in the Institutional Repository (<https://dspace.lboro.ac.uk/>) under the following Creative Commons Licence conditions.



For the full text of this licence, please go to:
<http://creativecommons.org/licenses/by-nc-nd/2.5/>



Pilkington Library

Author/Filing Title TEO, K.C.
.....

Accession/Copy No. 040147113

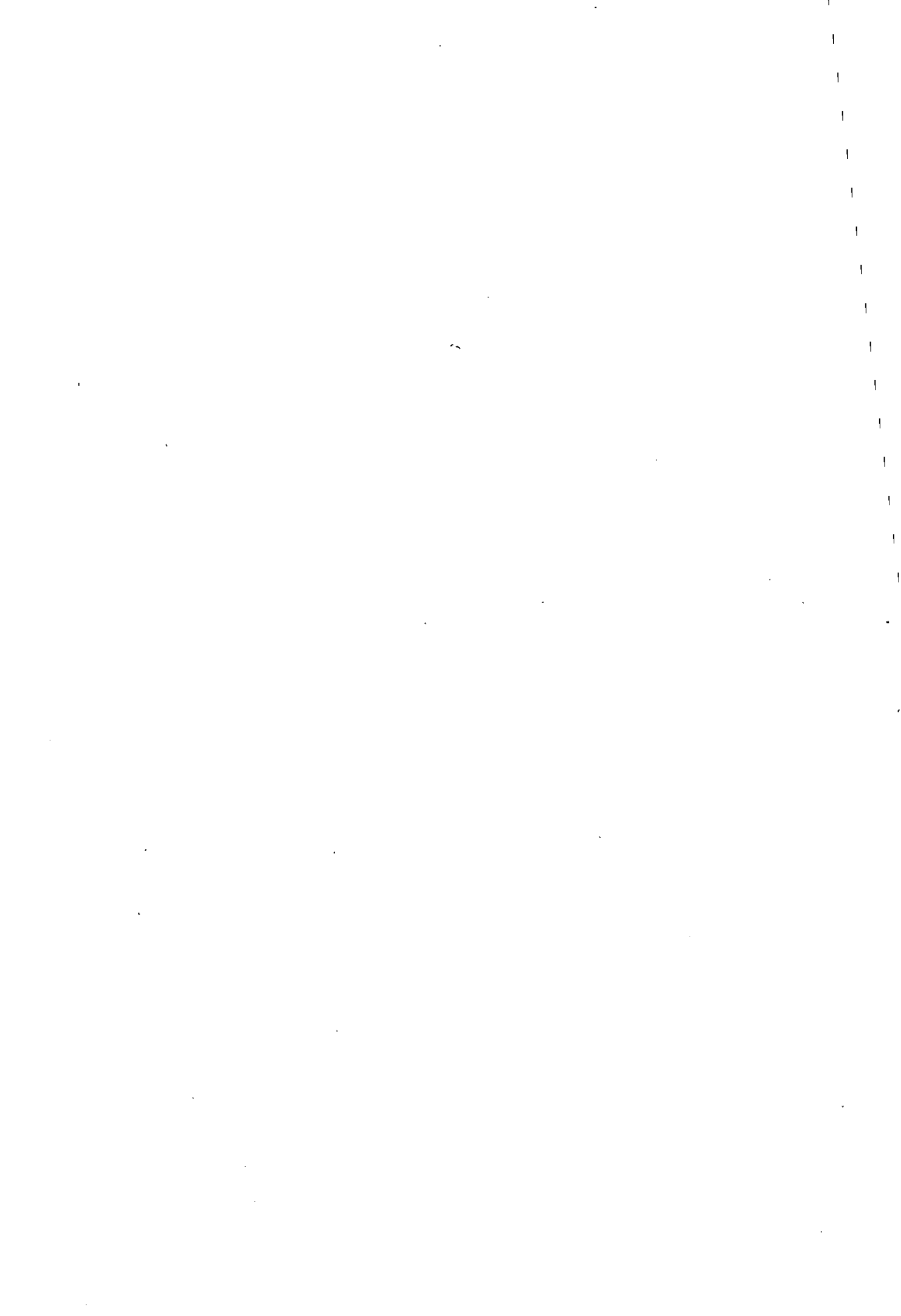
Vol. No.	Class Mark
---------------	------------------

	LOAN COPY	
--	-----------	--

0401471136



BADMINTON PRESS
18 THE HALECROFT
SYSTON
LEICESTER, LE7 1LD
ENGLAND
TEL : 0116 260 2917
FAX : 0116 269 6639



An Empirical Study of Fine-Pitch Assembly Faults And Their Correction

By

Teo Kiat Choon

MSc; MIIE

A Doctoral Thesis

Submitted in partial fulfilment of the requirements for
the award of

Doctor of Philosophy

of the Loughborough University

December 1996

© by Teo Kiat Choon 1996

 Loughborough University Primary
D. <i>July 97</i>
Class
Acc No. <i>040147113</i>

9/903115

SUMMARY

The explosion of SMT and highly-density packages has resulted in more complex and higher density board designs in order to incorporate more features into products while reducing overall package size. This has, in turn, created major challenges for the surface mount manufacturing process, particularly in solder screen printing, component placement, and reflow soldering. Investigation into these areas will contribute to our understanding of the origin of post reflow defects in surface mount assembly and improvement in product quality.

The thesis particularly explores empirically the relationship between screen printed paste deposit, the final joint geometry and the fluxing behaviour within the reflowing solder. The thesis also demonstrates the effect of modified screen printing parameters and the lead geometry.

Acknowledgments

I would like to express my sincere thanks to Professor David J. Williams for his expert supervision and guidance throughout this research. His knowledge in interconnect and soldering technology has been of great benefit in the progress of this thesis.

I would also like to extend my thanks to Director of Research Mr. Allen Hodgson, Mr. Paul P. Conway, Mr. David C. Whalley, Dr. F. Sarvar, Dr. S.H. Mannan and Ph.D student Low M.K. of Manufacturing Engineering Department, Loughborough University for their support and help. To those engineers and managers of Aztech System Ltd and Kester Solder which participated in the research, I would like to express my sincere thanks and appreciation.

Lastly, but not least very grateful thanks are due to my mother and late father who laid the foundation of my education. I am also thanks my wife, Geok Yian and daughter Yin Ling for their constant support, encouragement and patience, without their understanding this work would not have been completed. I am grateful to my nephew Goh Chee Ming and niece Chin Jia Min for diligently typing this thesis. To them I dedicate this thesis.

Abbreviations

IR	-	Infrared
Kg	-	Kilogram
mm	-	Millimetre
PCB	-	Printed Circuit Board
PLCC	-	Plastic Leaded Ceramic Chip
QFP	-	Quad Flat Pack
SOIC	-	Small Outline Integrated Circuit
TCE	-	Thermal Coefficient of Expansion
T _g	-	Glass Transition Temperature
TSOP	-	Thin Small Outline Package
μm	-	Micrometre
DSC	-	Differential Scanning Calorimetry
FEA	-	Finite Element Analysis
FEM	-	Finite Element Method
SOT	-	Small Outline Transistor
a	-	Thermal diffusivity

A	-	Surface Area
α	-	Heat transfer coefficient
c	-	Specific heat capacity
γ or ν	-	Surface tension
μ	-	Wetting tension
E	-	Total energy
F	-	Force
θ	-	Contact angle
g	-	Acceleration of gravity
h,d,l,L,x,y	-	Length, thickness, distance
η	-	Viscosity
λ	-	Heat conductivity
M	-	Mass
P	-	Pressure
ρ	-	Density
t	-	Time
T	-	Temperature

ΔT	-	Temperature interval
v	-	Velocity
V	-	Volume
ACA	-	Anisotropic conductive adhesive
ACF	-	Anisotropic conductive film

Soldering Terms

Open Joint: Is a term used to describe a gap that can occur between a component lead and a printed circuit board pad after solder reflow.

Solder Bridge: Bridges (short circuits) are connections between metal parts created by solder and which are unwanted and not required in the design.

Coplanarity: Is the distance of the fine pitch IC device lead tips above a plane, which is defined as that upon which the device will rest when placed on the board.

Solder Wicking (Insufficient Solder): Wicking is when the solder moves to a hotter section of the lead during reflow because of the greater thermal mass of the printed circuit board.

Component Misalignment: Misalignment resulting from the pick & place operation and station to station material handling.

Blow hole: A void in the solder joint caused by reduced and / or heat (outgassing).

Bonding time: The duration from heat start-up until the reflow profile is completed.

Capillary action: A phenomenon of force, adhesion and cohesion that prompts liquids (molten solder) to flow against gravity between closely spaced solid surfaces, such as component leads and pads.

Coefficient of Thermal Expansion (CTE): The change in dimension of a material vs a unit change in temperature expressed in $\text{ppm} / ^\circ\text{C}$.

Load test: A mass reflow soldering system test for the capacity repeatedly to process boards regardless of their volume through the oven.

Meniscus: The contour or shape of molten solder as formed by surface tension forces in turn controlled by wetting.

Preheat: The process portion of the reflow heat curve in which the PCB is heated from ambient at a preset rate and prior to full liquidus at the solder joint areas

Reflow Soldering: Joining components to substrates by placing the parts into solder paste and then the melting the paste to achieve reflow and interconnection.

Repeatability: The ability of a system to return to a specific parameter, said of equipment when evaluating its consistency of processing.

Shadowing: In reflow soldering, a condition in which component bodies block the infrared energy to other areas of the board. In wave soldering, the solder fails to wet some leads due to other devices blocking the flow of solder.

Soak: The period after preheat and before reflow peak temperature differences between parts are allowed to equalize.

Termination: The part of a component that makes contact with a pad on a substrate.

Test board: A PCB suitable for determining the solderability of a batch of boards produced with the same process. A representative board.

Dewetting: A solder coating that has receded, leaving irregular deposits and indicating the base metal has not be adequately deoxidized.

Double sided assembly: A PCB with components mounted on both sides.

Drying time: Within the reflow process after preheat and before peak reflow temperature where volatile materials escape from the solder paste.

Fillet: The concave formation of a solidified solder between the land or pad and the component lead.

Fine-pitch: The center-to-center lead spacing of SMDs measured between 0.025" (0.635mm) to 0.032" (0.813mm).

Forced air convection: Convection, consisting of flow, velocity and temperature, for heat transfer of fluid or gas over solder joints to be reflowed.

Halides: Chemical compounds present in flux and serving as the activators for deoxidization. Their residues are corrosive and must be washed.

Hot zone: The section of a reflow oven held at maximum temperature. Other zones include preheat and cooling.

Land: On a PCB, the conductive area (s) to which components are attached. Also called pad.

Thermocouple: A device made of two dissimilar metals which, when heated, generates a voltage that is used to measure temperatures.

Wave soldering: The technique of joining parts to a PCB by passing the assembly over a solder wave to coat the prefluxed areas to be joined.

Wetting: A reduction of surface tension on a metal introduced with molten solder resulting in the latter collapsing into a thin film, spreading and making intimate contact over all surfaces.

Contents

Summary	i
Acknowledgements	ii
Nomenclature	iii
List of Figures	xvi
List of Tables	xxi
1. Introduction	1
1.1 Introduction	1
1.2 The Areas of Investigation	2
1.3 Outline of The Thesis	3
1.4 Contribution of The Thesis	4
2. Literature Review	5
2.1 Introduction	5
2.2 Trends in SMT And Advanced Packaging Technologies	6
2.2.1 Evolution in Electronics Manufacturing	6
2.2.2 Ball Grid Array (BGAs)	10
2.2.3 Tape Automated Bonding (TAB)	14
2.2.4 Chip-On-Glass (COG)	15
2.2.5 Flip Chip Mounting	16
2.2.6 Wire-Bonding	18
2.2.7 Chip-On-Board (COB) Management Issues	20
2.2.8 Multi-Chip Module (MCM)	22

2.3 Interconnection Technology Using Anisotropic Conductive Adhesives (ACAs) and Anisotropic Conductive Films (ACFs).	25
2.4 Solder Reflow	28
2.4.1 Basic Reflow Processes	28
2.4.2 Pure IR Vs Forced Air Convection	29
2.4.3 Vapour Phase Solder Reflow	29
2.4.4 Laser and Optical Beam Soldering	30
2.5 Description of Phenomena in Reflow Soldering	31
2.6 The wetting Balance	33
2.7 Analytical Models of Solder Defects And Wetting of Surfaces.	36
2.8 Evolver And Computational Models of Solder Defects And Wetting of Surfaces.	48
2.9 Open And Effect of Lead Coplanarity	53
2.10 The Impact of Screen Printing On Reflow Defects	55
2.11 Bar Printing, Reflow And Bridging Defects	58
2.12 Summary	59
3. The Origin And Prevention of Post Reflow Defects in Surface Mount Assembly.	61
3.1.1 Introduction	61
3.1.2 Classification of Process Defects After Reflow.	62
3.2 A Survey On The Performance of Singapore-Based SMT Plants.	63
3.3 Defect Origin of Insufficient Solder, Bridges, And No Solder (Opens), Missing Component And Misalignment.	64

3.3.1 Observations	64
3.3.2 Screen Printing Studies	66
3.3.2.1 Results	68
3.3.2.1.1 Design of Experiments (DOE)	68
3.3.2.1.2 Response Surface Method (RSM)	75
3.3.3 Missing Components	78
3.3.3.1 Observations	79
3.3.4 Vibration Alignment During IR Solder Reflow of Quad Flat Pack.	81
3.3.4.1 IR Reflow Vibration Experiment	82
3.3.4.2 Results	82
3.3.4.3 The Component Placement Accuracy Problem.	83
3.4 Conclusion	84
4. Insufficient Solder And Solder Bridges: An Experimental Study of The Interrelations Between Assembly Process Faults.	86
4.1 Introduction	86
4.2 Approach	87
4.3 Results	88
4.3.1 A Correlation Between Bridges And Insufficient Solder.	88
4.3.2 Bridging And Insufficient Solder On The Same And Adjacent Leads.	90
4.3.3 Changing The Solder Paste Thickness.	92
4.3.4 The effect of Rework	94
4.4 Summary And Discussion	94

4.5 Conclusion	96
5. Stencil Optimization Via Flow Control	98
5.2 Approach	99
5.3 Results	101
5.3.1 Solder Bridging	101
5.3.2 Component Misalignment Or / And Displacement	107
5.3.3 Insufficient Solder (Solder Wicking)	108
5.4 Discussion	116
5.4.1 Solder Bridges	116
5.4.2 Component Misalignment And Displacement.	117
5.4.3 Insufficient Solder (Solder Wicking)	117
5.5 Conclusion	119
6.0 A Study of Solderability And Solder Spreading For SMT Open Joints.	120
6.1 Introduction	120
6.2 Philosophy of The Experimental Programme	122
6.2.1 Solder Spreading Test	123
6.2.2 Solder Paste Type	125
6.2.3 Lead Geometry Design And Bond Test Procedure	126
6.2.4 Lead Coplanarity Test	127
6.3 Results And Analysis	130
6.3.1 Solder Spreading Test	130
6.3.2 Bond Testing With Respect To Solder Pastes	136
6.3.3 Bond Testing With Respect To Lead Geometries	138

6.3.4 Lead Coplanarity Test	142
6.4 Discussion And Recommendations	145
6.4.1 Solder Spreading	145
6.4.2 Bond Test With Respect To Solder Pastes	146
6.4.3 The Interrelations of Bond Strength, Solder Fillet, Lead Geometries And Solder Spreading.	147
6.4.4 Bond Testing With Respect To Lead Shapes.	149
6.4.5 Lead Coplanarity Test	150
6.4.6 Microsection of Bonded Area	151
6.5 Conclusion	157
7. Conclusions	160
7.0 Introduction	160
7.1 The Solder Bridge Problem	161
7.2 The Insufficient Solder Problem	162
7.3 The Open Circuit Joints Problem	163
7.4 The Lead Coplanarity Problem	164
7.5 The Component Lead Misalignment Problem	164
7.6 Summary	165
7.7 Suggestions For Further Work	165
8. Appendices	167
Appendix A - Factorial Design	167
Appendix B - One-way Analysis of Variance (ANOVA) And Duncan's	174

Multiple Range Test

. Appendix C - Regression Analysis	181
. Appendix D - The Relationship Between The Normal, X^2 , t And F-Distributions.	187
. Appendix E - Contingency Tables	191
. Appendix F - Response Surface Methods (RSM)	193
9.0 References	204

List of Figures

Figure 2.0 - SMT basic process	6
Figure 2.1 - The number of device pins on surface mount packaging continue to grow as does the gate count of these devices.	7
Figure 2.2 - Interconnection pitch reduction with time.	7
Figure 2.3 - The trend towards higher pin-counts and fine-pitch	8
Figure 2.4 - The relationship between the technologies involved in packaging design.	8
Figure 2.5 - Construction of TAB in tape state and mounted to PCB.	15
Figure 2.6 - Component pitch and trends.	21
Figure 2.7 - A Wetting Balance Curve.	35
Figure 2.8 - Some representative shapes of wetting balance curves.	35
Figure 2.9 - Schematic of solder wicking on a gull-wing lead.	37
Figure 2.10 - A liquid surface ABCD having principal radius of curvature R1 and R2 expanding a distance δx radially.	39
Figure 2.10a - Vertical sections through sessile drops of liquid on a flat surface, defined by equation (e): [1] calculated for solder with $\frac{gP}{\gamma} = 0.2mm^{-2}$ and [2] defining the x-y axes and the radius of curvature R1 at angle ϕ .	41
Figure 2.11 - Force balance of a liquid on substrate.	42
Figure 2.12 - Energy of liquid on substrate.	44

. Figure 2.13 - The "elastica" curve for liquid solder.	46
. Figure 2.14 - The configuration of bridge between two parallel walls, w: distance of walls.	47
. Figure 2.15 - Illustration of experimental setup of optical paste observation. Spheres whose rotation opposes the rotation of the dotted sphere are labeled with an O and sphere which help the rotation are labeled with a h.	55
. Figure 2.16 - Sketch of paste flow out from a stencil aperture.	56
. Figure 3.1 - Result of solder bridge and insufficient solder.	65
. Figure 3.2 - Design of Experiment (DOE) setting.	67
. Figure 3.3 - Response Surface Method (RSM) setting.	67
. Figure 3.4 - Pareto chart for paste height	70
. Figure 3.5 - Main effect for paste height	72
. Figure 3.6 - Interaction effect of downstop and snapoff.	72
. Figure 3.7 - Normal probability plot for residual of paste height data.	73
. Figure 3.8 - Pareto chart for solder bridge.	73
. Figure 3.9 - Plot of main effect D, squeegee types.	74
. Figure 3.10 - Normal probability plot for residual solder bridge data.	74
. Figure 3.11 - A theoretical response surface showing a relationship between response h (paste height) as function of e1 (mechanical downstop) and e2 (snapoff-distance).	77
. Figure 3.12 - Paste height contour of above response surface, showing the relationship between response h (paste height) as function of e1 (mechanical downstop) and e2 (snapoff-distance).	78

. Figure 3.13 - Cross-section of IC's lead bonded area with vibration.	84
. Figure 4.1 - Bridge vs. insufficient solder (wicking).	89
. Figure 4.2 - Insufficient solder versus distance of occurrence from bridge.	91
. Figure 4.3 - Bridge versus solder thickness.	93
. Figure 5.1 - Lead geometry	100
. Figure 5.2 - Stencil design for "Centre"	101
. Figure 5.3 - Stencil design for "Quarter"	102
. Figure 5.4 - Stencil design with reduction in aperture length	102
. Figure 5.5 - Conventional stencil design	102
. Figure 5.6 - Solder bridge vs. paste thickness, Design 1 (Centre)	104
. Figure 5.7 - Solder bridge vs. paste thickness, Design 2 (Quarter)	105
. Figure 5.8 - Solder bridge vs. paste thickness, Design 3 (Reduction)	105
. Figure 5.9 - Solder bridge vs. paste thickness, Design 4 (Conventional)	106
. Figure 5.10 - Component misalignment vs. paste thickness, Design 1 (Centre)	109
. Figure 5.11 - Component misalignment vs. paste thickness, Design 2 (Quarter)	110
. Figure 5.12 - Component misalignment vs. paste thickness, Design 3 (Reduction)	111
. Figure 5.13 - Solder bridge vs. paste thickness, Design 3 (Reduction)	111
. Figure 5.14 - Insufficient solder (solder wicking) vs. paste thickness, Design 1 (Centre).	112
. Figure 5.15 - Insufficient solder (solder wicking) vs. paste thickness, Design 2 (Quarter).	113
. Figure 5.16 - Insufficient solder (solder wicking) vs. paste thickness, Design 3 (Reduction).	114

. Figure 5.17 - Insufficient solder (solder wicking) vs. paste thickness, Design 4 (Conventional).	115
. Figure 6.1 - IR-reflow temperature profile at peak temperature 213 degree C.	124
. Figure 6.2 - IR-reflow temperature profile at peak temperature 245 degree C.	124
. Figure 6.3 - Comb pattern with solder paste prior to reflow.	125
. Figure 6.4 - Pre-assigned non-coplanar leads at centre and two extreme corners of the QFP (quad-flat-pack).	130
. Figure 6.5 - K1 reflow at 213 degree C.	132
. Figure 6.6 - K1 reflow at 245 degree C.	133
. Figure 6.7 - K2 reflow at 213 degree C.	133
. Figure 6.8 - K2 reflow at 245 degree C.	134
. Figure 6.9 - K3 reflow at 213 degree C.	134
. Figure 6.10 - K3 reflow at 245 degree C.	135
. Figure 6.11 - A1 reflow at 213 degree C.	135
. Figure 6.12 - A2 reflow at 245 degree C.	136
. Figure 6.13 - Gull-Wing Outward L	139
. Figure 6.14 - Gull-Wing Outward L (with positive dihedral)	139
. Figure 6.15 a-d - Lead coplanarity test for solder paste K1.	143
. Figure 6.15 e - Close up view of lead coplanarity test for paste K1.	143
. Figure 6.16 a-d - Lead coplanarity test for solder paste A1.	144
. Figure 6.16 e - Close up view of lead coplanarity test for paste A1.	144
. Figure 6.17 - Thermal distribution of gull-wing during reflow.	146
. Figure 6.18 - Solder joint of gull-wing with dihedral angle.	152

- . Figure 6.19 - Cross-section of gull-wing lead bonded area. 152
- . Figure 6.20 - Lead joint with coplanarity defect after reflow using Kester R244 154
- . Figure 6.21 - Cross-section of lead joint with coplanarity defect using Kester R244. 155
- . Figure 6.22 - Lead joint of outward-L using Kester 587SA water soluble flux. 155
- . Figure 6.23 - Cross-section of outward-L lead joint using Kester 587 SA water soluble flux. 156
- . Figure 6.24 - Lead joint of outward-L using Alpha Metal A390DH3 RMA flux. 156
- . Figure 6.25 - Cross-section of outward-L lead joint using Alpha Metal A390DH3 RMA flux. 157

List of Tables

Table - 2.1 QFP coplanarity requirements.	11
Table - 2.2 Comparison of QFP and BGA technologies.	12
Table - 2.3 QFP vs. BGA yield comparison.	12
Table - 3.1 ANOVA table of solder paste height experiment.	69
Table - 3.2 ANOVA table of solder bridge experiment.	71
Table - 3.3 ANOVA table for the search of optimal paste height experiment.	76
Table - 3.4 Experimental result.	80
Table - 3.5 IR reflow without vibration.	82
Table - 3.6 IR reflow with vibration.	82
Table - 4.1 Bridge vs. insufficient solder (linear model $y=a+bx$).	89
Table - 4.2 Insufficient solder vs. distance of occurrence from bridge (exponential model $y=\exp(a+bx)$).	91
Table - 4.3 Bridge vs. solder paste thickness (exponential model $y=\exp(a+bx)$).	93
Table - 5.1 Solder bridge vs. paste thickness, Design 1 (Centre).	103
Table - 5.2 Solder bridge vs. paste thickness, Design 2 (Quarter).	103
Table - 5.3 Solder bridge vs. paste thickness, Design 3 (Reduction).	104
Table - 5.4 Solder bridge vs. paste thickness, Design 4 (Conventional).	106
Table - 5.5 Component misalignment vs. paste thickness, Design 1 (Centre).	107
Table - 5.6 Component misalignment vs. paste thickness, Design 2 (Quarter).	107
Table - 5.7 Component misalignment vs. paste thickness, Design 3 (Reduction).	108
Table - 5.8 Component misalignment vs. paste thickness, Design 4	110

(Conventional).

Table - 5.9 Insufficient solder (solder wicking) vs. paste thickness, Design 1 112

(Centre).

Table - 5.10 Insufficient solder (solder wicking) vs. paste thickness, Design 2 113

(Quarter).

Table - 5.11 Insufficient solder (solder wicking) vs. paste thickness, Design 3 114

(Reduction).

Table - 5.12 Insufficient solder (solder wicking) vs. paste thickness, Design 4 115

(Conventional).

Table - 6.1 Number of unions observed in spreading test on comb pattern. 131

Table - 6.2 Two-sample analysis on pull strength test. 137

Table - 6.3 One-way ANOVA table. 139

Table - 6.4 Test matrix for lead shapes and solder paste types. 141

Chapter One

Introduction

1.1 Introduction

The technology evolution in electronics manufacturing from the 70s to the 90s has been enormous. In the 1970s technology for digital devices consisted of through-hole devices ranging from 14 to 24 pin dual in-line packages. In the 1980s Surface Mount Technology(SMT) was rapidly accepted by the industry¹.

Today surface mount devices with connection pitch sizes ranging from 20 mil (0.020 inch) down to 8 mil (0.008 inch) are in common use and ball-grid-array(BGA) technology seems to be the next technology to achieve the assembly of devices with gate counts that approach or exceed one million per device, with package pin counts approaching 1000².

The SMT industry, despite the availability of improved screen printing and pick-and-place equipment, still has first-pass faults of 200 to 300 parts per million(PPM) after reflow³. The statistical implications of attempting to manufacture a printed circuit board with two thousand fine-pitch connections or more at a six-sigma quality level (i.e. 3.4 defects per million solder connections) indicate the need for a departure from the post process inspection and rework methods used in the past. This requires an understanding the origins of process defects in order to improve the process.

1.2 The Areas of Investigation

The focus of this thesis is the avoidance of SMT solder faults. This requires an understanding of how such fault form and how they can be avoided. The work begins with a study via a survey by the author to determine the common solder defects seen in the Singapore SMT industry. A total of three SMT suppliers for the original equipment manufacturer(OEM) where the author was employed were surveyed. In summary, the survey showed missing solder / components and solder bridges to be the top two defects faced by all three plants, in the production process, in spite of the difference between production process, machine supplies between the plants.

Misalignment and insufficient solder ranked 3rd and 4th faults respectively. This survey of faults before product rework was in contrast to the understanding of the importance of faults determined from customers returns, here the insufficient solder fault is known to be the top defect. This indicated that while it is easy to rework bridges and missing components, it is a difficult task for production operators to correct the fault of insufficient solder.

The bulk of this thesis therefore focuses on the bridging fault and the insufficient solder fault including the phenomenon of wicking. This follows a description of the effect of screen printing on paste reflow defects and the outline of a method to correct alignment faults. It includes a study of the correlation between open joints and solder bridges-- to indicate that volume related solder faults cannot be corrected by screen printing alone, stencil aperture modification to address the solder bridge problem, characterization of flux behaviour during the reflow stage and lead geometry -

modification to correct the wicking and coplanarity problems. The thesis particularly explores empirically the relationship between the screen printed paste deposit, the final joint geometry and the fluxing and flow behaviour within the reflowing solder.

1.3 Outline of The Thesis

There are total of seven chapters within this document inclusive of the introductory chapters, chapter 2 provides a literature review. The major topics are advanced packaging and technology trends, solder reflow, flux materials, screen printing, reliability, yield improvement, computational & analytical modelling of the reflow process. The review provides insights into how SMT solder faults can be addressed.

Chapter 3 presents the survey of common soldering defects and field failures in the Singapore SMT industry. A classification of defects and the quality requirements for solder joints are defined, Statistical experimental techniques such as design of experiments(DOE) and response surface method(RSM) are introduced. A vibration assisted alignment mechanism is presented in the multi-machine environment to address position-related component defects.

Chapter 4 presents a study of the interrelations between insufficient solder and solder bridge faults. This experimental correlation study is also linked to the computer simulation studies of the fundamental fluid mechanical phenomena within the soldering process. This also indicated promising avenues for modifications to stencil designs and hence paste print modification to design against solder bridging, and eliminate solder wicking as a result of bridging.

Chapter 5 focuses on optimised stencil design through solder flow control.

This thesis examines during solder reflow to reduce the formation of faults.

Chapter 6 focuses on the control of component solderability by considering the interrelations between the wettability of the lead's geometrical design and its thermal demand with respect to flux kinetics i.e. movement of the contact line⁸ in order to reduce the number of open joints created in manufacture.

Chapter 7 provides a summary of the major results, reviews the contribution of the thesis, and suggests areas in which it will be fruitful to conduct future research.

1.4 Contribution of The Thesis

The explosion of SMT and highly-dense packages has resulted in more complex and higher density board designs in order to incorporate more features into products while reducing overall package size. This has, in turn, created major challenges for the surface mount manufacturing process, particularly in solder screen printing, component placement, and reflow soldering. Investigation into these areas will contribute to our understanding of the origin of post reflow defects in surface mount assembly and improvement in product quality. The work in this thesis indicates how the faults of misalignment, bridging, insufficient solder and opens due to coplanarity errors can be corrected and avoided. Much of this work has been published in references^{134,137}.

Chapter Two

Literature Review

2.1 Introduction

This literature review discusses the main topics of post-reflow soldering and defect origin in the SMT process as examined by other workers. This is presented in the context of technology trends. The main contributors are emphasized in each topic area. These topic areas are advanced packaging and technology trends, ACAs (anisotropic conductive adhesives), wire interconnect technology (WIT), SMT process flow (include ultra fine pitch technology), solder reflow and reliability.

This chapter also present a review of the significant work describing and understanding the origin of defects. Research related to SMT processes has been carried out in many countries. Some of theses countries have pilot plants to assist the study of a particular topic. This literature survey attempts to review work reported by the main workers in each topic. It is appropriate to begin with an introduction to electronics assembly technology and its basic processes. The flow below shows a typical method of attaching components to surface mount boards. Here, solder paste is printed onto the board using a stencil, components are then placed precisely on the board, taking advantage of the solder tackiness to hold the components in place. Next, the board is reflow soldered en mass by a heat source, as mass reflow is used most widely in production line because of its productivity. Various reflow processes are available in the market namely infrared, vapour phase, and hot air for mass reflow,

and laser or optical beam soldering for localized reflow. This research focuses on infrared (IR) and convective reflow for SMT assembly of lead pitch size of no less than 0.017 inches.

Complementary techniques for ultra-fine-pitch manufacturing i.e. spacing 0.015 inches and below have been discussed in the review articles written by H.Hirai (1993)⁴, Degani, et al (1996)⁵, Lee (1996)⁶, Baba & Carlomagno (1996)⁷ and Tsunoi, et al (1996)⁸.

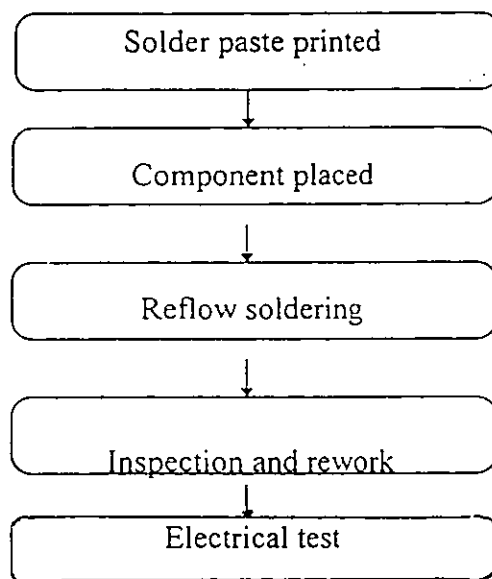


Fig 2.0 SMT Basic Processes

2.2 Trends in SMT and advanced packaging technologies

2.2.1 Evolution in Electronics Manufacturing

Williams, Conway and Whalley (1993)⁹, have discussed the evolution in electronics manufacturing and trends likely in future generations of electronic products. Surface mount and pin-grid-array technology packaged, LSI and VLSI components contain,

nearly 100000 gates in a single device, to give pin counts of several hundred. Today, ball-grid-array (BGA) technology promises to package gated counts that approach or exceed one million per device, giving in pin counts approaching 1000, see fig 2.1¹.

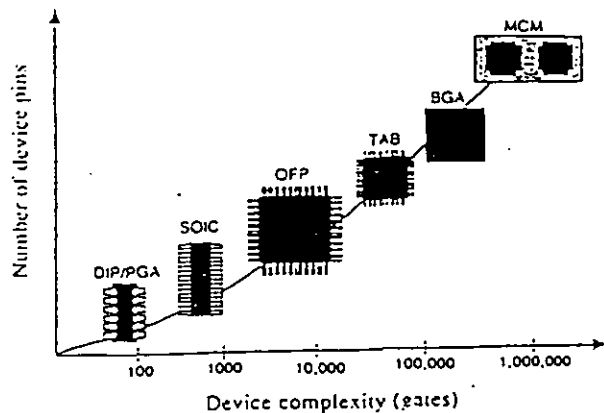


Fig 2.1 The numbers of device pins on surface mount packaging continue to grow as does the gate count of these devices (Adams et al, 1995)¹.

Loughborough work⁹ confirmed that the explosion of SMT and **highly dense packages** resulted in more complex and higher density board design by continually reducing pitches of surface mount components (shown below in fig 2.2), in order to incorporate more features into products while reducing overall package sizes. These changes in turn created major challenges in the electronic assembly process.

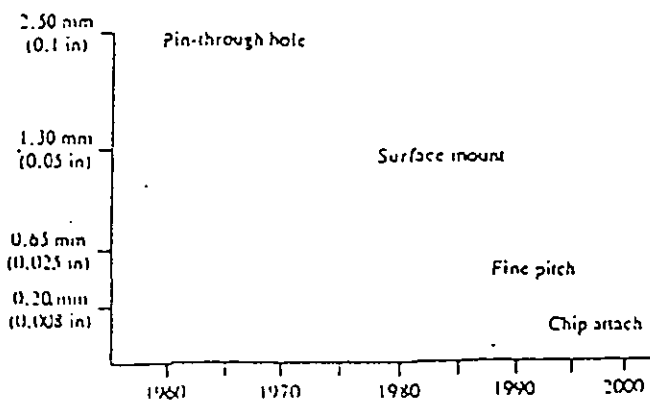


Fig 2.2 Interconnection pitch reduction with time adapted from Williams et al (1993)⁹

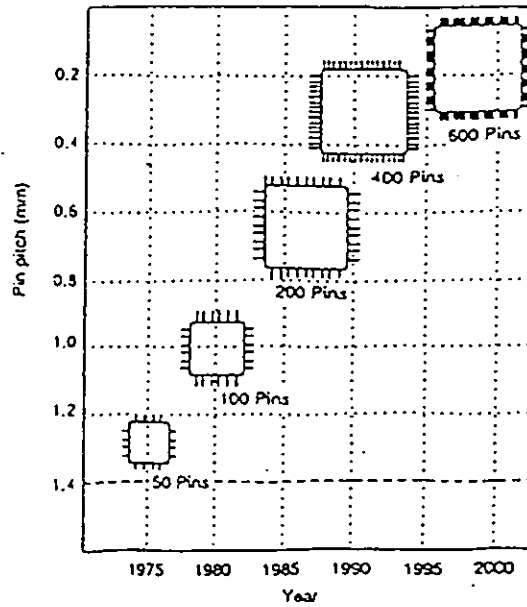


Fig 2.3 The trend towards higher pin-counts and fine-pitch (Oyama,1993)¹⁰

Williams et al (1993)⁹, identified the relationships between the different skills required for the improvement of the manufacturing process. Fig 2.4; essentially the integration of many disciplines: materials, science, manufacturing technology, and product design considering both mechanical & electrical functional performance (see below).

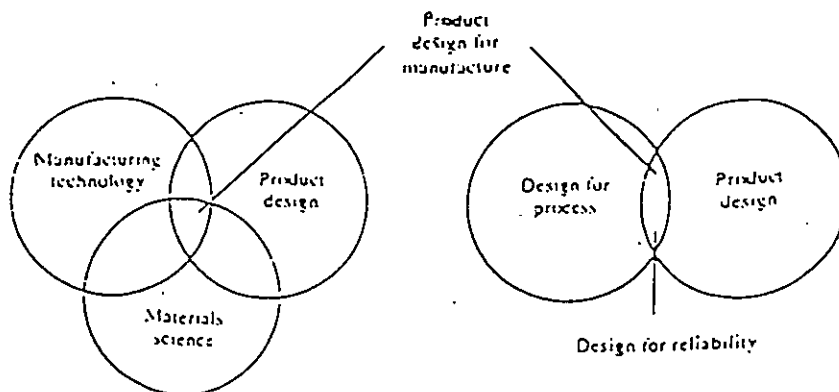


Fig 2.4 The relationship between the technologies involved in packaging design

(Williams.et al, 1993)⁹

They also suggested that the trends in second level packaging i.e. assembly of components on the printed circuit boards (PCB) will be driven by increasing complexity of microprocessors in all types of products such as computers, automotive components and domestic appliances including video cameras and HDTV (high resolution television).

Reviews (Jahn & Conway, 1993)¹¹ and Williams et al (1992)¹² all indicate that multi-chip module (MCM) technologies also represent a solution to design problems requiring high processing speed and reduced size, better functional performance in term of operating frequencies, minimal parasitic, cross-talk and transmission line effects. Nishida (1993)¹³ of IBM Japan Ltd showed the leadless components and SMT packages have major contributions by reducing floating capacity, decreasing wire length and improving propagation delay, thereby extracting maximum performance from LSI chips.

Perhaps the most challenging SMT package to assemble is the Quad Flat Pack (QFP) much of the work in this thesis targets the solder assembly of QFP. Recently, as evidenced by Chip on board (COB) and Chip on glass (COG) methods, the recent packaging trends are blurring the traditional distinction between first and second level packaging. Removing the secondary packaging level by mounting the LSI packages onto the PCB directly, the process cycle time reduced drastically and improve product reliability. It may also eventually be possible to further integrate all necessary product circuitry onto one silicon chip with consequent packaging cost reduction. This evolution indicates that the volume joining of high pin out, small geometry electronic

assemblies remains a major issue. The following sections discuss the major current leading edge technologies in more detail.

2.2.2 Ball Grid Array (BGAs)

Walshak and Hashemi (1994)¹⁴ discussed current and future directions for plastic, ceramic and tape BGAs. Ball Grid Array (BGA) packaging and assembly technology is a current issue throughout the packaging and interconnect community. The level of interest is similar to that which was focused on surface mount technology (SMT) and tape automated bonding (TAB) in the early 1980s. The plastic BGA was developed by the Motorola in the late 1980s. There it was called an overmolded pad array carrier (OMPAC) and used primarily in Motorola paging and portable products. This author first encountered it when it was adopted by Compaq Computers Corporation for their notebook computers (Compaq News, 1993)¹⁵.

The advantages of BGAs compared to conventional leaded surface mount plastic packages are: higher interconnect densities are possible even with a relatively large pitch (typically 0.05 inch pitch), higher assembly yields due to elimination of lead coplanarity issues (See table 2-1 on QFP coplanarity requirements) and less-stringent placement and screen printing requirements, package robustness, board space efficiency, and relative ease of thermal and electrical enhancement. It therefore more suitable for high speed ICs, high I/O application specific IC (ASIC), and MCMs. Bernier et al (1993)¹⁶ of IBM Microelectronics division make a comparison between BGA and QFP technologies (See table -2.2). It is commonly found that BGA

attachment to boards during assembly is as simple as placing 1.27 mm QFP components, since their I/O spacing for interconnect is the same. The BGA technologies offer extendibility in the high I/O range from 250 to 1089 interconnects depending on the type and size of the BGA package. The alternate QFP technology offers interconnection in the high I/O range from 250 to 450 in the ultra fine pitch large body size offerings. Given these selected facts, it would seem apparent that BGA technology is likely to dominate in the future, given its greater ease of assembly and greater extendibility.

Pitch	Required Coplanarity
0.02 inch	0.004 to .00425 inch
0.01 inch	0.00325 to 0.0035 inch
0.0075 inch	0.00275 to 0.003 inch

Table -2.1 QFP Coplanarity requirements (Bernier et al, 1993)¹⁶

Yield performance between BGAs and QFP in IBM's lab is shown in table - 2.3. The comparative yields of the BGA technologies and the QFP technologies shows the BGA class has a clear advantage. Experience in Compaq Computer Corporation shows a general yield defect levels in the 0.3 to 5 ppm/ lead for the initial pass. QFP yield defect levels are significantly higher but it is notable that they are trending downwards and are currently 5 to 30 ppm/lead for the initial pass. So although the difference is narrowing, it is generally known that BGAs are less expensive to assemble.

	PQFP	CQFP	BGA
Body material	Plastic	Ceramic	Ceramic, plastic and tape
Body size	12-30 mm	20-40 mm	12-44 mm
Pitch	0.3, 0.4 0.5 mm	0.4, 0.5 mm	1.27, 1.5 mm
I/O range	80 - 370	144 - 376	72 - 1089

Table - 2.2 Comparison of QFP and BGA technologies (Bernier et al, 1993)

	QFP Pitch			BGA
	0.5 mm	0.4 mm	0.3 mm	1.27 mm
Industry	200 ppm	6000 ppm	speculative	0.5-0.3 ppm
IBM	75 ppm	600 ppm	NA	0.5-0.3 ppm
IBM APD Lab	<10 ppm*	<25 ppm*	<30 ppm*	<1 ppm

Table - 2.3 QFP vs BGA Yield Comparison (Bernier et al, 1993)

However, there are some issues for concern as revealed by Walshak and Hashemi (1993)¹⁴ of MCC labs:

Price - the current package-level BGAs are not at parity with QFPs, but the higher prices of BGAs are countered by the reduced manufacturing cost due to the higher yields with BGAs. Plastic BGAs have about a 20 percent premium over QFPs, but price parity is expected in the near future as production and general usage increases.

Signal escape routing concerns for high I/O arrays - routing the I/Os from dense array patterns on the next level board requires that either the number of layers on the PCB be increased because of limitations in line widths and the line widths and spaces become smaller. Both of these approaches require additional cost in fabricating the next-level board. A system-level design study is recommended, so as to minimize the

routing lengths and in turn minimize the electrical parasitics and to determine the optimum assignment of the signal I/O versus power and ground pads.

Solder ball uniformity / inspectability - process control of the solder paste deposit and, solder ball thickness, are critical to the overall success of the assembly. This process requirement is coupled with the inability to visually inspect the resulting solder joints (X-ray inspection is commonly used) and to perform touch-up. All of the solder balls on the package must contact the solder paste deposit on the board. With the typical low occurrence of BGA solder joint defects i.e. <0.5 ppm/joint, it is claimed that 100 percent inspection can be eliminated¹⁷.

Moisture absorption of plastic packages - PBGAs, similar to PQFPs are subject to popcorn failure and die-bond delamination during solder reflow. The plastic materials used in the package readily absorb moisture from the environment. Package failure can occur due to the rapid expansion of the entrapped water vapour during the reflow process. As with PQFPs, users are recommended to bake the packages prior to assembly to reduce the moisture content of the packages.

Repair-touch-up of a BGA is impossible, thus the rejected component must be removed. The removal of BGAs is not difficult, however care must be taken to prevent the application of excess temperature. After removal, the site must be dressed, leveled and paste added. The new BGA is then placed and reflowed.

Solder joint reliability - data presented to date suggests that BGA packages are extremely reliable¹⁸. However, depending upon the application requirements, there are limitations in the thermo-mechanical life of the joints. The fatigue life is dictated by the CTE mismatch between the PCB and the package substrate. For PBGAs, the area of the highest stresses is located around the perimeter of the chip¹⁹. The TBGA (tape BGA) can be CTE-matched to the printed circuit board, due to the tape flexibility, thus essentially eliminating fatigue life concerns. In summary, while offering an alternative to QFP packages BGAs present a different set of joining and assembly problems. Another package form is that associated with Tape Automated Bonding (TAB) discussed below.

2.2.3 Tape Automated Bonding (TAB)

Suzuki (1993)²⁰, revealed that recently advanced interconnection technology is becoming particularly applied to office automation systems in the form of, high-pin-count LSI drivers for flat panel displays application with minimal size and weight specifications. With TAB, the IC die is mounted above a thin polyimide tape (typically 75 micro-metre thick) and inner-lead-bonded (ILB) to the tape's thin copper foils (35 micro-metre). The TAB device, in the tape state, can be readily tested and reworked if necessary. The device is subsequently mounted and outer-lead-bonded to the fine pitch pads of the PCB. Devices can also be tested and reworked if necessary at this stage. A TAB device achieves its thinness because epoxy encapsulation is applied only to the underside or active side of the die (the inner mold). The thickness from PCB to the back of the die is typically less than 1.0 mm (see fig 2.5)

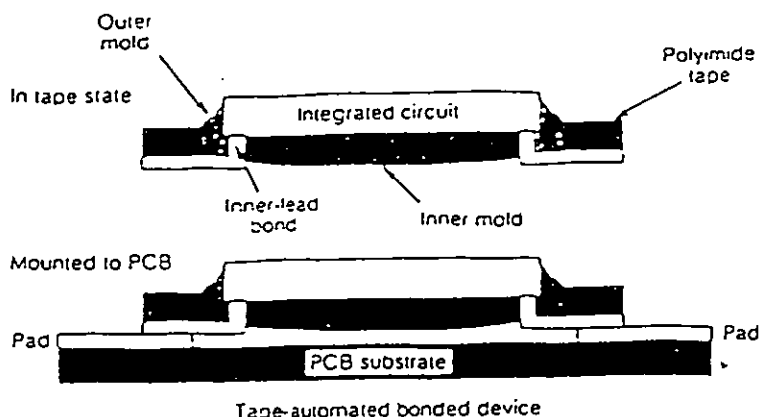


Fig 2.5 Construction of TAB in tape state and mounted to PCB (Perry,1991)²¹

Liquid crystal modules are typical products using tape automated bonding (TAB). TAB was introduced in liquid crystal modules because the pads of liquid crystal panels and the outer leads of a TAB package can be bonded relatively easy by using anisotropic conductive sheet. Consequently, development of TAB advanced rapidly and the market share of TAB reached 3 percent of IC packages according to Hatada (1993)²³.

2.2.4 Chip-On-Glass (COG)

Applications of liquid crystal modules are expanding from view finders of TV cameras to computer displays and large screen TVs. As displays make advances in resolution and colour, there is a trend towards narrower pad pitches of 100 micrometre, but cross-talk is likely to occur in anisotropic conductive sheets²³. Further, packaging cost must be kept low to hold down the cost of liquid crystal modules. It is anticipated that chip-on-glass (COG) will solve the issues encountered by TAB in liquid crystal modules, and companies are shifting in this direction²². Many COG

technologies using organic materials have been developed in which the LSI is bonded to the glass substrate using conductive adhesives²³.

The objective of bonding a liquid crystal panel's pad to the LSI's pad is to use as little force as possible. The Japanese company, Citizen, has had good results over a prolonged time with an interconnect method using organic materials²⁴. TAB interconnection will be one of the primary systems used in the creation of multichip modules where many packageless chips are placed on a very high technology substrate. The resulting package emulates a conventional package available now with conventional board assembly using the module approach^{24,25}. Total elimination of the package and lead-interconnect solution as in the TAB case is possible when using flip chip technology. The connection of the chip to a substrate is created by implementing a solder ball on the surface of the chip connected electronically to the internal wiring of the chip. When the chip is turned face down, 'flipped', the solder balls on the face of the chip are available for direct attachment to the substrate leadless package TAB and flip chip approaches are again viable outside Japan for new generations of product implementations (Buschbom et al, 1993)²⁴.

2.2.5 Flip Chip Mounting

Chip-on-board (COB) techniques use variations of tape-automated-bonding (TAB), flip chip, and conventional wire-bonding techniques to mount bare chips directly on the printed-circuit-board (PCB), eliminating most pin-related problems entirely²⁶.

Besides TAB, two other most commonly used techniques are flip chip and wire-bonding.

Flip chip mounting; whereby bare chip I/O pads are bumped and the chips are mounted face down on the PCB/substrate. Flip chip assembly offers advantages over other methods of bare-die mounting such as TAB and wire bonding technology²⁷. It requires the lowest footprint area on the PCB and allows a significant reduction in package height. Because of the face-down assembly, the whole surface of the IC can be used for different area array configuration allowing the highest density and number of I/Os^{26,27,29}.

Another advantage of the area array configuration is that, compared to standard ICs using wire bonding with peripheral pads, pitch and the pad size can be greater. As wire bonding and TAB technology using peripheral pads more to pitches below 100 micro-metre^{30,31} a comparable area configuration for flip chip is possible at >300 micro-metre pitch. Because most chips are currently designed for wire bonding or TAB, an area configuration can be achieved only with an additional redistribution layer²⁷. This additional step in the bumping process increases the cost and reduces the electrical parasitic life. Therefore, many users prefer to avoid this by performing flip chip with peripheral pads³².

2.2.6 Wire-Bonding

The next primary method of electrically interconnecting bare chips is wire-bonding. A proprietary assembly process, Bonded Interconnect Pin (BIP) technology developed by Raychem Corporation, combines the simplicity of wire bonding, the pretest capability of TAB, and the packaging density of flip chip³³. BIP technology enables large numbers of chips to be interconnected to a wide variety of circuit boards and makes it possible to access and take advantage of the very high routing density of high-density interconnect microcircuits. The BIP process utilizes thermosonic ball bonding and reflow soldering to create electrical interconnections between the chip and the circuit board.

Silicon chips that can be thermosonically ball-bonded can be electronically interconnected using BIP. A BIP chip is assembled face-down on the high-density interconnect microcircuit minimizing the path length of electrical signals and optimizing routing and packaging densities. The BIP length can be varied to accommodate the thermal coefficient of the flip chip structure^{34,35}. BIP assemblies are repairable using reflow soldering techniques. In addition, BIP can be applied to individual die; thus availability of the wafers (presently a sensitive issue for semiconductor manufacturers) is not an issue³³.

Solderless flip chip mounting using stud bumps and adhesive^{59,60}; flip chip mounting is notorious for poor chip-to-substrate connection reliability due to widely differing coefficients of thermal expansion of the mating surfaces³⁶. To address this problem,

the chip-printed wiring interstices are filled with enough thermosetting adhesive to ensure that the sides of the chip are covered. A stud bump is formed on each I/O pad and covered with a conductive paste³⁶. The conductive paste compensates for variations in stud-bump height, making the connection more secure. Reliability^{36,37} appraised later showed no abnormality.

The process of stud-bump formation^{59,60} is the same as that of wire-bonding IC die to lead frames. A gold wire is passed through the hole in a capillary tube and subjected to an electrical discharge to form a gold ball, which is bonded to the chip I/O pads by thermocompression and ultrasonic energy. The next step is to apply a conductive paste to the stud bumps. This is done by squeezing a conductive paste film of a predetermined thickness onto a jig, then pressing the stud-bump surface against the film to transfer the paste. The chip mounting sequence begins by feeding thermosetting adhesive onto the PCB pads by screen printing or dispenser process. The mounting is placed with high precision (15 micro-metre), the chip is then heated and pressurized from the reverse side to set the adhesive and thus make the PCB pad and chip bump connection. This process eases thermal and mechanical stresses resulting from differences in die and board coefficients of thermal expansion, and is relatively inexpensive. There is an increase in the development of a new array package - the CSP (chip size package) in the large Large-Scale-Integration (LSI) package using for example stud-bump-bonding (SBB)^{62,63}. The SBB techniques have favorable thermal and electrical characteristic⁶² with almost the same size as the LSI chip. LSI packaging has changed from QFP to array packages such as BGA, the CSP package is now the new alternative to realize high density interconnect with larger pitch^{61,62}.

2.2.7 Chip-On-Board (COB) Management Issues

Lau (1993)³⁸ and Martin et al³⁹ (1993) state that chip on board (COB) technology is still evolving, but that economics and the necessity of this technology for small product packages make it of significance. The lack of infrastructure within the industry has limited implementation of this technology to date. The most severe limitation has been the availability of known-good-die (KGD). It's unavailability can be attributed to the difficulty in testing raw die. It has been only recently that tested die have been made available to the industry³⁹. As SMT components reach their limits i.e. around 0.3 mm for both TAB & QFP and pin out trends further move towards 0.2 mm in one to two years (see fig 2.6 Goward et al, 1993)²³ COB technology will surpass TAB with a mounting density of 20 points / cm² when compared to 15 points per cm² for TAB. BGA's can achieve a smaller density to that of COB or TAB when a lead pitch of 1.5 mm compared to 0.3 mm for TAB & QFP^{16,23} but still include the extra joints associated with second level packages and their reliability impacts.

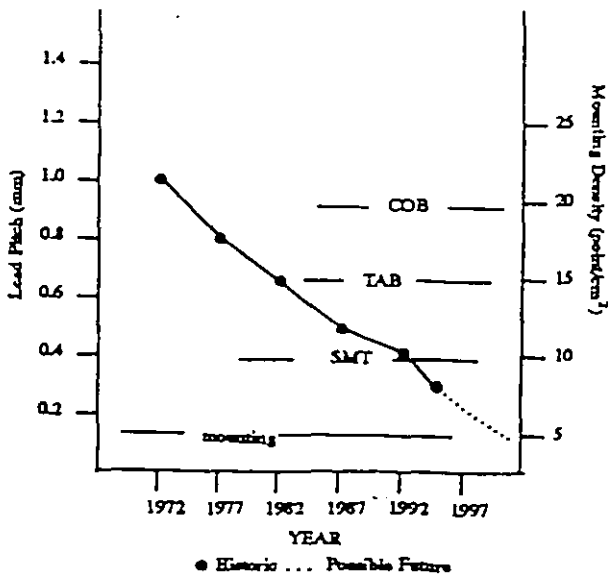


Fig. 2.6 Component pitch and trends (Goward et al, 1993)

Like the implementation of SMT, COB will require assemblers to invest in different pieces of capital equipment and develop new processes.

Users will be required to develop processes that include die mounting/bonding, plasma cleaning, wire-bonding and encapsulation.

Assemblers of COB will also have to provide the environment required to handle raw die - cleanrooms, and semiconductor-related equipment.

In spite of the number of negatives currently associated with COB, there are a number of positives. First, and probably most important, is that many designs would not be possible without the use of COB e.g. particularly in telecommunication products such as mobile phones, pagers, LCD modules and others such as the thermal printer. Another important point is that the COB can provide economic advantages, especially in volume i.e. the elimination of IC packaging cost. While

COB is in evolution there is still industry skepticism³⁸. But, like SMT, economics and the necessity of COB will make it a near term reality, with more die fabricators providing tested raw die and a growing infrastructure.

2.2.8 Multi-Chip Module (MCM)

The introduction of multichip modules evolved mainly from the demand for high density packaging for computers for example RISC processor modules, Motorola 68080, IBM RS9000 and SUN's Sparc processor, and NEC's ACOs S1500 supercomputer^{9, 11, 22}.

According to Hatada (1993)²², multichip packaging technology can be broadly divided into two types. The first type is a multichip packaging technology whose primary component is the functional substrate.

Typical products include LCD modules and thermal printers. The packaging technology applied here are those already described namely chip-on-board (COB) and tape-automated bonding (TAB). Thermal management issues are more important than the packaging technology for dies, and inexpensive packaging technologies are required other than high level packaging technologies, and therefore will not be elaborated here.

In this section, we will focus on the second type of multichip module.

The primary components are LSI devices, circuit modules such as

microprocessor modules and memory modules, such as those for the computers described earlier. This multichip packaging technology aims at large capacity and high functionality, high density is an important technical issue.

In modules for microprocessors, die with different functions such as gate array and memory are mounted on a multilayer wiring substrate at fine pitch with high density and completed as a module that functions as a circuit. Important module characteristics are high speed and power dissipation. Less high function computers are becoming more compact, this technology is indispensable as a next generation packaging technology^{11, 12, 40}.

MCM packaging technologies in the industry are widely classified into three types^{9, 11, 41, 42}:

MCM-L - High density laminated circuit board.

MCM-C - Ceramic substrate, either co-fired or low dielectric constant.

MCM-D - Cover modules with deposited wiring on silicon, ceramic or metal substrates.

Modules which use laminate as a substrate for packaging and electronics interconnect are now in volume production. This is primarily driven by various performance needs, such as cost, size,

weight and computational speed^{9, 11, 12, 43}.

MCM-L as a low cost substrate interconnect medium is evolving from simple to complex applications. Improvements in the material and process for laminate manufacturing have increased the performance level of the substrates rapidly over the past few years⁴⁴. Laminated substrates have gone from being a very low density wiring approach to being fully competitive with MCM-C and competitive in many cases with MCM-D in term of wiring density⁴⁴.

The laminate method has offered high electrical performance and improve processes have given the designer the flexibility to take full advantage of the superior performance level of the laminate material. The result is that current MCM-L is superior to both MCM-C and MCM-D in term of electrical performance^{44, 45, 46}.

Degani et al (1996)⁴⁴ and Zamborsky (1996)⁴⁷ suggested that the infrastructure necessary to support BGAs is nearing the point where the ball grid format can be a viable alternative for virtually any packaging application. It is quite likely that MCM applications will become viable in BGAs before single chip BGAs are in wide use. BGA formats for laminate based MCM are less costly than for other packaging formats. In addition BGA formats have thermal and electrical performance advantages over other surface mount formats, and higher assembly

yield than conventional surface mount components. Thus, BGA will become less expensive on a piece part basis than MCMs built on conventional surface mount formats. In short, the ball grid format is anticipated to be perfect package format for laminate based MCMs. All these processes require solder joining or the alternatives of wire-bonding or the use of anisotropic conducting adhesives. After a brief introduction to wire-bonding and anisotropic conductive adhesive (ACA) as discussed below, the review will focus on soldering.

2.3 INTERCONNECTION TECHNOLOGY USING

ANISOTROPIC CONDUCTIVE ADHESIVES (ACAs) AND ANISOTROPIC CONDUCTIVE ADHESIVE FILMS (ACF)

Anisotropic Conductive adhesive (ACAs) - A conductive adhesive consisting of conductive particles and adhesive has been widely used for coarse - pitch interconnections of I/O pads, has a low interconnection temperature, and has begun to find further practical applications, such as in interconnecting TAB outerleads bonding (OLB) and COG to an LCD panel ^{48, 49, 50}.

The conventional ACA is a paste adhesive consisting of conductive particles dispersed in an adhesive matrix. Conductive particles can be pure metal such as gold, silver or nickel; or metal-coated particles whose cores are plastic, quartz, or glass ^{51, 52}. The adhesive matrix can

be thermosetting, thermoplastic, or UV-curable. ACAs typically contain only 5 to 25 volume percent conductive filler, with a spherical particle shape^{49, 50, 51}. Mean ACA particle sizes range from 5 to 15 micro-metre, with smaller particles used for fine-pitch interconnections⁵¹. When the IC is placed into the adhesive and applied by force, the adhesive is pressed into a monolayer of conductive particles, creating z - axis electrical contacts. ACAs are available both from the United States and Japan. American suppliers include Zymet, 3M, AI technology and Alpha Metals. Japanese suppliers include Hitachi Chemical, Three Bond, and Sony Chemical⁵¹.

Anisotropic Conductive Adhesive films (ACFs) - ACFs consist of conducting particles and adhesives which provide both attachment and electrical interconnection between electrodes. ACFs are widely used for high-density interconnection between liquid-crystal display (LCD) panels and tape carrier packages to replace the traditional soldering⁵³. ACFs have achieved broad acceptance for direct chip interconnections such as chip-on-board (COB) assembly in the interest of product miniaturization, multiple connectivity, and cost reduction^{53, 54, 55}. ACFs are widely used today, ranging from larger notebook computer displays to smaller alphanumeric displays found in pagers (beepers).

ACF is in film form, typically packaged in tape-on-reel format. ACFs

utilizing the adhesive matrix can be thermosetting or thermoplastic ⁵⁶.

First, the ACF is placed between the tape carrier package and the glass substrate, and the electrodes to be bonded are aligned. Second, pressure and heat are simultaneously applied to effect interconnection between electrode surfaces, where connecting particles are deformed between electrode surfaces ^{56,57}. Bonding conditions for interconnecting a tape carrier package to glass substrate and PCB are usually 170 degree C, 20 kgf/cm² and 20 seconds ⁵⁶, during which time no adjacent electrodes are short-circuited by nondeformed conducting particles.

The interconnection is then retained by the compressive force between electrode surfaces because of the curing shrinkage of the adhesive. When electrode surfaces are bonded, adhesive resin is squeezed out and conducting particles are trapped between conductor surfaces.

Consequently, electrical conduction in the ACF is restricted in the z direction (normal to the plane of adhesive films) while electrical insulation in xy plane is maintained ⁵⁶. Therefore, ACF does not need to be patterned, unlike soldering, and therefore is more versatile ^{56, 57}.

However, ACFs are not commonly used for flip chip application yet ⁵¹.

Nevertheless, some suppliers have begun producing ACFs for this application, and trials using ACF for flip chip assembly are increasing ⁵⁸.

2.4 SOLDER REFLOW

2.4.1 BASIC REFLOW PROCESSES

The basic process of infrared reflow (IR) uses the radiated heat of the infrared beam to apply heat to the board and is the most common reflow method ⁶⁴. The rate of heat absorption differs according to the subject materials, the emissivity of the board, PCB layout and the wavelength of the infrared light. However, there is increased use of forced air convection as in the Vitronics Oven used in some of the author's experiments. In this case the heat distribution of the IR technology across the entire board is more even and homogenous and thus less dependent on above factors ⁶⁵.

Klein (1993) ⁶⁵ and Whalley, et al (1991) ⁶⁶, discuss the important issues in reflow soldering. These authors point out that for more complicated PCBs with large fine pitch devices, it is not always easy to meet the requirements defined in the temperature profile specified for the reflow process. The problem of large temperature differences between components can be resolved with the use of forced air convection but not at the expense of process control needed to get to the required temperatures and dwell time at specified temperatures.

2.4.2 PURE IR VS FORCED AIR CONVECTION

Research work ^{68, 69, 70}  have compared low cost (pure IR) and a large Senju furnace (with forced air convection). The combined IR/ Convection oven was found typically to be 70:30 to 90:10 convective : radiative heating. In this research, it is suggested that convection is accounting for only 20 to 30 percent of heat transfer for this machine, but that this convection was found of significant help in uniform heating on the board. This is important, for large circuit boards with less copper on inner layers and large fine pitch devices. If the temperature difference between the coldest and the hottest location on a board in the peak zone of reflow system is more than the distance between the maximum and minimum temperature to be reached, then there is a need for more forced air convection.

Klein (1993) ⁶⁵, Langen et al (1990) ⁶⁷ and Adam (1993) ⁷¹, suggested using nitrogen as a protective atmosphere, as it will enlarge the process window because the wetting process needs less time and takes place with higher wetting forces. This is critical when low residue solder pastes are used, as reproducible wetting behaviour is essential for the no clean soldering process.

2.4.3 VAPOUR PHASE SOLDER REFLOW

Next, vapour phase soldering (VPS) uses the heat from the vapours of a hot, fluorinated, inactive solvent to cause the solder to melt and reflow.

As the heat conductor has a specific boiling point and the latent heat emission due to vapourisation is large, the uniformity and rapidity of heating is good ⁷². Also, the soldering temperature will not rise beyond the boiling point of a solvent. However, maintenance of the machine's complex structure and the running costs and environmental impacts of consumable solvent are big disadvantages for this process ^{73,74}.

The hot air reflow (IR with forced air convection) process involves heating air with a heater and forcing the heated air to circulate within the oven. The solder is melted and reflowed by the heat transferred from the hot-air. The uniformity of hot air reflow falls midway between those of pure infrared and VPS methods. In most cases, the use of an inert atmosphere (i.e. nitrogenous environment) is encouraged to eliminate the fear of oxidation after a prolonged period of heating. Hot air reflow has the advantage of being maintenance free when compared to the VPS method ^{73,74}.

2.4.4 LASER AND OPTICAL BEAM SOLDERING

Laser soldering is accomplished quickly with the high energy density of a laser, but the abrupt rise in temperature sometimes causes solder balls to form. However, due to the nature of the precisely focused energy of the laser, it is found most suitable for fine pitch soldering i.e. 10 mil (0.010 inch) and below ^{73,74}.

As the above discussion has revealed, there is no general purpose reflow device available. The appropriate reflow method must be chosen by taking into account the thermal capacity, types of mounted devices, and the production quantity of the PCBA assembly.

2.5 DESCRIPTION OF PHENOMENA IN REFLOW SOLDERING

Boettinger et al (1995)⁷⁵, Singler (1994)⁷⁶, and research work in Loughborough^{66,67,77,78,79,80,81,82,83,84,85,89,90} have carried out fundamental investigations into the IR-reflow process and the mechanism of solder alloy wetting and spreading. These studies are important as they provide an understanding of the reflow soldering process and the mechanics of reactive wetting and intermetallic formation.

Early work done in Loughborough^{66,77,78} investigated the phenomenology of the reflow sub-process, namely fluxing and solder particle reflow phenomena, using high speed video microscopy. With respect to fluxing, it was observed that solvent temperature rise and solvent evaporation (boiling) took place in the early stage of the reflow process. As heat transfer increases, the flux begins to melt and its viscosity falls. At this instant, the low viscosity activated flux starts metal oxide removal. Similar work⁷⁵ was done by research workers of NIST in an U.S. Army lab with rosin (R) and rosin mildly activated (RMA) fluxes, representing two extremes for the importance of heat flow even through the rates of heating for the

experiments were identical. For the RMA flux, the wetting is so rapid that the geometry and the rate of flux melting influences the geometry (shape) and the rate of solder spreading process. Thus, the rate of temperature rise is important. With the R flux, melting is clearly completed before the solder spreads to any significant extent. Thus, the spreading process of R flux occurs non-isothermally. These observations represent the complexities of addressing practical aspects of soldering process. Work^{77,78,79,84} at Loughborough revealed that solder paste reflow is subjected to a number of changes, prior to reflow and at reflow. These are solder particle reflow movement, partial reflow into mashy material, bulk melting, wetting and spreading. The mashy behaviour was observed to occur between 180 to 200 degree C. Following the formation of the mashy zone, structure in the paste collapses and the flux is forced to the surface of molten solder. Then the sub-process of wetting, flow / spreading and intermetallic formation take place. These sub processes do not occur instantaneously but appear controlled by thermal energy input.

In the U.S.Army lab⁷⁵, two limiting cases of the wetting and spreading of molten solder on a substrate were studied. The first case is limited by the rate of fluid flow in the solder and the second case is limited by the contact line kinetics.

Ehrhard & Davis's (1991)⁸⁶ constitutive equation: $v = k(\theta - \theta_e)^n$ describes the contact line kinetics, where v is the velocity of the contact line, k is the rate constant, θ and θ_e are the instantaneous and the equilibrium microscopic contact angles, respectively. The wetting / spreading behaviour is dominated by the

variation of the flux surface tension as the flux composition changes during the reflow process. These studies indicate the many variables it is necessary to understand for an informed approach to solving technical problems.

2.6 The Wetting Balance

Flux activity evaluation through wetting balance analysis. The wetting balance is an important tool to explore this phenomena. Huang et al (1995)¹¹⁶ presents a paper on an approach to evaluate the influence of the flux activity in promoting wetting through the use of wetting balance analysis. The results obtained can serve as a bench mark for evaluating candidate fluxes for future use in the manufacturing process. it is therefore important to present the basis of this technique.

An overview of wetting balance analysis; the wetting balance method is a quantitative investigation of solderability through the measurement of wetting speed and wetting force¹¹⁷. It is typically used to evaluate the solderability of a component lead. The specimen is suspended from a sensitive balance and immersed at a predetermined speed and at a controlled depth into molten solder at a specific temperature. The resultant vertical forces of buoyancy and surface tension on the immersed specimen are detected by a transducer and converted into an electrical signal. Solderability performance is determined by the examination of the vertical forces as function of time after component lead immersion. A component's solderability is inversely proportional to the wetting time (the time needed for the recorded signal crossing the buoyancy corrected zero axis) and directly proportional

to the wetting force.

This work concluded, there that is reasonable correlation being observed between the wetting scenario on the specimens and data collected by the wetting mechanism.

A specimen with a shorter time to zero buoyancy and higher wetting forces generally exhibits better wetting performance. Poor wetting was observed for the specimen with negative wetting forces. Correlation between the 'Dip and Look' and Wetting Balance analysis was not found to be significant in prior research (Elkins, 1994)¹¹⁸. The wetting performance of flux was found to correlate to the pull strength of the solder joint (Denny, 1994)¹¹⁴.

Lea (1995)¹²⁰ discussed the six stages of the measurement of a specimen that is readily wet by the solder are as shown in figure 2.7.

- a. just prior to the moment of immersion.
- b. immediately after the moment of immersion, when wetting has not begun and there is an upward summation of buoyancy and surface tension forces;
- c. after wetting has begun and the meniscus has risen up the specimen to the point where the vertical force from surface tension is zero and the wetting force acting on the specimen is that due to its buoyancy;
- d. when the meniscus is curved and the surface tension force is acting downwards;
- e. as the specimen is being withdrawn; surface tension and a possible oxide film on the solder are causing a dragout of solder;
- f. when the specimen has been withdrawn and is heavier than at the start of the test because of its different solder coating.

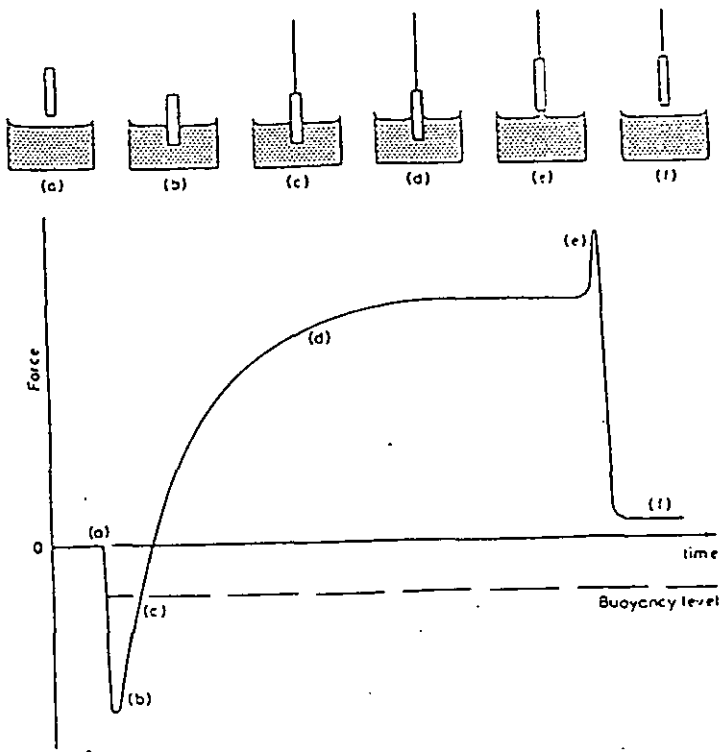


Fig 2.7 A wetting balance curve, Lea (1995)120

Some representative curves are shown in figure 2.8. In each case the full horizontal line represents the force condition at the start of the test cycle and the dotted horizontal line: buoyancy level at which the wetting force is zero i.e. the contact angle is 90 degree.

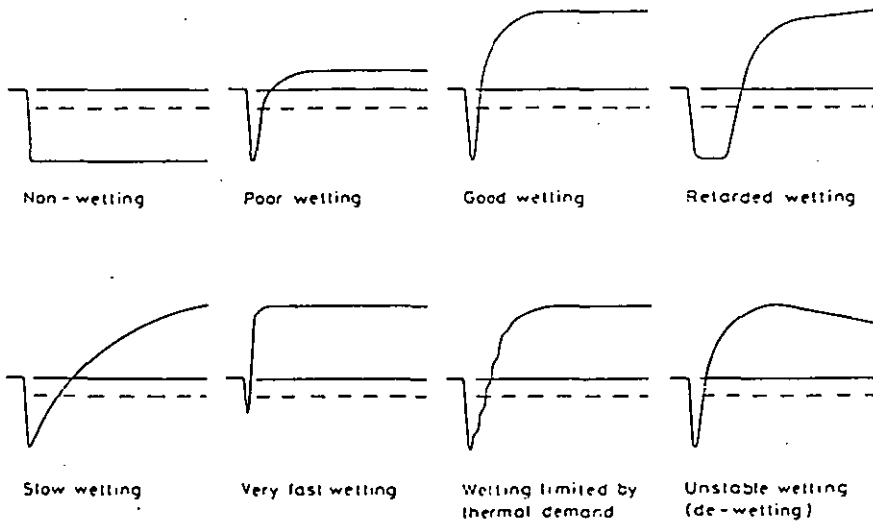


Fig 2.8 Some representative shapes of wetting balance curves, Lea (1995)120

2.7 ANALYTICAL MODELS OF SOLDER DEFECTS AND WETTING OF SURFACES.

A number of authors^{75,76,86,87,88,91,92,93,94,95,96,97,98} have addressed the modelling of the formation of solder joints and wetting behaviour of surfaces.

Singler (1994)⁷⁶ particularly discussed the fluid mechanics of soldering processes.

He considers a solder bridge from the perspective of the stability of an equilibrium capillary surface. Bridging problems have largely been dealt with empirically, usually by adjusting process parameters until the phenomenon has been substantially mitigated.

This approach usually does not involve any fundamental understanding of the problem. However, it is our intention here to take an approach of combining the fundamental understanding of physical science and empirical study through vigorous testing in a mass production environment to ensure any recommendation is sufficiently robust (eg. sensitivity of problems) to provide a scientific guide for process tool & equipment design, board layout, component's lead design etc.

Singler (1994)⁷⁶ concluded that where the gull-wing lead has very positive structural properties (eg. flexibility etc.), it has some potentially detrimental characteristics from a solder flow perspective (i.e. solder wicking), due to the fundamental relationship relating the pressure jump across a liquid-fluid interface to the curvature of that interface. Considering the gull-wing lead shown in fig 2.9, the relationship can be expressed using Laplace's equation.

$$P_B - P_A = \sigma \left(\frac{1}{R_1} + \frac{1}{R_2} \right) = J P_B - P_A = \sigma \left(\frac{1}{R_1} + \frac{1}{R_2} \right) = J$$

P_A and P_B are the pressure in the fluid on either side of the interface, R_1 and R_2 are the principle radius of curvatures, and the sign of first curvature J is chosen such that $P_B \geq P_A$, provided that the surface is on average concave towards region B.

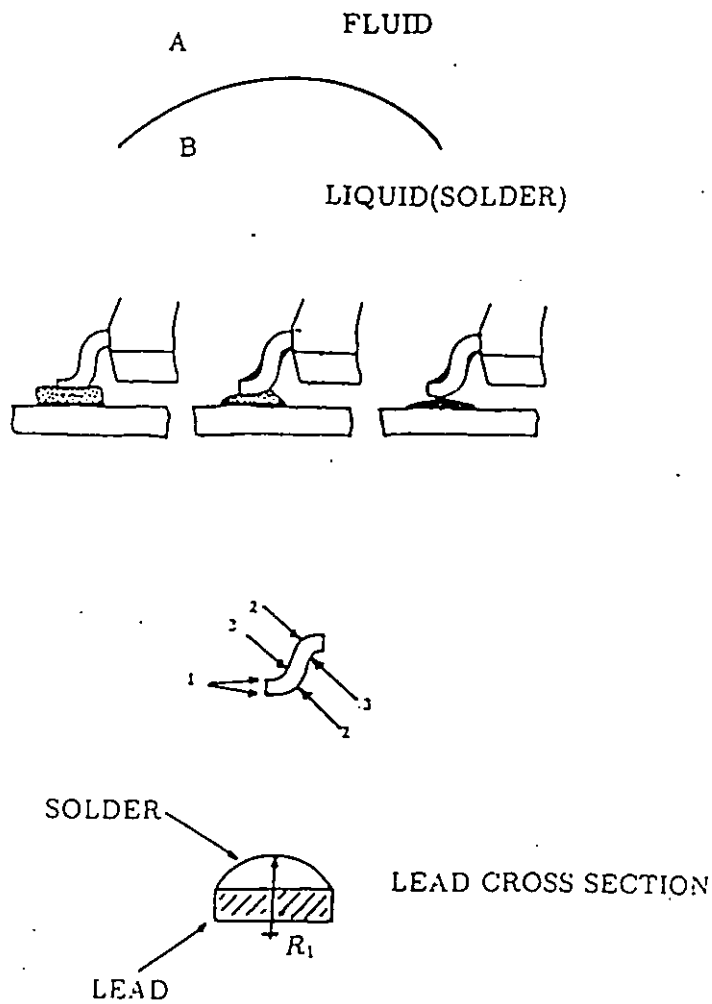


Fig. 2.9 Schematic of solder wicking on a gull-wing lead (Singler, 1994)⁷⁶.

The detrimental features arise from the lead configuration itself, assuming the solder has a uniform shape at any cross section along the lead, then one principal radius of curvature, say R_1 , is constant along the lead. At the points designated 2 on the lead, the sign of R_2 is the same. Therefore the pressures in the fluid at the points labeled 2 are higher than at the points labeled 3. Consequently, fluid is effectively squeezed from the regions 2 towards region 3; the capillary pressure gradients established by the curvature of the leads effectively confines the solder to region 3 on both the top and bottom of the lead resulting solder wicking faults.

Lea (1988)⁸⁷ described the surface tension of a liquid in its basic form and it was found that the amount of energy needed to enlarge the liquid surface area. It has dimensions of $J.m^{-2}$.

The intermolecular structure of liquid is attracted uniformly in all directions. At the surface due to the lesser number of neighbouring atoms in the surrounding environment, the outside attraction is smaller and there exists a resultant force acting inwards perpendicularly to the surface and consequently a pressure across the surface. The surface atoms are drawn into the interior of the liquid more rapidly than their replacement by other molecules moving outwards so that the surface contacts to a minimum area for the particular volume of liquid.

The system thermodynamically strives to obtain a minimum value of its free energy, and this it does by minimising its surface area. A floating droplet therefore assumes the shape of a sphere since a sphere has the minimum surface-to-volume ratio.

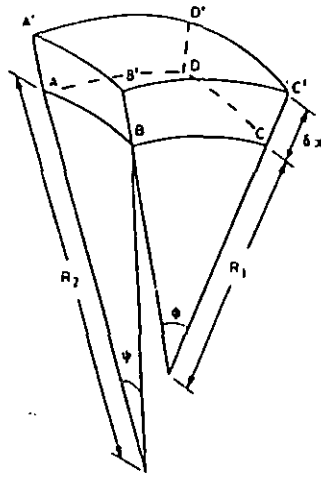


Fig 2.10 A liquid surface ABCD having principal radius of curvature R_1 and R_2 expanding a distance δx radially⁸⁷.

Figure 2.10 described a curve liquid surface of resultant forces mathematically in term of pressure, area and expansion distance. The liquid surface is having a principal radius of curvature R_1 and R_2 . If γ is the surface tension, the energy of surface ABCD is γ times the area, i.e. $\gamma \cdot R_1 \delta\phi \cdot R_2 \delta\psi$. If the pressure difference across the curved surface, arising from the resultant forces acting inwards is δp , then the work done to cause this expansion is (pressure) x (area) x (expansion distance), i.e. $\delta p \cdot R_1 \delta\phi \cdot R_2 \delta\psi \cdot \delta x$. Thus

$$\gamma \delta\phi \delta\psi [R_1 + \delta x)(R_2 + \delta x) - R_1 R_2] = \delta p \delta\phi \delta\psi R_1 R_2 \delta x$$

$$\text{when } \delta p = \gamma \left[\frac{1}{R_1} + \frac{1}{R_2} \right] \quad (a)$$

This is known as the Laplace equation.

In equation (a) a radius is positive when it is measured inside the liquid and negative if measured outside the liquid. For a floating droplet, sphere of radius R , therefore

$$\delta p = \frac{2\gamma}{R} \quad (b)$$

As the volume of the sessile drop increases, so its top surface becomes flattened by the effect of gravity. The difference in pressure across the surface, at any point on the liquid surface is then

$$\delta p = \delta \rho g h + \text{constant} \quad (c)$$

where g is the acceleration due to gravity, ρ the density of the liquid and z the vertical co-ordinate measured from the apex of the drop. The normal to the curve at any point (x, z) makes an angle ϕ to the vertical, and the radius of curvature of the surface in the plane subtended at angle ϕ is $R_2 = x/\sin\phi$. The radius of curvature in the plane of the section is R_1 as shown in fig.2.10 a. At the apex of the drop, $z=0$, $R_1=R_2=r$, the maximum radius of curvature, and hence the constant in equation c is $2\gamma/r$. Thus the equation for the shape of the cylindrically symmetric sessile drop is obtained as shown below.

$$\frac{r}{R_1} + \left[\frac{r}{x}\right] \sin \phi = 2 + \frac{r^2 g \rho}{\gamma} \left[\frac{z}{r}\right] \quad (d)$$

The linear dimensions, R_1 , x and z , appear as ratios to the maximum radius of curvature, r . Also, the parameter:

$$\zeta = \frac{r^2 g \rho}{\gamma}$$

is a dimensionless constant for the particular liquid and its quantity. For 60:40 tin-lead solder $\zeta=0.20r^2$. If r is expressed in millimetres, r depends upon the volume of liquid solder present. Thus, a given value for the constant ζ gives the same drop shape regardless of drop size, and changing the size of the drop without altering its

shape. However, by changing the size of the drop while holding surface tension and density constant causes both ζ and r to change simultaneously.

Both R_1 and ϕ involve derivatives of z with respect to x , to give:

$$r \frac{d^2 z}{dx^2} + \frac{r}{x} \left\{ 1 + \left[\frac{dz}{dx} \right]^2 \right\} \frac{dz}{dx} = \left[2 + \frac{\zeta z}{r} \right] \left\{ 1 + \left[\frac{dz}{dx} \right]^2 \right\}^{3/2} \quad (e)$$

This equation describe the shape of a liquid sessile drop shown in fig.2.10a.

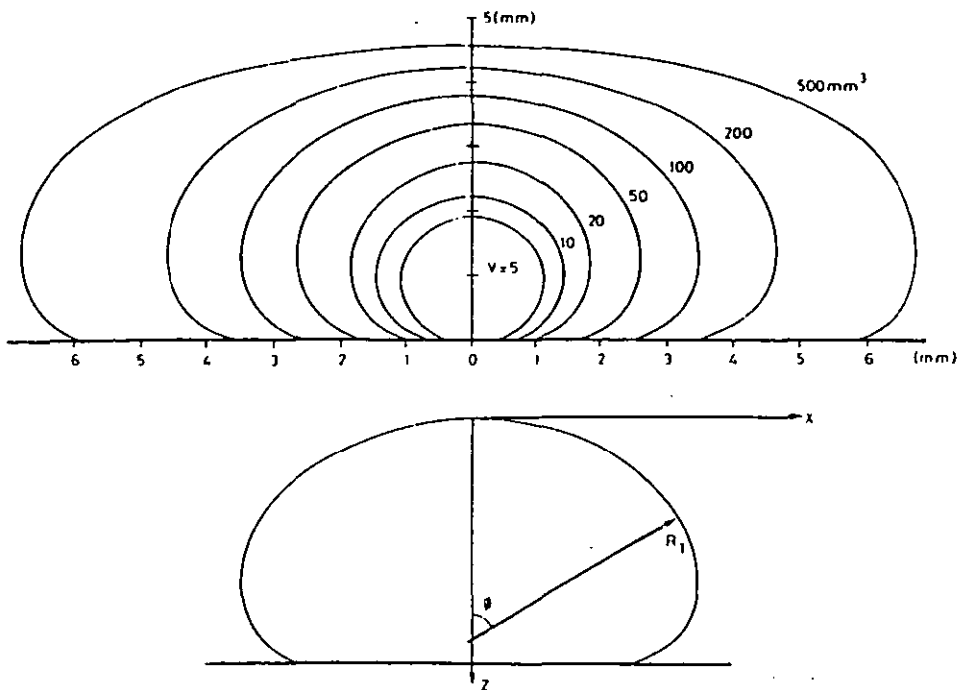


Fig. 2.10a Vertical sections through sessile drops of liquid on a flat surface, defined

by equation (e): [1] calculated for solder with $\frac{8\rho}{\gamma} = 0.2 \text{ mm}^{-2}$ and [2] defining the x-y axes and the radius of curvature R_1 at angle ϕ ⁸⁷.

The thermodynamics of wetting of a liquid spreading on a solid surface was originated by Young⁹⁹, whom originally considered the equilibrium qualitatively in 1805 and Dupre⁸⁷, in 1869, put in mathematical terms. As every system tends towards minimum free energy, the areas of the interfaces and the free surfaces tend to become as small as possible. In doing so, however, they counteract one another.

Thus an equilibrium condition is reached with the total free energy, F , given by Young⁹⁹ as:

$$F = \sum_i \gamma_i (\text{surface area})_i$$

$$\gamma_{sv} = \gamma_{sl} + \gamma_{lv} \cos \theta$$

where γ_{LV} is the surface tension of the liquid/vapour interface, γ_{SV} is the solid/vapour interface surface tension, γ_{LV} is the solid/liquid interfacial tension and θ is the contact angle. The degree of wettability can be obtained from the value of the contact angle

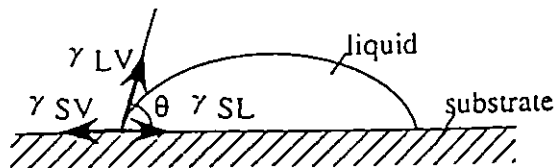


Fig 2.11 Force balance of a liquid on substrate.

From the Young-Dupre equation, it is clear that wetting, i.e. a small contact angle θ is promoted by small value of γ_{LV} and γ_{SL} in combination with a relatively large value of γ_{SV} ^{87,88}. This means that an oxide covered substrate will not wet because the surface tensions of oxide (γ_{SV}) are distinctly lower than the corresponding unoxidised metals¹⁰⁰. The total surface energy of the system is expected to be reduced when flux is applied to remove the oxide on the substrate, causing an increase of the surface tension γ_{SV} ^{87,88}, hence promoting wetting. However this effect is arguable, experiments by Tabelev et al¹⁰¹ show that oxidized solder gives a larger wetting speed than unoxidised solder. In any case, the influence of γ_{SV} in general dominates that of γ_{LV} , because its magnitude is much larger⁸⁸, hence it is recommended that in soldering practice complete oxide removal must always be the goal.

Shimokawa et al (1995)⁹³ argued that the Young-Dupre equation is difficult to apply to such complicated forms such as solder bridges, since the method is based on local balance at the edge of a wetted part. As a result, a new energy-based method for analyzing the wetting behaviour is proposed^{93,102}. This method is used to estimate the effects of physical properties on wetting behaviour by studying the spreading of solder balls. The new method defines the wetting tension and surface tension thermodynamically as follows⁹³:

The wetting tension is the amount of energy required for the liquid to wet a unit area of the solid. The surface tension is the amount of energy required for the liquid

to form the unit area.

From these definitions, the total energy can be expressed as follows¹⁰²:

$$E = \nu S_\nu + \mu S_\mu + \rho g M_s$$

E : total energy

S_ν : surface area of the liquid

S_μ : contact area of the liquid and solid

ν : surface tension

μ : wetting tension

$\rho g M_s$: potential energy of the liquid

ρ : density of the liquid

g : gravitational acceleration

The above equation is considered in the stable form, as the total energy E of liquid is minimum, and applied to the spreading of solder balls as follows:

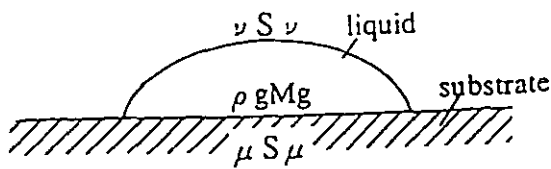


Fig 2.12 Energy of liquid on substrate⁹³.

The spreading form of solder is approximated as an ellipse. Find the wetting tension μ of the liquid become parameters determining the total energy E . Likewise, in

calculating surface tension γ , the equation is obtained from the sessile drop method and the liquid form of solder is approximated as an ellipse. Adding the condition that the stable form has minimum E and that the liquid volume is constant, the surface tension can be obtained. In this report⁹³, the effects of physical properties on wetting behaviour are examined. It is found that the physical property which influences the wetting behaviour the most is the ratio of wetting tension to surface tension, and this ratio is suitable as a parameter for analyzing soldering defects such as solder bridges⁹³.

Wassink (1984)⁸⁸ and Lea (1988)⁸⁷ discussed the profiles of some surfaces relevant for soldering. The contour of the liquid meniscus shapes are defined by the Young-Laplace equation plus gravity in the form of hydrostatic pressure

$\Delta P = \rho g \Delta z$, where Δz is a difference in height between two points in the liquid.

Both height and curvature shape are related, this contour is stable if it represents a situation of minimum energy with regard to small changes of the profile at a constant volume. For the situation of two-dimensions, a mathematical representation of the profile of the meniscus was given by Rayleigh (1892)¹⁰³ and the curve is known as the 'elastica'. This curve is shown for liquid solder in fig 2.13. The curve can be described as a function of the angle ϕ , and x and y coordinates can be determined from the function. ϕ is the angle between the curve and the x -axis.

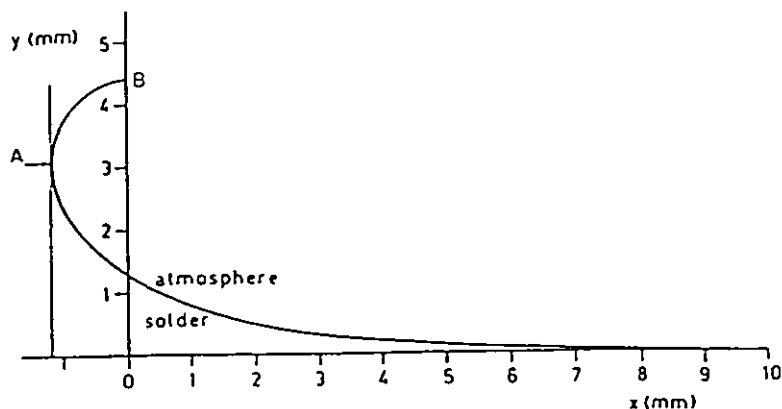


Fig 2.13 The 'elastica' curve for liquid solder⁸⁸.

The x and y coordinate are defined as follows⁸⁸:

$$x = \sqrt{\frac{\gamma}{\rho g}} \left(\ln Co \tan \frac{\phi}{4} - 2 \cos \frac{\phi}{2} \right)$$

$$y = \sqrt{\frac{\gamma}{\rho g}} 2 \sin \frac{\phi}{2}$$

The parameter representation of the curve $\sqrt{\frac{\gamma}{\rho g}}$ is a combination of surface tension γ (liquid solder $\cong 0.4 J / m^2$), and density $\rho \cong 8 g / cm^3$ using SnPb (60:40) solder with flux. Also, the acceleration due to gravity, g , is $9.81 m.s^{-2}$, so that the

parameter $\sqrt{\frac{\gamma}{\rho g}} = 2.25 mm$. The angle ϕ between the elastica and the x-axis ranges

from 0 to 180 degrees as shown in fig 2.13.

$\phi=0$ degree at $x = \infty$ and $y=0$

$\phi=90$ degree for $x=-1.2mm$ and $y=3.1mm$ in point A, to

$\phi=180$ degree for $x=0$ and $y=4.4 mm$ in point B.

Lee et al (1995)¹⁰⁴, present a mathematical model bridge between the leads of a quad flat pack (QFP) based on a thermodynamics view point, in order to find out the analytical properties of bridge configuration between leads. The physical

properties of the bridge can be approximated with a bridge that is constructed by the Laplace formula, and therefore describe the potential of occurrence of bridge accurately as follows. Using thermodynamic theory, the total energy concerned with the configuration of fluid is considered. The total energy of a configuration of fluid

$$\text{is: } E = \nu S_f + \mu S_w + g\rho M,$$

ν : surface tension

S_f : area of free surface

μ : adhesion tension

S_w : area of surface in contact with solid

ρ : density of fluid

g : gravitation constant

It is assumed that the configuration of a bridge is approximated by a solid rotation, in which the rotating curve is given as $r+ax^2$ as shown in fig.2.14.

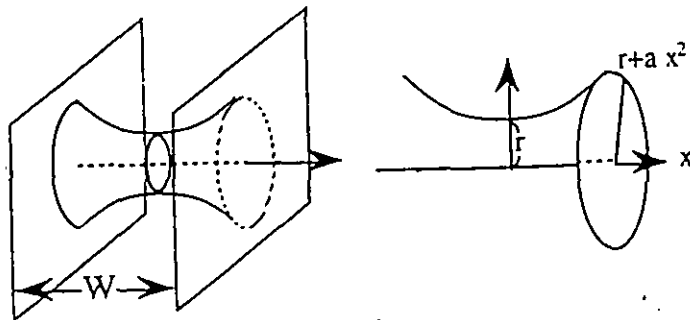


Fig.2.14 The configuration of bridge between two parallel walls, w : distance of walls¹⁰⁴.

By using the above equation, an energy function for the bridge $E(r, a, w, v, u)$ is constructed and by solving the Laplace formula, the local minimal and maximal points of energy with respect to r can be calculated. In this research, the minimal value for bridge (MVB) between two walls was deduced and a saddle point on the energy surfaces of system modelling the soldering of a QFP is found. From this, the mechanism of bridging can be seen and the significant factors on bridge creation identified as follows:

1. good wettability of solder decreases the probability of bridges occurring.
2. for a particular pitch of QFP, there is the optimal width of lead
3. the effect of a gap between lead and pad can be very serious.

2.8 Evolver and computational models of solder defects and wetting of surfaces.

Brakke (1992)¹⁰⁵ Presents a numerical computational program to perform energy minimization calculations. It is called Surface Evolver. Evolver is an interactive program written for the purpose of studying surface tension defined shapes.

Evolver can handle arbitrary topology and a wide range of constraints. This makes it particularly well suited to modeling the complex meniscus problems that arise in circuit board attachment^{106,107,108}.

Evolver (Racz & Szekely, 1993), operates by using a gradient descent on a space of admissible surfaces to try to find the local minimum energy on the surfaces. For the gull-wing lead, the geometry most commonly found in QFP devices, classical techniques as described in Section 2.5 are inadequate¹⁰⁶. As Evolver and its

algorithm have also proven useful tools in tackling more exotic geometries as presented in Whalley's et al model^{107,108}.

Whalley (1996)¹⁰⁷ used Surface Evolver to explain SMT open circuit joints associated with adjacent solder bridges. This computational model helps to understand the formation and stability of solder bridges and how these bridges may also result in adjacent lean (insufficient solder) or open circuit joints, successful simulation of the process of short formation and of short stability should allow the design of assemblies that are less prone to short circuits. However, Whalley (1996)¹⁰⁷ asserted this may be at the expense of a greater susceptibility to, for example, open circuit defects. It is therefore difficult to design a product/process to be fully robust against all types of process defect and therefore the use of simulation tools to help identify the most effective compromise may provide significant cost savings over traditional experimental approaches to product/process optimization.

Singler et al (1996)¹⁵⁴ also examined the solder bridging phenomena using Evolver. This tool revealed that, gravity exerts a very small effect on the interfacial shape, which is consequently dominated by surface energy effects. For a given pitch, the rectangular pad geometry allows the maximum solder volume deposition over the pad geometries e.g. circular or square pads, such that, should a bridge inadvertently form between adjacent pad, it would be ultimately unstable and incapable of existing in the steady state. It was also found that bridge stability exhibited sensitivity to contact angle, bridges being less stable for larger contact angles. Low

sensitivity of stability on surface tension and density was established. Finally, the instability of bridges was shown to be connected with the phenomenon of bifurcation. This phenomena is concerned with the configuration of fluid, in this case, solder bridge is approximated by a solid of rotation, which the rotating curve is given as $r + \alpha x^2$ ¹⁰⁴. And there is a branch point to decide whether bridge occurs or not. The low sensitivity of bridge stability has indicated the need to understand the respective wetting forces of Young-Laplace equation, so as to explain the bifurcation behaviour between two parallel walls.

This work, was in parallel to the author's observations described in Chapter Three. Whalley et al (1995)¹⁰⁸, identified that model in Surface Evolver that simulate the formation of solder joint geometry could feed directly into finite element models of solder joint thermal fatigue and reliability, reliability issues are discussed in 110, 111, 112, and 113. Evolver has also been used to predict solder joint shapes for conventional SMT components¹⁰⁹, such as chip capacitors and gull-wing packages. Possible applications of these geometric models are as part of the study of sensitivity of fatigue life to design rules and process technology, or in the estimation of solder joint reliability for new package styles.

Whalley & Conway (1996)¹⁵³ presents a study on simulation and interpretation on wetting balance tests using the computational modelling tool Surface Evolver. This paper presents the results from an evaluation of conventional and globule wetting balance tests using both computational modelling and experimental techniques. The results from the experimental tests showed that reasonable consistency in the measured force can be obtained, but that the wetting angle to this force is

insensitive to the globule block test. Instead, a computational model Evolver is used to simulate the behaviour of molten solder in wetting balance tests. The results also confirmed that the use of a solder surface tension figure appropriate to the solder atmosphere/flux conditions is vital to accurate modelling of solder wetting forces and it has been observed that the solder rise in these tests cannot be fully explained by a static surface tension model.

The work has confirmed that Evolver is an effective tool for examining the surface tension influenced behaviour of molten solder. However, in predicting the distances of solder flow over wettable surfaces require understanding of the effects of the microscopic surface geometry and explanation of Marangoni convection caused by temperature gradients in the fluid. Further work is required to establish the relative magnitude of these effects on the solder wetting behaviour.

Moon et al (1996)¹⁵⁵ investigated the dynamic aspects of wetting balance tests by studying the relationships between the force measured during wetting balance tests and the observed changes of contact angle and meniscus shape. The meniscus shapes are computed using the elastica solution (Wassink, 1984)⁸⁸ for wide plates and Surface Evolver for narrow plates. The study highlighted through the wetting balance measures wetting force, the time dependent contact angle and height rise are the important quantities. This is because the final contact angles must be small enough to permit sufficient solder spread over the substrate pad or lead to produce the desired joint geometry. The rate of change of the contact angle must be sufficiently fast to respond to wave soldering travel rates or to solder paste reflow rate. In this chapter, the consistency of the wetting force with both the contact

angle and meniscus height was closely examined. The theoretical framework for the static effect of a plate on the meniscus shape can be described analytically by the 'elastica' curve (Wassink, 1984)⁸⁸. For the dynamical effects, the force versus time curves from wetting balance tests after reaching the zero balance point can be expressed by the relationship.

$$\frac{F_{\max} - F}{F_{\max}} = \exp\left(\frac{-t}{t_0}\right)$$

Where F_{\max} is the maximum force and t_0 is a characteristic time. However, in the field of fluid mechanics (Ehrhard & Davis, 1991)⁸⁶ assume that the contact angle varies with contact line speed, V as $V=K(\theta - \theta_e)^n$, where K is an empirical constant, and θ and θ_e are the instantaneous and equilibrium macroscopic contact angle.

Other theoretical work⁹¹ includes the Marangoni effect on spreading i.e. when a temperature variation exists along a free surface of a fluid, the resulting variation in surface energy induces a flow towards the direction of the high surface energy. This flow can alter the dynamics of spreading the final shapes achieved.

The report concluded that the rise of the meniscus as well as the downward force exerted on the plate, when the meniscus is stationary for the non-isothermal tests using silicone oil may be due to the Marangoni flow generated by the surface energy gradient associated with temperature gradients the fluid near the contact point. For solder, the discrepancies between the measured and theoretical meniscus shape are too large to be explained by the thermally induced Marangoni flow. Other

factors such as oxidation of the liquid solder and flux effects are possible sources of the discrepancy that require further investigation.

2.9 Open And Effect of Lead Coplanarity

Ugur and Adriance (1994)¹¹⁴ determined the assembly yield and quality of the ultra fine pitch mass reflow process with lead coplanarity error. Six major attributes of ultra fine pitch mass reflow assembly, solder paste, stencils, screen printer process parameter, printed circuit boards, component placement and solder paste reflow were studied.

A wide range of component lead coplanarity errors were used to determine acceptable limits based upon the developed assembly process. In this assembly yield experiment, "near optimum" attachment pad/stencil aperture geometries of various device types were evaluated with respect to two solder paste print processes (metal with single thickness stencil and rubber with 85 durometer hardness and step stencil) and two reflow processes (single and double sided). This evaluation procedure was carried out in the form of assembly yield analysis. Two defect types, solder shorts and open joints were considered.

Solder paste deposition volume and the coplanarity of the component leads were found directly and proportionally related to the formation of open solder joints. The amount of solder paste volume deposited in a given attachment pad, the center of this deposition on a given attachment pad, the center of this deposition with respect to the center of attachment pad and distance between the adjacent attachment pads

are believed to be the significant contributors to solder bridging or shorts in this investigation. Regression models were developed to estimate the contribution of each individual variable on the defects. Two separate models were used for each experiment and are referred to as the short model and open model in this paper.

The experiment shows high pre-measured lead coplanarity values do not always correspond to the high lead coplanarities after solder deposition, nor do they always cause the formation of a open solder joints. The most significant attribute that the results show is that insufficient solder deposition greatly increases the probability of the formation of an open joint.

Ugur and Adriance (1994)¹¹⁵ also carried out empirical work in yield improvement by studying the effect of how attachment pad length influences the assembly process for 0.5, 0.4 and 0.3 mm pitch mass reflow devices and to help optimum attachment pad lengths. The response variables for the experiment were assembly yield (shorts and open), solder paste deposit volume / height. The report concluded that open solder joints were the only type of defects produced during the investigation and longer attachment pads produced higher assembly yields, the higher yield produced from these pads is a function of the larger solder paste volume that is deposited. Poor correlation was found between open solder joints and maximum lead coplanarity errors, some of the open joints were not caused by excessive lead coplanarity errors and suggested that such faults may be linked to solderability related problems.

Lastly, the report concluded there is no significant difference in the size of solder joint at the foot of the lead when comparing short, medium and long attachment pads. The larger amounts of solder that were applied on the medium and longer attachments pads, wicked to the lead, instead of remaining at the lead foot.

2.10 The impact of screen printing on reflow defects.

Mannan et al (1994)¹²¹ presented two papers on the computer simulation of solder paste flow (part 1 and 2). Part 1, examines skipping the main defect in solder paste printing and part 2, studying the behaviour of solder paste while withdrawing from a stencil aperture (see fig.2.15). These researches provide insights to the defect origins from the screen printing process.

Particles inside the aperture play a crucial role in the formation of the skipping fault.

This is because of the jamming of the particles across the width of the aperture.

These individual particles are forced into a mono-layer which increases the extent of this clumping inside the aperture. Further if the stress on the solder paste becomes greater than its tensile strength skipping will occur.

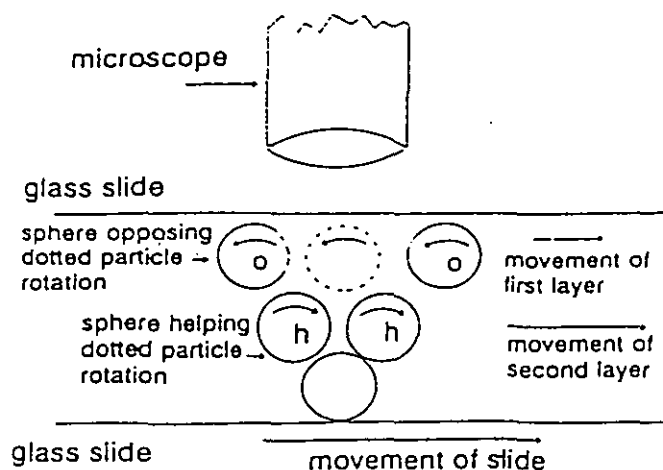


Fig. 2.15 Illustration of experimental setup of optical paste observation. Spheres whose rotation opposes the rotation of the dotted sphere are labeled with an O and sphere which help the rotation are labeled with a h. Mannan et al (1994)¹²¹.

Part 2 of this research focuses on the flow out of the stencil aperture. The aperture width, height, angle of wall inclination, particle size and concentration of the suspension are varied to examine the effect of flow patterns. Firstly, the withdrawal of paste from a stencil aperture is studied. In the simulation model, as the paste is pulled out of the aperture (see fig 2.16) by the contact with the PCB due to paste thickness on the board (both the walls and PCB are assumed perfectly smooth and flat), the average drag force on a particle was observed to be increased as this particle gets closer to the walls and eventually leaves the aperture, this phenomenon continues until a sudden drop in the total drag force and hence the tensile stress. For the practical applications of this model, electropolishing of the aperture wall must be pre-specified in order to make the surface smooth to make the analysis valid. It is clear that electro-polishing does assist paste release by smoothing the inner aperture walls¹²³.

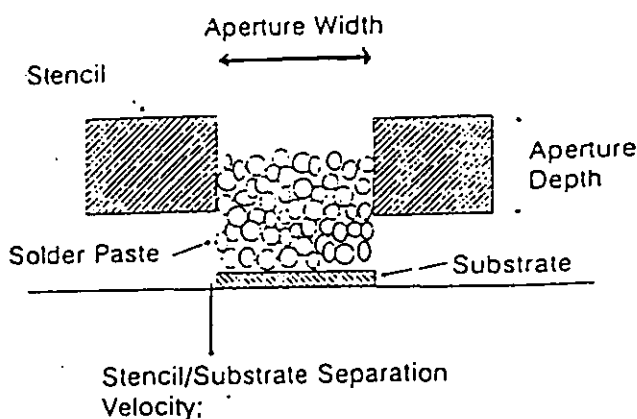


Fig.2.16 Sketch of solder paste flow out from a stencil aperture.

Warwick & Hedges (1994)¹²⁴ suggested that to minimize the skipping problem in fine-pitch printing smaller solder particles should be used, as this allows easier paste flow. Solder particles should not be so large that they cause a restricted flow into the stencil openings because this might promote segregation of the paste, which would cause inconsistent metal deposition and skipping as observed by Mannan¹²¹ and his colleagues. It is generally felt that powder particles in the range of 25 to 38 micrometers can be used for printing lead pitches down to 20 to 16 mil (0.020 to 0.016 inch) devices.

Nevertheless, Mannan et al (1994)¹²¹ pointed out that with smooth walls and smooth spherical particles, a larger particle size distribution would not automatically cause more skipping if the tensile strength of the paste can be kept reducing as the stress on the paste reduces.

The smoothing effect of electropolishing to the inner aperture walls and the stencil must be understood¹²¹. For example, if the stencil surface exhibits the same degree of smoothness as the aperture walls, what effect does this have? It is very likely that the solder paste will skip rather than roll during the printing operation, which is not desirable, since the stress will be equal or greater than the tensile strength of solder paste, skipping will occur. A comparison of stress and wall inclination of different angles e.g. 0, 5, 10 degrees was examined in this paper¹²¹. It concluded that, the effect of wall inclination has significant effect in reducing the skipping effect. However, the effect of the stencil thickness is equal influential, the stress decreases as the depth gets smaller. The recommendation for a QFP trapezoidal

aperture stencil is taper mil / side 0.5 to 0.7 and stencil thickness 2 to 7 mils (0.002 to 0.007 inch) depending on the pitch size¹²³. There is no clear evidence in this research that reduction in the shear rate of solder paste during printing will produce a reduction in bridging.

2.11 Bar Printing, Reflow and Bridging Defects.

It is important to recognize screen printing and reflow contribute together to process faults. There is little work that takes this view. Singler & Curran(1994)¹²⁵, however present an experimental investigation of solder bridging, observed primarily in the context of the bar printing process. The work explores the effects of solder alloy type, component pitch, metallization coating, substrate surface properties, stencil parameters and process atmosphere on bridging incidence.

In the course of this investigation, two phenomena were observed to influence bridging at least as significantly as many of the above parameters. The phenomena are: (1) Thermally-driven Marangoni motion and (2) Segregation of the liquid alloy from the flux vehicle liquid with extensive wetting of the flux over the substrate material.

The bar print process is a soldering technique that employs a simple stenciling procedure in which solder is deposited in the form of a continuous bar of paste spanning an entire row of pads on a printed circuit board. After the board is

populated with SMT components, it is subjected to a reflow cycle during which the

solder paste undergoes a phase transformation resulting in a liquid metal bridge instantaneously spanning the entire row of pads. It is expected the bridges between adjacent pad break. Since bridge breaking occurs with the solder in its molten state, the dynamics of this phenomenon are determined by the laws of fluid physics and the discussions presented are developed from this view point.

The driving force behind these motions is thought to be a thermal Marangoni effect deriving from non-uniform heating of the substrate. The existence of a Marangoni-driven flow can have both positive and negative consequences in the bar print process. A weak Marangoni motion is able to facilitate bridge breaking by serving as an added perturbation to the bridge surface. Strong Marangoni motions, however, can transport significant amounts of liquid along a pad row, often resulting in inadequate amount of solder on pads. This phenomena is further discussed in this thesis (chapter 5).

2.12 Summary

Following a review of the field of surface mount assembly, this chapter gave an overview of the origins of defects observed after solder reflow. In particular we have identified some problems and limitations of the traditional reflow soldering methodology, including IC package lead geometry design, stencil aperture and screen printing process design, the lead coplanarity problem and issues associated with the characterization of flux activity. The review of the trends in SMT and advanced packaging confirms that lead spacings and joint geometries grow

increasingly smaller to support demands for ever higher densities in modern microelectronics circuitry. Radical measures are needed to achieve consistent defect free assembly.

In spite of the mathematical and computational modelling available today there are limitations to our ability to apply these techniques to the real problems as encountered in complex systems in mass production environments. To address these problems, it is valuable to conduct empirical work on the critical processes within the SMT assembly.

The author therefore conducted such empirical research on screen printing, reflow soldering, joint lead geometry design and optimization, and wetting phenomena within fluxes and solder pastes. This work particularly recognizes that each of the processes cannot be considered in isolation. The next chapter of this thesis concentrate on the discussion and presentation of a survey on the performance of Singapore based SMT plants to determine a ranking of defects of these plants. In the balance of the thesis statistical experimental techniques such as design of experiment (DOE) and response surface method (RSM) and non-parametric tests are applied to explore defects. Also innovative solder joint design and formation processes are generated to determine process conditions that avoid defects.

Chapter Three

The Origin and Prevention of Post Reflow Defects in Surface Mount Assembly

3.1.1 Introduction

As has been indicated in the review and in the 1970s technology for digital devices consisted of through-hole DIP(dual in-line package) components containing SSI (small scale integration) and MSI (medium scale integration) circuitry. Typically, the electrical gate count for these ranged from ten to several hundred gates contained in 14 to 24-pin packages.

In the 1980s surface mount technology (SMT) was rapidly accepted by the entire industry¹. The emergence of surface mount and pin-grid-array (PGA) technology introduced LSI (large scale integration) and VLSI (very large scale integration), components contain nearly 100000 gates in a single device with pin counts of several hundred, and with connection pitch size ranging from 20 mil down to 8 mil. Today, ball-grid-array (BGA) technology seems to be the next promising technology to help achieve the assembly of devices with gate counts that approach or exceed one million per device, with package pin-counts approaching 1000².

The explosion of SMT and high-density packages resulted in more complex and higher density board designs in order to incorporate more features into products while reducing overall package size. This has in turn, created major challenges for the surface mount manufacturing process, particularly in solder paste screen printing,

component placement, reflow soldering and product testing. An understanding of the origin of post reflow defects in surface mount assembly has become the core issue in meeting this challenge.

3.12 Classification of process defects after reflow

For the reflow process, the quality requirements for solder joints are usually³:

- No bridges or floating leads when the solder melts
- Sufficient solder
- Good solder wetting
- No solder balls
- Sufficient bond strength
- No flux residues (in case of flux with halide-content and other corrosive substances)

Soldering defects that tend to occur with the fine pitch packages, for example Quad Flat Packs, include bridges, voids and fillet defects, and for chip components (e.g. 1206, 0805, SOT and D-case packages), missing components and tombstones are quite common. The causes of these defects and the results of investigations carried out to avoid them are discussed in the following sections.

As has been shown in the review, there has been considerable work within the research community on these processes however, there has been little working reporting industrial experience of the relative occurrence of faults and their origin. The contribution of this chapter therefore has a number of elements. It begins with a short summary of process faults occurring in a number of Singaporean plants and then

addresses some of these faults particularly optimisation of screen printing and correction of misalignment. Other faults are addressed in the balance of the thesis.

3.2 A Survey on the Performance of Singapore-based SMT Plants

A survey was carried out to understand the common solder defects seen in the Singapore SMT industry before rework. A total of three SMT plants were surveyed, and in this benchmarking exercise all plants involved manufactured the same product for the original equipment manufacturer (OEM) where the author is employed.

This product is a single-sided board, populated with 800 SMT components ranging from 0805 chip components to QFP 160-pin, 25 mil pitch ICs. In addition, there are some through-hole connectors, audio jacks and headers which require hand-stuffing and wave soldering.

Of the factories involved in this survey, two are located in Batam, Indonesia and they are Singapore-based companies, B-1 and B-2, respectively. One is located in Singapore and is an American based company, namely S-1. These companies are subcontractors for printed circuit board assembly (PCBA) for major OEM and Multinational Corporations (MNCs). The equipment used by these factories varies and includes primarily Japanese made pick and place machines (e.g. Fuji, Panasert, Citizen), and Japanese and U.S made screen printers (e.g. MPM & Fuji, all printers are not equipped with any closed loop feedback system). Ovens are primarily U.S and Japan made forced air convection IR-Reflow, e.g. Vitronics, Universal, Electrovert and Fuji.

In summary, missing solder/component and solder bridges are the top two defects faced by all these plants, despite the difference in machine suppliers. Misalignment and insufficient solder ranked 3rd and 4th respectively, followed by component overturn which is unique to plant S-1. The following sections explore the origins of the key defects, e.g. insufficient solders, bridges, no solder (open) and missing components, etc. The following is a summary and the ranking of the most significant defects detected at the post-IR reflow process, for a period of three weeks.

Plants/Wk	Solder Bridge			Missing Solder/Component			Insufficient Solder			Tombstone			Misalignment			Component Overturn		
	1	2	3	1	2	3	1	2	3	1	2	3	1	2	3	1	2	3
B-1	1	2	1	3	3	2	2	1	3									
B-2			3	1	2	1	2			3			3	1	2			
S-1	1	1				1					2		3	3		2	2	3
Score	54			58			32			14			36			22		
Overall Rank	2			1			4			6			3			5		

Weekly rank	Score
1st	10
2nd	8
3rd	6

It should be noted that it is difficult for operators to detect the insufficient solder fault (see page 94). This table does not therefore show the correlation shown in section 4.3

3.3 Defect Origin of Insufficient Solder, Bridges, and No Solder(Opens), Missing Component and Misalignment.

The following investigations were carried out in order to ascertain the defect origin of the top three defects listed above. A batch of customer return boards(40 pieces) was used in the failure analysis to ascertain the process performance.

3.3.1 Observations

A careful examination of the returned boards sought to explain the origins of insufficient solder and solder bridges. It was observed that the volume of the solder

forming the bridge is typically drawn from the adjacent leads or its own lead (see fig. 3.1) and as a result solder bridges and insufficient solder faults occur concurrently. Figure 3.1 shows six soldered leads from a surface mounted component assembly. A bridge is present across the pair of leads at the left of the figure. Good solder fillets and well wetted pads can be seen on each of the three joints at the right of the figure. The fillet and pads of the leads with the bridge shows insufficient solder at their toe as does the lead adjacent to these two. This, and other observations, suggests that the solder in the bridge is drawn from the other areas of the joints and adjacent joints. It is always easy for the production operators to spot a solder bridge via visual inspection but is frequently forgotten that the lead has insufficient solder at the point of contact on solder pad. Hence, if the origins of solder bridge fault can be removed, some of the faults due to the insufficient solder will be resolved too. This observation also forces us to reconsider our investigation paradigm as two of the faults are related. This identifies the need to do more work on the correlation between insufficient solder and bridges as presented later in chapter four.

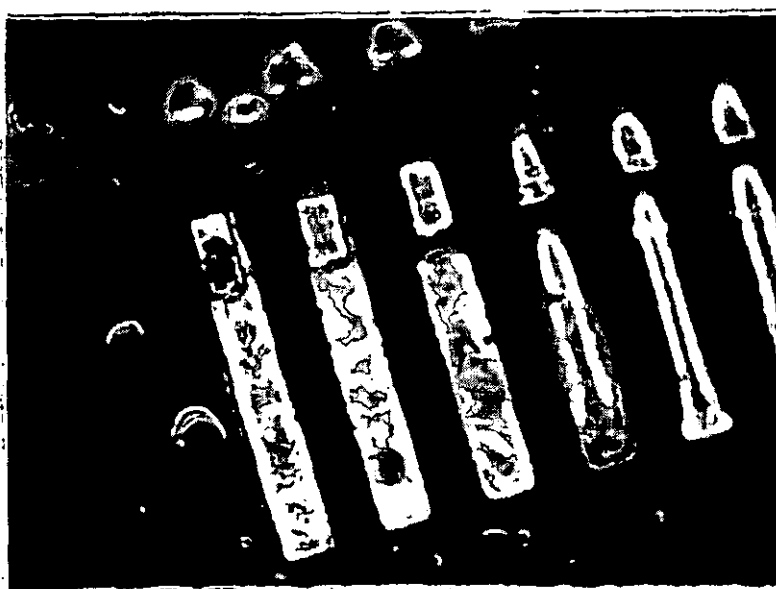


Fig.3.1 Result of solder bridge and insufficient solder.

3.3.2 Screen Printing Studies

Post reflow defects related to either insufficient or excess solder (i.e. bridges) are clearly related to the volume of solder paste applied by screen printing. The machines parameter requires to establish a consistent low ppm printing process were therefore explored on a MPM Corporation printer. Parameters that affect the process must be optimized in order to make the process robust against all noise (e.g. human factors, humidity and room temperature etc.), inner noise (deterioration) and process noise (manufacturing imperfections).¹²⁶

The critical parameters for screen printing can be identified as Down-stop, Speed, Snapoff Distance and Squeegee types, as defined below. The response variable to be investigated were solder paste height and solder bridge (solder short). The values of variables are used in fig.3.2 shown below.

Response Surface Methods¹²⁷, a set of techniques designed to find the “best” value of the response, are used here to quantify the relationship between the values of paste height and those of a set of experimental factors, i.e. Speed, Snap-off Distance and Downstop, the values of variables used are in fig 3.3. Squeegee types were removed from this experiment as metal squeegees were found to give good definition of solder paste during the print cycle.

No	Name	Low	High	Units
A	Speed	0.8	2.4	inch/sec
B	Downstop	0.2	0.6	inch
C	Snapoff	0	0.03	inch
D	Squeegee	Rubber	Metal	types

Response Variables

No	Name	Units
1	Height	0.001 inch
2	Bridges	ppm

(SI: 2.54 cm = 1 inch)

Fig. 3.2 Design of Experiments setting.

RSM Setting

Experiment Factors

No	Name	Low	High	Units
A	Speed	0.8	2.3	inch/sec
B	Downstop	0.020	0.12	inch
C	Snapoff	0.004	0.03	inch

Response Variables

No	Name	Units
1	Height	0.001 inch

(SI: 2.54 cm = 1 inch)

Fig. 3.3 Response Surface Method setting

Definitions

- **Speed---** This is the squeegee/or print speed, the rate at which the squeegee blade moves across the stencil during the print cycle. Typical speeds range between 0.4 to 0.6 inch per second.¹²⁸
- **Snap-off---** The height that the stencil is set above the board for "off contact" printing, also commonly known as snap-off distance. This is to determine the amount of deflection that occurs during the snap-back action of the stencil. Snap-off distance is typically in the range of 0.003 to 0.005 inch¹²⁸ (on contact printing would have a zero snap-off distance).

- Squeegee--- A rubber or metal blade that wipes across the stencil to force the solder paste through the stencil apertures and on to the printed circuit board (PCB).
- Downstop--- This is the squeegee Downstop, i.e. the travel in the Z-axis of the squeegee to the stencil, which has direct influence over the pressure exerted on the stencil during the print cycle.

3.3.2.1 Results

The objectives of the experiments were two-fold:

- To determine the paste height solder bridge, dispersion effect of the process parameters identified above and their relative significance, and
- To identify the appropriate settings of significant parameters, to search for the optimal conditions and obtain the nominal paste height.

Traditional factorial designs were employed in the experiments, as first developed by Fisher and Yates in the 1920s, in this case a 2 x 4 full factorial of sixteen runs were used to investigate all the four main effects of four two-level factors and eleven possible interactions.

3.3.2.1.1 Design of Experiment (DOE)

FIRST RESPONSE: Paste Height

Table 3.1 ANOVA table of solder paste height experiment.

Effect	Sum of Squares	DF	Mean Sq.	F-Ratio
A SPEED	75180.89	1	75180.9	0.81
B DOWNSTOP	86022.46	1	86022.5	0.92
C SNAPOFF	124325.01	1	124325.0	1.33
D SQUEEGEE	1505578.49	1	1505578.5	16.16
AB	138053.16	1	138053.2	1.48
AC	45557.95	1	45558.0	0.49
AD	1871.79	1	1871.8	0.02
BC	510510.23	1	510510.2	5.48
BD	113869.24	1	113869.2	1.22
CD	178421.47	1	178421.5	1.92
block	166677.91	1	166677.9	1.79
block	1805.03	1	1805.0	0.02
Total error	3260890.56	35	93168.3	
Total (corr.)	6241798.12	47		

R-square = 0.477572 R-square (adj. for d.f.) = 0.298454

Statistical analysis software (STATGRAPHICS) was used in computation of all the effects. The analysis of variance (ANOVA) shown in Table 3.1, revealed the main effect "squeegee types" yields a significant effect on paste height (F-ratio is 16.16, t-statistic 2.08 at 95 percent confidence level).

The Pareto chart (shown as Fig.3.4) and the analysis of the main effects for paste height in Fig.3.5 confirmed that the squeegee is most significant. The interaction effect between downstop and snapoff (BC), shown in Fig.3.6, was also found to be statistically significant (F-ratio is 5.48, t-statistic 2.08 at 95 percent confidence level).

When the downstop is set at the low-level, the snap-off distance is recommended to be set at the low-level as this yields a paste thickness closer to nominal value, i.e. 6 mil (0.006 inch). Similarly when the downstop is set to high-level, the snap-off distance must be set at high-level in order to obtain a desirable paste height. The normal

probability plot for residual of the data, shown in Fig.3.7, appeared to be satisfactory.

All the points of this residual plot lie close to the line, confirming the conjecture that

effects other than 2, 3, 6, 10, 12 and 15 are readily explained by random noise¹²⁹.

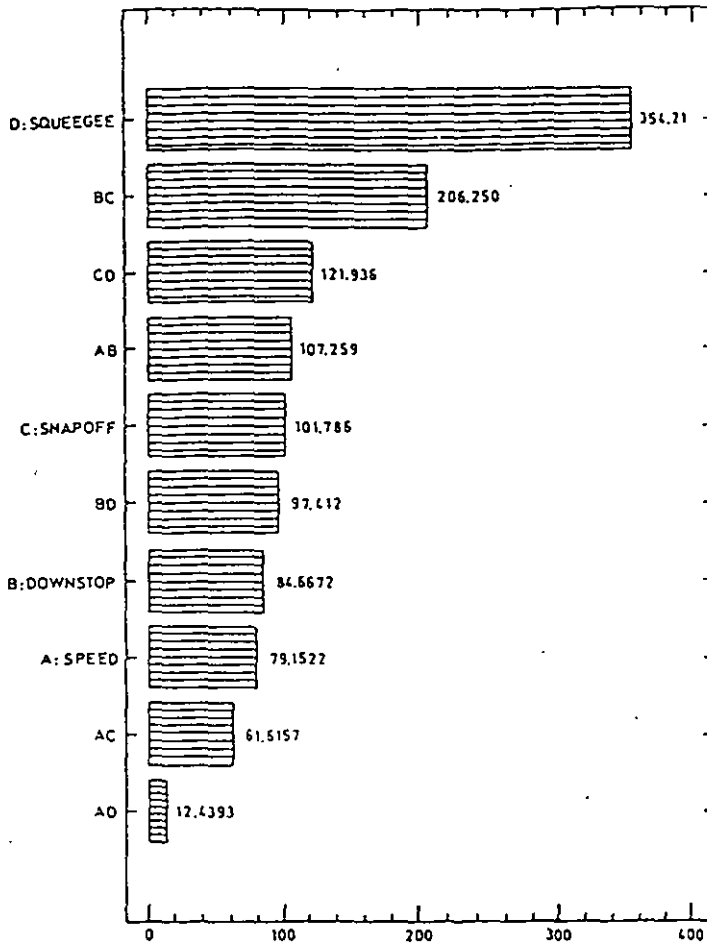


Fig.3.4 Pareto chart for paste height.

SECOND RESPONSE: Solder Bridge (Solder Short)

Table 3.2 ANOVA table for solder bridge experiment.

Effect	Sum of Squares	DF	Mean Sq.	F-Ratio
A SPEED	1367.1348	1	1367.1348	2.57
B DOWNSTOP	7.6457	1	7.6457	0.01
C SNAPOFF	30.0475	1	30.0475	0.06
D SQUEEGEE	6388.5761	1	6388.5761	12.01
AB	472.3404	1	472.3404	0.89
AC	84.2462	1	84.2462	0.16
AD	383.9280	1	383.9280	0.72
BC	1167.6172	1	1167.6172	2.20
BD	36.0860	1	36.0860	0.07
CD	1052.2998	1	1052.2998	1.98
block	153.7027	1	153.7027	0.29
block	55.2220	1	55.2228	0.10
Total error	18610.5039	35	531.7287	
Total (corr.)	29756.1533	47		

R-square = 0.374566 R-square (adj. for d.f.) = 0.160132

t-statistic = 2.10 at 95 percent confidence

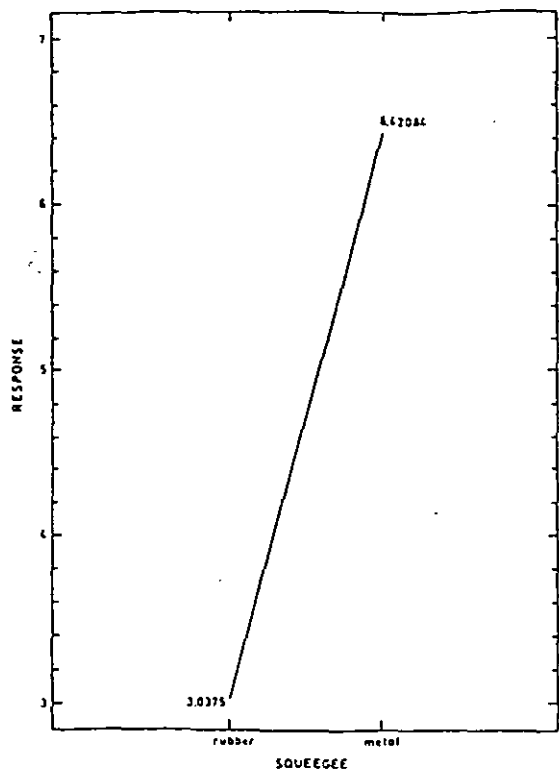


Fig.3.5 Main effect for paste height

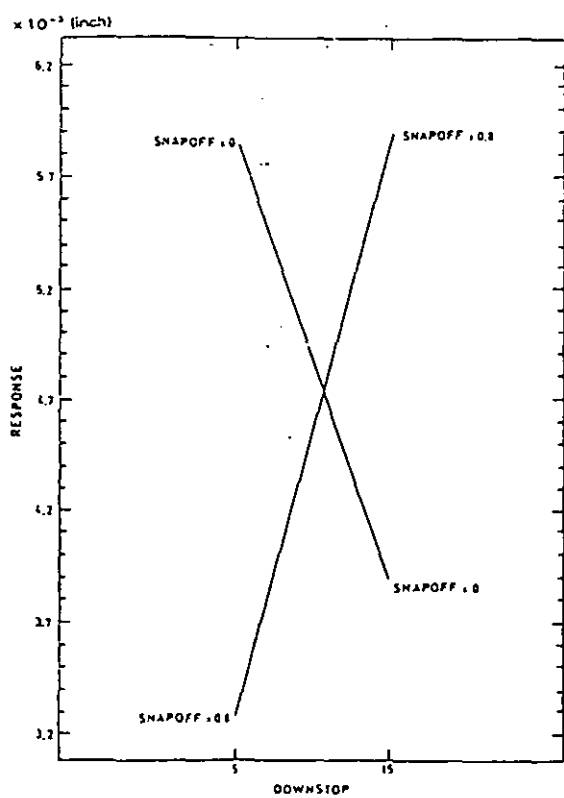


Fig.3.6 Interaction effect of downstop and snapoff (BC)

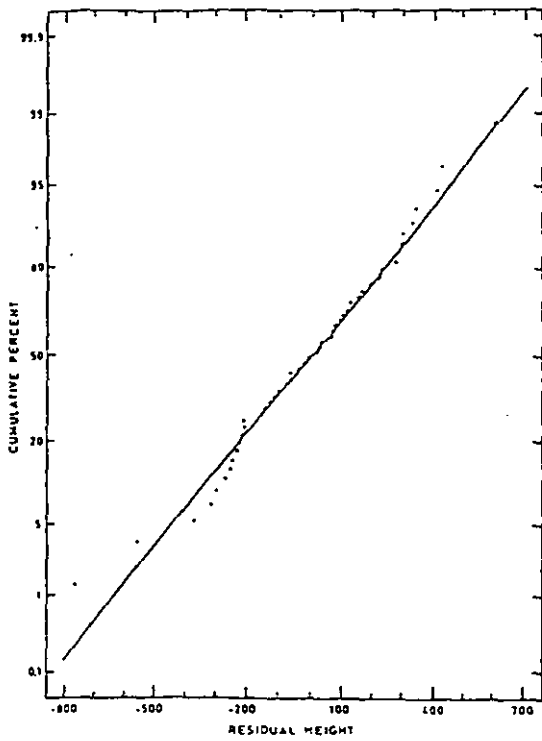


Fig.3.7 Normal probability plot for residual of paste height data.

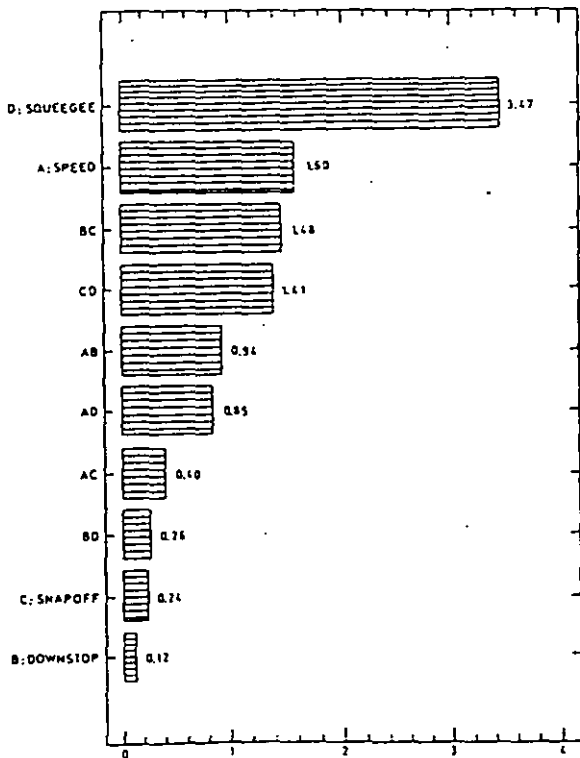


Fig.3.8 Pareto chart for solder bridge

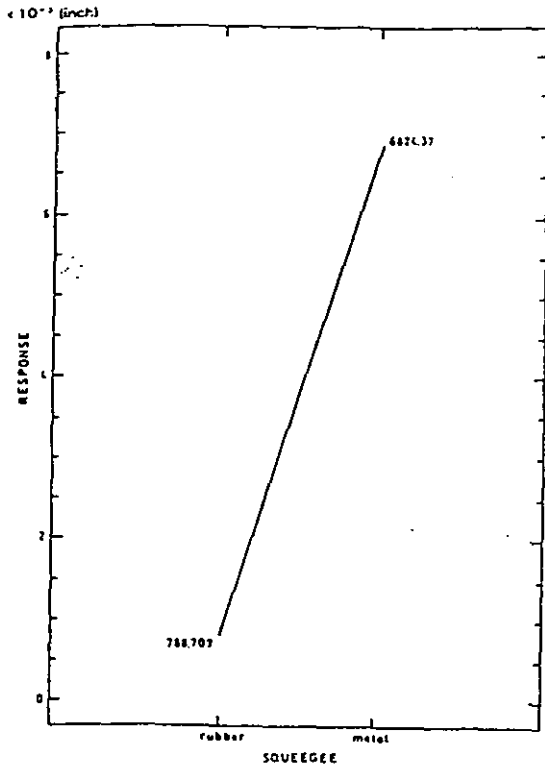


Fig.3.9 Plot of main effect D, squeegee types.

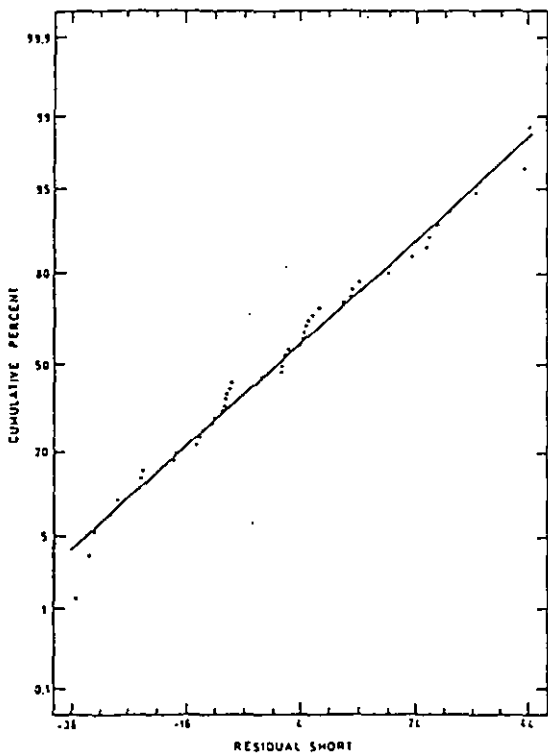


Fig.3.10 Normal probability plot for residual solder bridge data.

The analysis of variance(ANOVA) again confirmed that the main effect “squeegee types” significantly influences the solder bridge(solder short) (F-ratio is 12.01, t-statistic equal to 2.10 at 95 percent confidence). The Pareto chart in Fig. 3.8 outlines the significant defects affecting the solder bridge. “ Speed” was found to be marginally significant, as shown in the ANOVA table (table 3.2). The metal squeegee yielded a much higher paste height(well expected above the expected the nominal value of 6 mil thickness), and therefore a greater risk in producing a solder bridges due to excess solder volume, as revealed in fig.3.9. The normal probability plot for residual of solder bridge data in 3.10 appeared to be satisfactory.

3.3.2.1.2 Response surface method (RSM)

Response Variable: Search for optimal paste height operating condition. For effective SMT assembly the screen printing of solder paste requires tight process control, especially as pad geometries become finer. Here this thesis examines the practical application of experimental design to solder paste printing for SMT. The experimentation concentrates on the important printer and squeegee parameters and their effect on paste deposition with measured solder paste height. The method is described in full in the Appendices.

Recognizing that the type of squeegee blade, travel speed and the interaction effects of downstop and snap-off are the major factors affecting the solder paste thickness variability and solder bridge, a response surface approach was adopted to identify the “best” value within the process window, i.e. to search for the optimal operating condition in order to center the process at the process at the nominal value.

First, the ANOVA table for the search of optimal paste height (table 3.3) revealed that

none of the effects were statistically significant. This was as a result of fixing the type of squeegee used, as a result of earlier analysis. The focus of this experiment was on the search of the optimal condition in order to obtain the nominal paste height (i.e. 0.006 inch).

A response surface showing a relationship between response h (paste height) as a function of predictor e_1 (mechanical down stop) and e_2 (snapoff distance) is shown in Fig.3.11. Indeed, several response surface contours can be estimated further from the responses generated, as shown in fig.3.12. It was found that to center the printing process at the nominal value of 6 mil (0.006 inch) paste thickness, the recommended setting for the printer's downstop was from near zero to maximum of 0.012 inch (0.3mm). Similarly, the snap-off setting should only vary from near zero to a maximum of 0.024 inch (0.6mm) depending on downstop setting along the x-axis of Fig.3.12. The curve XXX on the contour plot of Fig.3.12 denotes optimum paste height setting for a six thousandth of an inch (0.006) stencil.

Table 3.3 ANOVA table for the search of optimal paste height experiment.

Effect	Sum of Squares	DF	Mean Sq.	F-Ratio
A SPEED	1.69962301	1	1.6996230	1.06
B DOWNSTOP	0.39015858	1	0.3901586	0.24
C SNAPOFF	0.25013366	1	0.5201337	0.33
AB	2.53125000	1	2.5312500	1.57
AC	0.91125000	1	0.9112500	0.57
BC	0.45125000	1	0.4512500	0.28
AA	0.01731225	1	0.0173122	0.01
BB	0.29653687	1	0.2965369	0.18
CC	0.63529050	1	0.6352905	0.39
block	1.35878957	1	1.3587896	0.84
Total error	8.04921111	5	1.6090422	
Total (corr.)	18.1375000	15		

R-square = 0.556212

R-square (adj. for d.f.) = 0

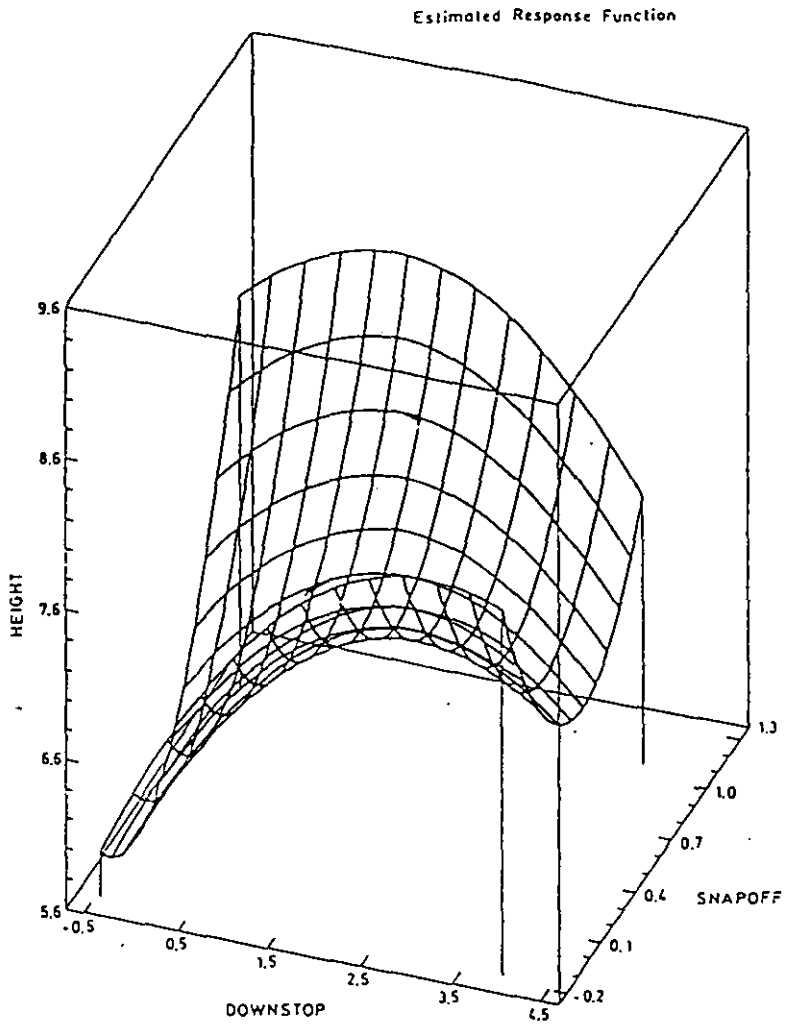


Fig 3.11 A theoretical response surface showing a relationship between response h (paste height) as function of e_1 (mechanical downstop) and e_2 (snap-off distance).

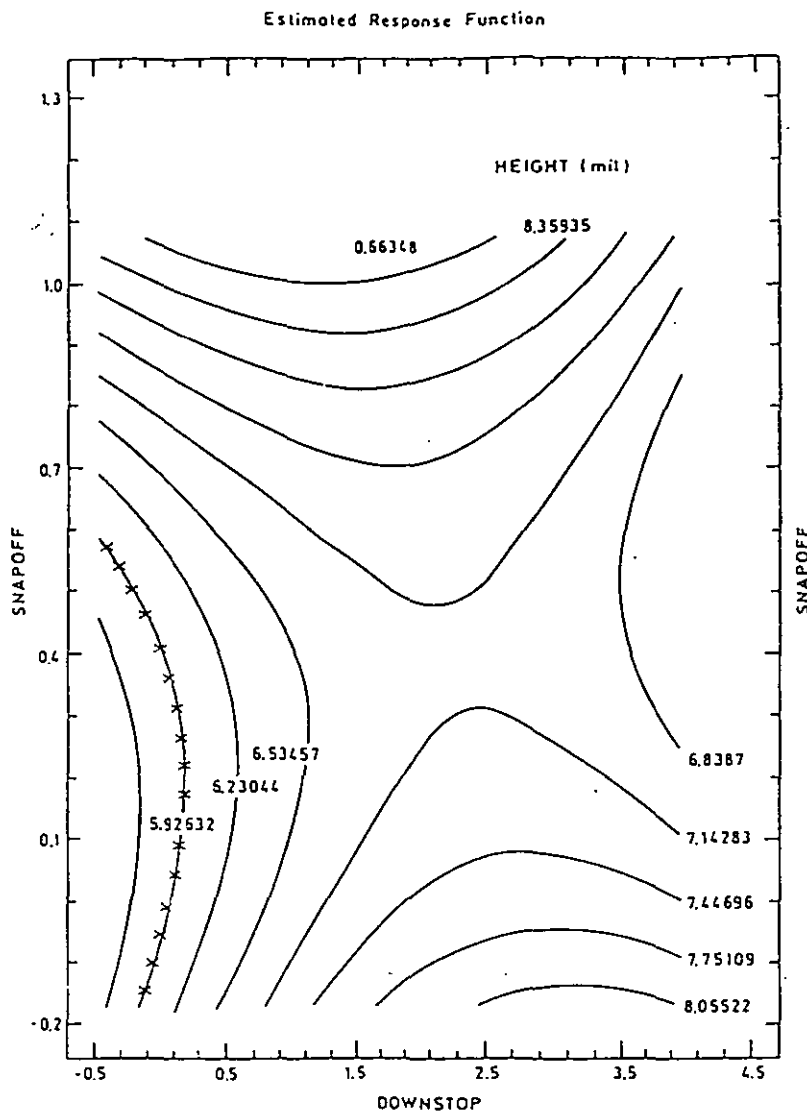


Fig 3.12 Paste height contour of above response surface, showing the relationship between response h (paste height) as function of e_1 (mechanical downstop) and e_2 (snap-off distance).

3.3.3. Missing Components

Missing components was found to be one of the top defects listed in the SMT plant survey. This problem appears to be acute for smaller chip components, e.g. 0.805, 0603 and 0403 case size. An experimental study was carried out in an attempt to establish the root-cause of this.

This experiment involved water-soluble solder paste with powder particle size Type 3 (80% between 20 and 45 micrometer in diameter as specified in IPC-S-819). This paste was selected due to its ease of printability, as finer particle size is easier to print through the small stencil openings required.

Water-soluble pastes typically consist of a solvent such as water or alcohol, and a carrier such as glycol that is water-soluble.¹³⁰ This carrier acts as a wetting agent in removing metal oxides, chemical residues, salts etc.

3.3.3.1 Observations

An experiment was designed to analyze the print results with respect to time and the effect of immediate placement delay on process faults, as follows:

Definitions

Printer-- Visual inspection for screen printing defects such as no decomposition of solder, solder short and stencil clog etc.

IR1 -- Defects shown by post IR-reflow inspection with a time delay between screen printing and component placement.

IR2 -- Defects shown by post IR-reflow inspection without a time delay between screen printing and component placement.

Table 3.4 shows that as the time duration printing and placement increases, the inspection result (IR1) revealed that the no solder problem increased dramatically.

“No solder” was found to be the major defect here, as the paste dried up and lost its tack, the relative adhesion between the paste and stencil interface, and the paste and PCB deteriorated. As a result, when the stencil lifts (or the PCB is withdrawn from the stencil) the paste, instead of being pulled out of the stencil, follows the stencil and the no solder defect will then occur.

Duration (minutes)	IR1 (ppm)	IR2 (ppm)	Printer
11	0		good
30	729		good
75	3644	1457	good
120	1457		good
138	2915		good

Table 3.4 Experimental result.

The solder paste used in this experiment was applied in experimental amounts of 148g, 200g, 325g, 450g and 500g. A solder paste loading of 148g(approx. 150g), in contrast of the standard of the 500g, was found to be the best. This not only avoided unnecessary wastage of solder paste, but also eliminated defects due to paste dry up and paste oxidation.

The experimental results show that the relative adhesion between the paste and stencil interface and the paste and PCB interface is crucial. This is a major weakness of water soluble paste due to its low tackiness(poor adhesion) and short tack-time. Thus determining the right amount of solder paste for the screen printer is critical to eliminate solder defects such as no solder.

3.3.4 Vibration alignment during IR solder reflow of Quad Flat Packs

Pick-and-place equipment manufacturers have made many significant improvements in their products over the years.¹³¹ Vision system and high precision motions controllers have been incorporated to ensure that every step of the machine operation is within the specification.

However, more recent products designs are combining high-lead-count Quad Flat Pack (QFP) devices and extremely small chip type components (0.04 inch X 0.02 inch) to optimize product performance and meet package requirements. In many instances, these two types of components are placed by different machines.

The resulting multi-machine environment, coupled with station-to-station material handling, increases the potential for position-related components defects, as revealed earlier in the chapter, where the misalignment problem ranked 3rd most common defect. Hence, in order to ensure proper X, Y, O positioning of these types of components, a mechanism can be incorporated in the reflow zone(last zone) of the oven, where the solder is fully molten. A vibration force is applied by the mechanism, this allows final corrections to be made before the solder joints are fully formed, hence reducing rework cost significantly.

The application of a similar technique to correct the misalignment of chip components with respect to solder pad geometry has been discussed by E.A Kress and Kent Warwick of AVX.¹³² This paper therefore concentrates on the application of vibration techniques to QFPs.

3.3.4.1 IR reflow vibration experiment

An electrically operated vibrator was installed at the exit of the oven equipped with a photo light sensor to sense the absence/presence of the boards coming out from the oven. The vibrator only triggers when it senses a board has exited from the oven, minimizing its effect on other mechanical parts of the oven.

3.3.4.2 Results

Samples of 10 QFP-160 pin and 25 mil pitch devices were evaluated. These ICs were all mounted on a printed circuit board and then broken into two groups of sample size, i.e. five each, then processed through the reflow oven with and without vibration for each run. The results are given in tables 3.5 and 3.6.

Table 3.5 IR reflow without vibration.

S/N	Component Offset Before IR Reflow in 0.001 inch	Inspection Result After IR Reflow in 0.001 inch	Percent Improvement in Alignment
1	Side A 4.3	4.1	4.7%
2	Side A 6.0	6.5	-8.3%*
3	Side A 3.2	3.3	-3.1%*
4	Side A 4.4	3.9	11.3%
5	Side A 5.2	5.0	3.8%

*Negative denotes further deterioration in alignment after IR reflow.

Table 3.6 IR reflow with vibration.

S/N	Component Offset Before IR Reflow in 0.001 inch	Inspection Result After IR Reflow in 0.001 inch	Percent Improvement in Alignment
1	Side A 3.5	1.2	66%
2	Side A 3.0	0.6	80%
3	Side A 4.4	1.1	75%
4	Side A 7.0	1.8	74.3%
5	Side A 7.5	2.1	72%

The vibrator imposed a 50 Hz vertical oscillation to the oven belt.

3.3.4.3 The component placement accuracy problem

Component mechanical placement accuracy needs and board registration tolerance can be significantly reduced by this approach. In comparison with through-hole technology, the current surface mount technology requires twice the accuracy, and this requirement can increase to five times higher when fine-pitch technology is used¹³¹. This requires an investment in new and more sophisticated capital equipment.

In this study, the user is currently employing first generation placement equipment, i.e. using a mechanical centering device instead of electronic vision commonly found in the more sophisticated capital equipment. The process capability index for the placement machine studied was relatively poor, typically the C_p equal to 0.6 and C_{pk} 0.4 as revealed in the above placement result (i.e. component mounting before IR reflow).

The lead alignment was measured by CyberOptic LSM InfraRed high-precision X-Y-Z measurement equipment in this entire evaluation. C_p and C_{pk} are process capability indices,

The above evaluation clearly shows the effectiveness of the use of vibration to remedy the QFP misalignment problem seen in the IR solder reflow. For example, a misalignment of the IC lead of 0.0075 inch overhang was corrected with vibration to 0.0018-0.002 inch overhang. Analysis of the lead bonded area using a scanning electron microscope (SEM) as shown in Fig.3.13 indicated that the solder fillet shows no abnormality.

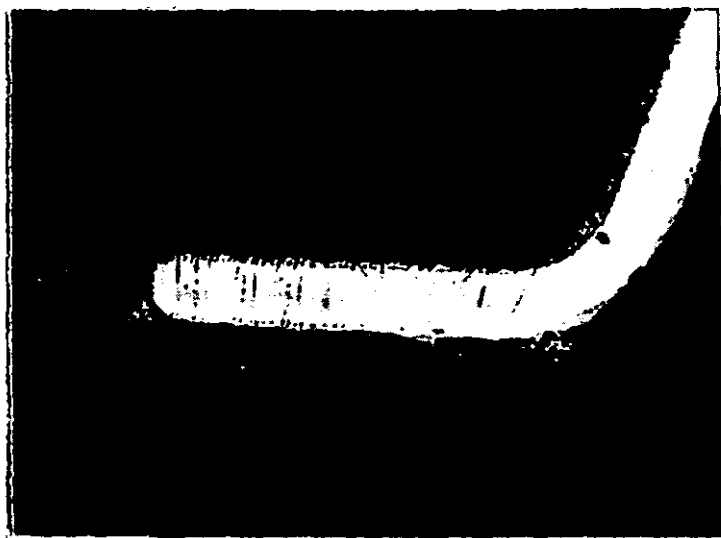


Fig. 3.13 Cross-section of IC's lead bonded area with vibration.

3.4 Conclusion

In the fine-pitch assembly of the SMT process, screening solder paste with typical deposit thicknesses (0.006 to 0.012 inch) will cause an increase in the number of bridges as lead pitches become finer, and this will also lead to insufficient solder and bridges, as these are observed together.

The SMT manufacturing process offers a variety of design, process engineering and control challenges. Crucial process parameters have to be maintained and optimized to obtain acceptable yields. Statistical experimental techniques such as design of experiments (DOE) and response surface method (RSM) are very effective tools in reducing common variation and help to center the process average. Consistent process control over areas such as pads and stencil tolerance design, the use of the right amount of solder paste at pre-specified time intervals, paste quality, placement accuracy and reflow profile are essential.

In the multi-machine environment, as seen in the survey, position-related components defects are increasing as the number of machines and station-to-station material handling increases. A vibration assisted alignment mechanism incorporated at the reflow zone of the oven can significantly improve component misalignment and hence reduce rework cost. The thesis now turn to address the challenge of insufficient solder and bridges occurring together.

Chapter Four

Insufficient Solder And Solder Bridges : An Experimental Study of The Interrelations Between Assembly Process Faults

4.1 Introduction

Early printed circuit board assembly inserted component leads into through-holes in the board. Surface mount has now become the most frequently used method, and is now possible to anticipate boards requiring even higher densities as bare chip mounting methods, in which a semiconductor chip is mounted directly to the board, will be routinely applied within the next five years.^{9,133} However, it is also clear, that soldering, with its numerous strong points, will remain a mainstream mounting method until the end of the millennium and beyond.

Against this backdrop, solder connections that join components to the board must become ever finer. In this chapter we focus on the defects in soldering processes. There are many types of solder defects, and many arise from a given process and joint technology.⁷⁶ This chapter examines the quality in high-density soldering, and presents an investigation of the bonding characteristics of a soldered gull wing QFP (Quad Flat Pack) having a lead pitch of 0.65 mm. The soldering defects that usually arise here are short circuits, usually in the form of solder bridges, component displacement and/or misalignment, and insufficient solder, which can result in joints formed with inadequate solder volume or, in extreme cases, open circuits.

The particular contribution of this chapter is to quantify the interrelationship between solder bridges and insufficient solder using regression analysis. These findings confirm the fundamental experiments on the phenomena of bridge stability described by Singler (1994)⁷⁶ and Whalley (1996)¹⁰⁷ and help formulate guidelines for stencil design to avoid solder bridging in the future.

4.2 Approach

In this experiment, a typical current generation PCBA (printed circuit board assembly) was used, and observations were made on locations on the board. At each of three sites, 100 pin, 0.65 mm pitch QFP devices were placed and reflowed. Printing was carried out on a MPM (Ultra-2000 Model) screen printer, with a 0.006 inch (0.152 mm) thickness stencil, and a total of 40 samples reflowed using a convection oven on a commercial production line. The boards were then inspected. The definition of bridge is self-explanatory but insufficient solder is defined to be minimum solder fillet on four sides of the lead joint (i.e. less than 25% solder fillet). Regression analysis was carried out in an attempt to understand the correlation between the solder bridge defect as a dependent variable and insufficient solder as an independent variable. It is important to understand this correlation, as the first likely action to be taken to avoid process faults is to change the screen thickness to modify the quantity of solder paste deposited to either increase or reduce solder bridges or insufficient solder (wicking) faults unless these process faults are correlated.

Informal observations and modelling work suggests¹²⁵ that motion of solder between joints causes this correlation. It is therefore important to explore the correlation between insufficient solder and bridges as a function of distance from the bridge.

Even if only a few correlated observations are made, they are still significant when expressed as ppm (part per million), and help explain the phenomena of the processes going on in the formation of bridges and wicks. All boards were inspected soon after IR-reflow, and the solder paste thickness reading was also recorded via laser operated off-contact paste height measurement equipment. The results were compiled and data processed using STATGRAPHIC statistical software. All boards with solder bridges were then repaired and reinspected. Earlier observations had caused the author to assert that while operators could easily identify and rework bridges, they found it more difficult to identify and therefore repair insufficient solder faults.

4.3 Results

4.3.1 A correlation between bridges and insufficient solder.

Regression analysis (Table 4.1) with dependent variable bridge and independent variable insufficient solder was employed to determine the significance of correlation, and a linear model ($y=a+bx$) was used to fit the variables, as shown in Fig 4.1. The results show that the bridge fault is correlated positively with the insufficient solder fault (wicking). The R-squared value of 50.58 indicates that 50.58% of the variability in bridging is correlated with insufficient solder. This clearly indicates that many of the bridging and insufficient solder faults occur on the same assemblies and are unlikely to be avoided by changes in solder volume alone. The number of results indicates that coplanarity errors alone are unlikely to account for the insufficient solder faults.

Table 4.1 Bridge versus insufficient solder (linear model

$y = a + bx$).

Parameter	Estimate	Standard Error	T Value	Prob. Level
Intercept	0.287649	2.7211	0.10571	0.91772
Slope	0.437286	0.1303	3.35526	0.00642

Dependent variable: QFP BRIDGE
Independent variable: QFP INSUFF

Analysis of Variance

Source	Sum of Squares	Df	Mean Square	F-Ratio	Prob. Level
Model	215.07758	1	215.07758	11.2578	0.00642
Residual	210.15319	11	19.10434		

Total (Corr.) 425.23077 12
Correlation coefficient = 0.711189 R-Square = 50.58 percent
Std. Error of Est. = 4.37091

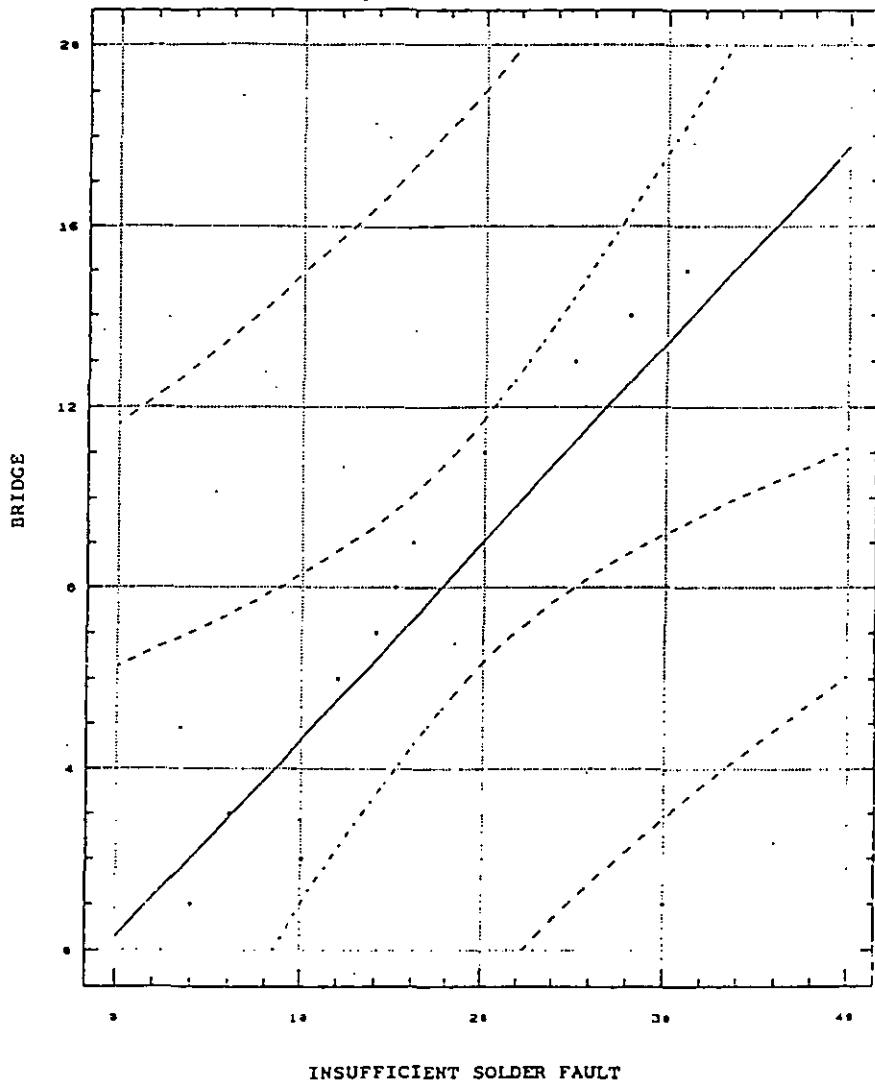


Fig. 4.1 Bridge versus insufficient solder (Wicking).

4.3.2 Bridging and insufficient solder on the same and adjacent leads.

Regression analysis (Table 4.2) with dependent variable insufficient solder and independent variable distance of insufficient solder from bridge is shown in Fig 4.2.

The figure shows the number of occasions on which both faults were observed on the same lead (zero distance), on the adjacent lead (distance 0.65 mm) and on subsequent leads. The pitch of the devices used was 0.65 mm (0.024 inch), which determines the unit of the abscissa. The model using an exponential fit $y=\exp(a+bx)$ shows that at least 87.93% of the insufficient solder faults occur at the bridging fault, i.e. the bridge fault and insufficient solder fault are on the same lead.

This quantitatively confirms the qualitative observation of Singler (1994)⁷⁶. The occurrence of the defects together reduces exponentially as the distance from the bridge increases. The observation of eight (of a total of 12 000 joints) insufficient solder faults on adjacent leads to a bridge and the frequent occurrence of bridges on adjacent pairs of leads suggests that the bridge is formed from a continuous bridge across many joints which “snaps” to form a single bridge, and that the drawing of material by surface tension from adjacent sites to remove bridges in the final assembly leads (as suggested by Whalley (1996)¹⁰⁷ does take place. It is difficult to attach significance to the other two experimental observations as they may have been caused by coplanarity or other errors.

Table 4.2 Insufficient solder versus distance of occurrence from bridge (exponential model $y = \exp(a + bx)$).

Parameter	Estimate	Standard Error	T Value	Prob. Level
Intercept	3.6674	0.683774	5.36347	0.03305
Slope	-0.0716374	0.0182746	-3.92005	0.05934

Dependent variable: DIST. INSUFF

Independent variable: DIST. DIST

Analysis of Variance

Source	Sum of Squares	Df	Mean Square	F-Ratio	Prob. Level
Model	10.263529	1	10.263529	15.3667	0.5934
Residual	1.3358076	2	0.6679038		

Total (Corr.) 11.599337 3

Correlation coefficient = -0.940658 R-Square = 83.48 percent

Std. Error of Est. = 0.817254

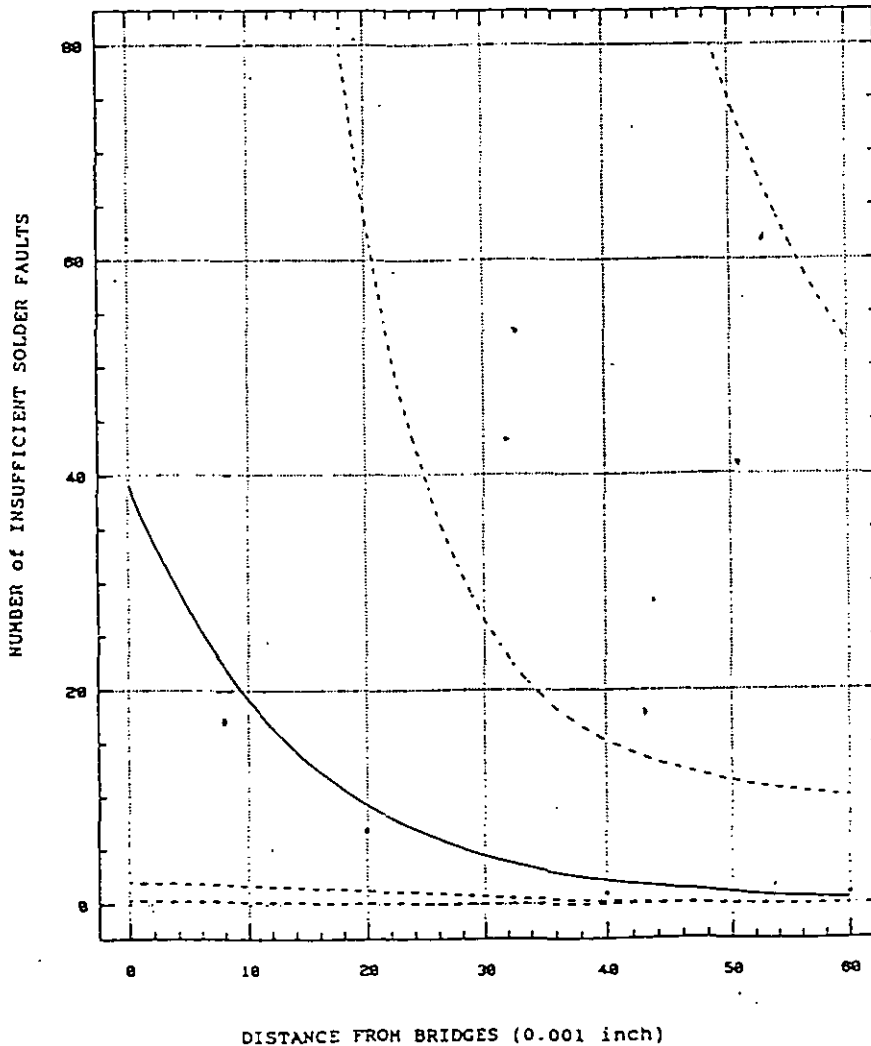


Fig.4.2 Insufficient solder versus distance of occurrence from bridge.

4.3.3 Changing the solder paste thickness

A further experiment was carried out to determine the effects of changing the deposited solder paste thickness by adjusting the screen printing parameters namely squeegee speed, pressure and snapoff distance.

Regression analysis (Table 4.3) was carried out once again with dependent variable bridge and independent variable paste thickness. The model $y = \exp(a + bx)$ indicates that 64.8% of bridges are explained by the increase of paste thickness, i.e. from 0.006 to 0.0105 inch (0.152 - 0.267 mm) as shown in Fig 4.3. This indicates that solder paste thickness plays a significant part in the likelihood of bridges forming, but this must be considered with respect to the earlier results that clearly show that insufficient solder is clearly related to solder bridges and increasing thickness will not remove the insufficient solder fault.

Table 4.3 Bridge versus solder paste thickness (exponential model $y = \exp(a + bx)$).

Parameter	Estimate	Standard Error	T Value	Prob. Level
Intercept	-19.6433	1.90222	-10.3294	0.00000
Slope	1.997636	0.236282	8.36443	0.00000

Dependent variable: Bridge
 Independent variable: Paste Thickness

Analysis of Variance

Source	Sum of Squares	Df	Mean Square	F-Ratio	Prob. Level
Model	436.98550	1	436.98550	69.9637	0.00000
Residual	237.34392	38	6.24589		
Lack of fit	20.508901	2	10.254451	1.70249	0.19657
Pure error	216.83502	36	6.02330		

Total (Corr.) 674.32942 39
 Correlation coefficient = 0.805003 R-Square = 64.80 percent
 Std. Error of Est. = 2.49918

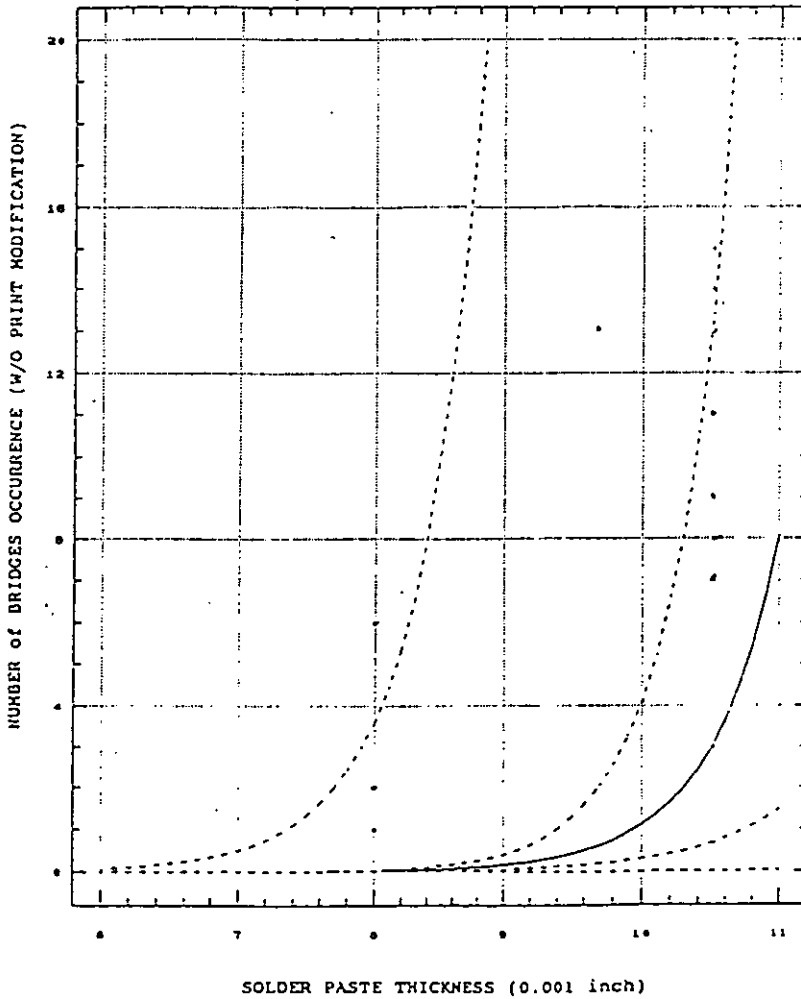


Fig.4.3 Bridge versus solder thickness.

4.3.4 The Effect of Rework

This supports the assertion that bridges are easier for repair operators to identify, but that a process alteration that just adds solder and therefore makes bridges, will more likely not improve the occurrence of insufficient solder defects. All the rejected boards with solder bridges were passed on for repair. 75 joints with solder bridges were repaired but 60 joints were still found with insufficient solder (wicking) after repair.

Part of the initial motivation for this work was to identify the causes or faults identified by end-users of the board after all the production processes after repair. Insufficient solder was identified as the major process fault, but further investigation of processes before repair indicated that a straightforward process change to remove this problem was not sufficient. It was therefore decided to carry out the experiments described above.

4.4 Summary and Discussion

The fluid mechanics of insufficient solder caused by solder wicking was first discussed by Singler,⁷⁶ and implies the undesirable migration (flow) of solder at the joint site. This migration results in either insufficient solder at the bridge or one or more leads from the bridge. Table 4.2 and Fig 4.2 show the regression model for this.

Both Singler⁷⁶ and Teo¹³ and chapter three reported that it is possible for enough solder to flow away from the joint to leave an inadequate solder volume for an effective joint to be formed. Typically, the volume of solder forming the bridge is drawn from the adjacent leads or its own lead, and as a result solder bridge and

insufficient solder faults occur concurrently. This is shown in the regression model in Table 4.1. The bridge is correlated positively with insufficient solder as shown in Fig 4.1. Similar work was done by Whalley¹⁰⁷ using computational modeling to describe the limits of formation and stability of shorts and how instability in an existing short may result in lean fillets, i.e. insufficient solder or wicking. The above regression study and findings match well with Whalley's model. Whalley's model, however, does not include the effect of termination geometry.

The consequences of the insufficient solder fault are most severe when an open joint occurs due to interactions within a joint with a coplanarity fault. This work has shown, as would be expected, that solder bridging is found to be correlated positively with paste thickness, as seen in Table 4.3 and Fig 4.3 i.e. if a large amount of solder is applied then a short may be inevitable (i.e. without modification of print pattern). On the contrary, if all other variables are held constant for the same paste thickness, the probability that a solder bridge will form and be stable increases as the separation between adjacent lands decreases. This is particularly critical as pitch values in modern microelectronics circuitry continue to decrease. Theoretical understanding of fundamental fluid mechanical phenomena in soldering processes has become important in product quality control.^{76, 135}

Singler⁷⁶ suggested that there is a need for fundamental experiments on bridge stability to provide more scientific guidelines on which board and joint layout could be based in order to design against soldering bridges. The author considers that there may be opportunities to change screen printing stencil designs in order to modify the print pattern to control the flow of molten solder so that bridge-less soldering can be

accomplished. This is discussed in chapter five. Also, Singler suggests that the application of solder resists to the terminations near to the component body would also help prevent bridges.

The rework results reported here have shown the difficult task for production operators of correcting the fault of insufficient solder after clearing the solder bridge. This clearly identifies the need for more work on print pattern modification to both prevent bridges and insufficient solder.

The motion of solder described in this work and that of Singler helps to account for the phenomenon of wicking, the motion of solder away from the foot of the lead to the portion of the lead adjacent to the component body. This work has shown that wicking-type phenomena may be driven by the formation of bridges as well as by temperature gradient and lead curvature effects. It may also be appropriate to further study alternative lead geometries in order to identify their effect on the instance of bridges and consequent insufficient solder faults. As it is explored in chapter five.

4.5 Conclusion

The regression models presented here suggest that solder bridge and insufficient solder (wicking) faults are strongly correlated. If a large amount of solder is applied, then a solder bridge is inevitable (i.e. without modification of print pattern). These results provide strong support for the importance of studies of the fundamental fluid phenomena of solder bridges and insufficient solder (wicking). Further study may provide design guidelines on which stencil design and perhaps board and joint geometry and layout can be based on, in order to address the issue of bridge stability

so that bridge-less soldering can be accomplished.

This chapter has indicated particularly the complex relationships between screen printing performance and the occurrence of process faults in reflow soldering.

Chapter Five

Stencil Optimization Via Flow Control

5.1 Introduction

There are many types of solder defects, and the most common soldering defects^{3,76,134} are short circuits, usually in the form of bridges, component misalignment or displacement and insufficient solder (solder wicking), in which molten solder climbs up the leads of QFP, PLCC or SOIC components during solder reflow resulting in inadequate solder volume or, in extreme cases, open circuits^{76,134}. All of the above defects are artifacts of the interactions between screen printing, component placement, solder reflow and joint technology⁷⁶.

If the soldering process was sufficiently well understood these phenomena could be explained by the chemistry and fluid mechanics of reflowing solder⁷⁶. There are also numbers of publications dealing with paste flow empirically usually by studying stencil tolerance design^{123,136} and flow out of the aperture with respect to its opening size and shape^{121,122}. However consideration of print pattern modification with respect to the fluid mechanics of the reflowing solder and the effect of the interaction of these two on soldering defects has not been explored to date. It is therefore the intention of this chapter to discuss modified stencil designs that modify the flow of the melting solder.

As has been indicated already, the fundamental aspects of the dynamic events of fluid

flow with respect to solder spreading have been discussed by Boettinger, Handwerker and Kattner (1993)⁷⁵ and further expanded by Singler (1994)⁷⁶ to include a simplified description of solder bridge dynamics in terms of energy equilibrium. Singler⁷⁶ also suggested the most important aspect this is that if a bridge is stable and is a part of an equilibrium capillary surface, it will freeze during the cool down phase of the process and form a permanent defect. Some of the driving forces behind these dynamics motion are thought to be liquid surface tension gradients  deriving from non-uniform heating of the substrate⁷⁶. Hence, if the process of print modification to be successful, the bridges between adjacent pads must break. The dynamics of molten solder flow is clearly determined by the laws of fluid mechanics and the discussions presented in this chapter are developed from this viewpoint.

5.2 Approach

In this investigation, a model "A" printed circuit board assembly (PCBA) was used and the observations were on the three locations U8, U27 and U31. These are all, 100 pin, 0.65 mm pitch QFP devices, with a lead geometry as shown in Fig. 5.1. The experiment was carried out using a MPM screen printer, with a 0.006 inch (0.152 mm) thickness stencil. The experiment was carried out on four different stencil designs as follows :

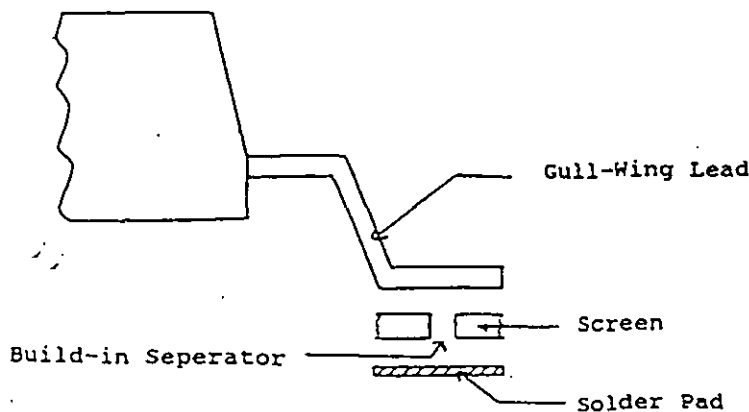


Fig 5.1 Lead Geometry.

(a) Design 1 : "Centre"

The overall stencil opening is divided into two sub-openings of equal area, and a separator at its centre. Fig. 5.2 shows a single opening of this type.

(b) Design 2 : "Quarter"

The stencil opening once again is divided into two sub-openings, with the ratio of the areas ratio 1:4, we shall call this Quarter. Fig. 5.3 shows a single opening of this type.

(c) Design 3 : Reduction

The stencil opening is solely reduced in size, with no solder paste printed at the heel of the pad. As shown in Fig. 5.4.

(d) Design 4: Conventional (Normal)

The stencil opening is normal, i.e. the stencil opening matches the pad size without any print modification to the IPC (The Institute for Interconnect and Packaging Electronic Circuits) standard.

We shall call this conventional as illustrated in Fig. 5.5. With each of the stencil designs forty pieces of model "A" PCBAs were printed with incremental changes in paste thickness on normal pads, i.e. the board pad has not been redesigned; it remains conventional. These boards were then populated with Panasert in-line placement machines and reflowed through a convection oven. Inspection was done immediately after reflow. The results were compiled and data processed through the STATGRAPHICS software using Regression Analysis and Correlation Study tools. (See Appendix C on regression method).

5.3 Results

The objective of this study is to select the optimum stencil design in term of robustness against solder bridging, component misalignment or displacement and insufficient solder (solder wicking). For the purpose of comparison between designs, the data are analyzed by the various defect modes as follows:

5.3.1 Solder Bridging

With Design 1, 2 and 3 (Centre, Quarter and Reduction respectively) there were no solder bridges observed for any increase of paste thickness as revealed in table 5.1, 5.2, 5.3 and Figures 5.6-5.8. Design 4, the conventional design, shows an exponential correlation: an exponential increase in solder bridges with an increase in paste thickness as shown in table 5.4 and Fig.5.9.

Dimensions:

Component pitch (inch)	Pad dimensions (inch)	Sub-opening (W x L) (inch)
0.025	0.014 x 0.095	two equal areas of 0.012 x 0.02
Aperture width (inch)	Separator (inch)	Maximum stencil thickness (inch)
0.012	0.010	0.0075

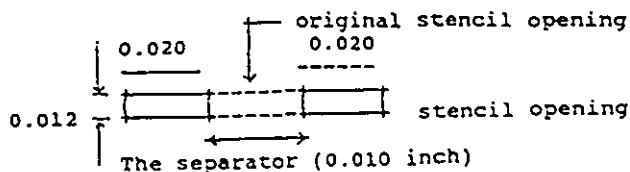


Fig 5.2 Stencil design for "Centre".

Dimensions:

Component pitch (inch)	Pad dimensions (inch)	Sub-opening (W x L) (inch)
0.025	0.014 x 0.095	one quarter area: 0.012 x 0.0125 three-quarter area: 0.012 x 0.0245
Aperture width (inch)	Separator (inch)	Maximum stencil thickness (inch)
0.012	0.013	0.0075

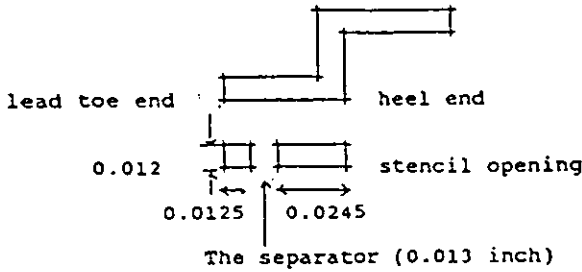


Fig 5.3 Stencil design for "Quarter".

Dimensions:

Component pitch (inch)	Pad dimensions (inch)	Sub-opening (W x L) (inch)
0.025	0.014 x 0.095	actual area: 0.012 x 0.050
Aperture width (inch)	Maximum stencil thickness (inch)	
0.012	0.0075	

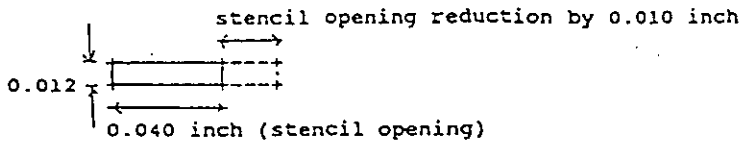


Fig 5.4 Stencil design with reduction in aperture length.

Dimensions:

Component pitch (inch)	Pad dimensions (inch)	Aperture width / length (W x L) (inch)
0.025	0.014 x 0.095	0.012 x 0.050
Maximum stencil thickness (inch)		
0.0075		



Fig 5.5 Conventional stencil design.

Table 5-1 Solder bridge versus paste thickness, Design 1 (Centre).

Parameter	Estimate	Standard Error	T Value	Prob. Level
Intercept	1E-3	0	9999.99	0.00000
Slope	0	0	9999.99	0.00000

Regression Analysis — Linear model: $Y = a + bX$

Dependent Variable: Bridge.Centre

Independent Variable: Bridge.Thickness

Analysis of Variance

Source	Sum of Squares	Df	Mean Square	F-Ratio	Prob. Level
Model	0.0000	1	0.0000	9999.999	0.00000
Residual	0.000000	38	0.000000		

Total (Corr.) 0.000000 39

Correlation Coefficient = 1 R-Squared = 100.00 percent

Std. Error of Est. = 0

Table 5-2 Solder bridge versus paste thickness, Design 2 (Quarter).

Parameter	Estimate	Standard Error	T Value	Prob. Level
Intercept	1E-3	0	9999.99	0.0000
Slope	0	0	9999.99	0.0000

Regression Analysis — Linear model: $Y = a + bX$

Dependent Variable: Bridge.Quarter

Independent Variable: Bridge.Thickness

Analysis of Variance

Source	Sum of Squares	Df	Mean Square	F-Ratio	Prob. Level
Model	0.0000	1	0.0000	9999.999	0.00000
Residual	0.000000	38	0.000000		

Total (Corr.) 0.000000 39

Correlation Coefficient = 1 R-Squared = 100.00 percent

Std. Error of Est. = 0

Table 5-3 Solder bridge versus paste thickness, Design 3 (Reduction).

Parameter	Estimate	Standard Error	T Value	Prob. Level
Intercept	1E-3	0	9999.99	0.00000
Slope	0	0	9999.99	0.00000

Regression Analysis — Linear model: $Y = a + bX$
 Dependent Variable: Bridge.Reduction
 Independent Variable: Bridge.Thickness

Analysis of Variance

Source	Sum of Squares	Df	Mean Square	F-Ratio	Prob. Level
Model	0.0000	1	0.0000	9999.999	0.00000
Residual	0.000000	38	0.000000		

Total (Corr.) 0.000000 39
 Correlation Coefficient = 1 R-Squared = 100.00 percent
 Std. Error of Est. = 0

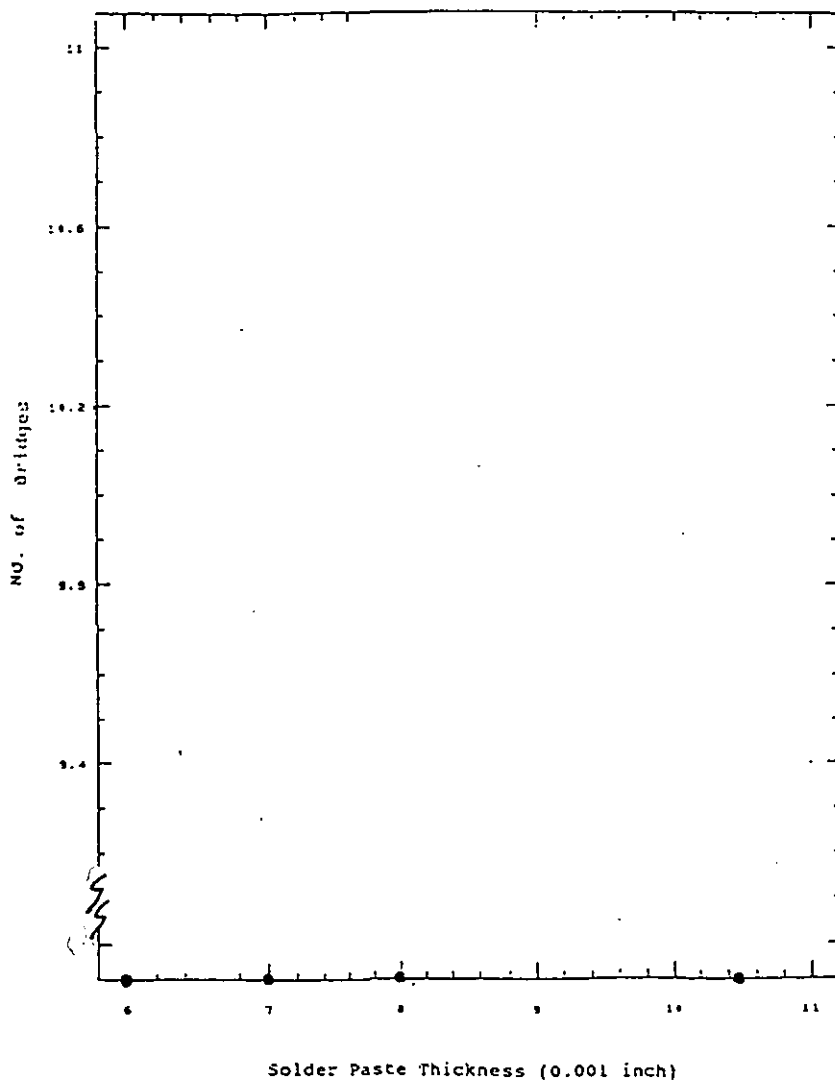


Fig 5.6 Solder bridge versus paste thickness, Design 1 (Centre).

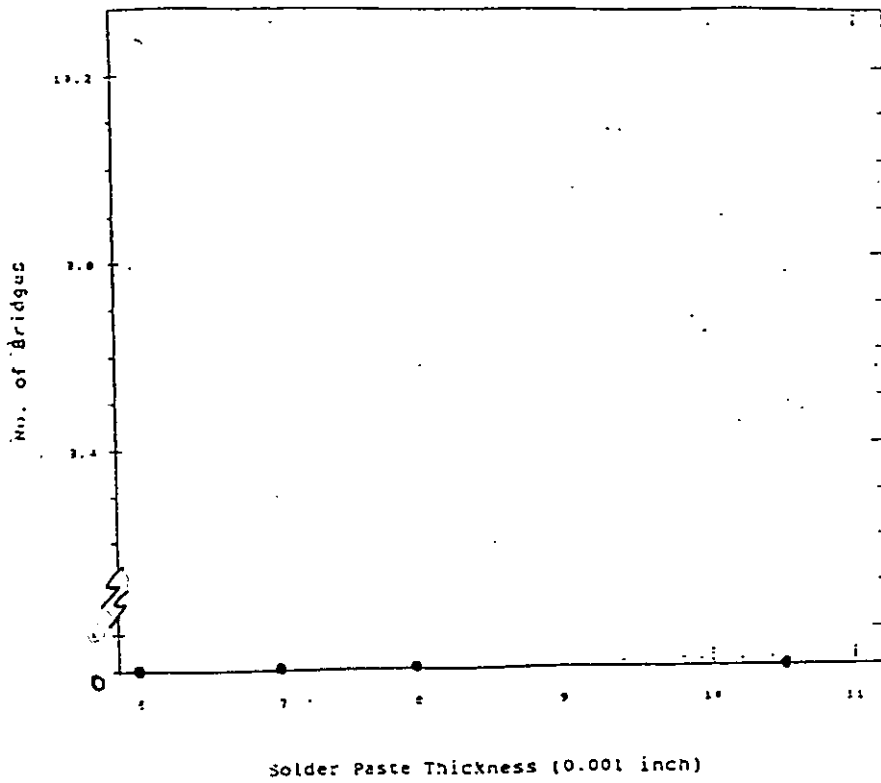


Fig 5.7 Solder bridge versus paste thickness, Design 2 (Quarter).

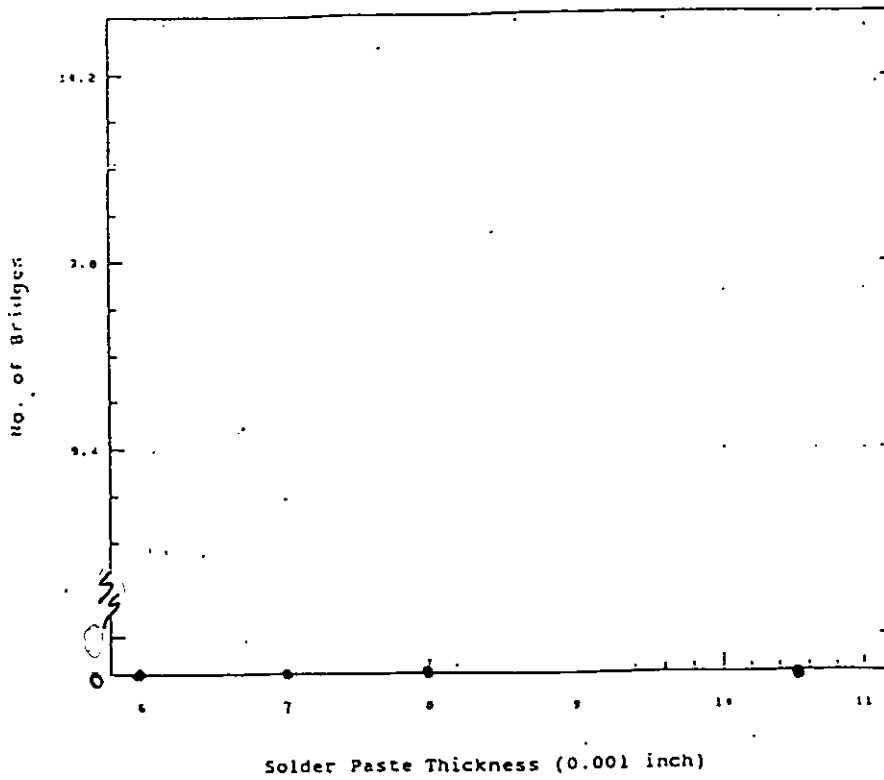


Fig 5.8 Solder bridge versus paste thickness, Design 3 (Reduction).

Table 5-4 Solder bridge versus paste thickness, Design 4 (Conventional).

Parameter	Estimate	Standard Error	T Value	Prob. Level
Intercept	-19.6488	1.90222	-10.3294	0.00000
Slope	1.97636	0.236282	8.36443	0.00000

Regression Analysis — Exponential model: $Y = \exp(a+bX)$

Dependent Variable: Bridge.Convention

Independent Variable: Bridge.Thickness

Analysis of Variance

Source	Sum of Squares	Df	Mean Square	F-Ratio	Prob. Level
Model	436.98550	1	436.98550	69.9637	0.00000
Residual	237.34392	38	6.24589		
Lack of fit	20.508901	2	10.254451	1.70249	0.19657
Pure error	216.83502	36	6.02320		

Total (Corr.) 674.32942 39

Correlation Coefficient = 0.805003 R-Squared = 64.80 percent

Std. Error of Est. = 2.49918

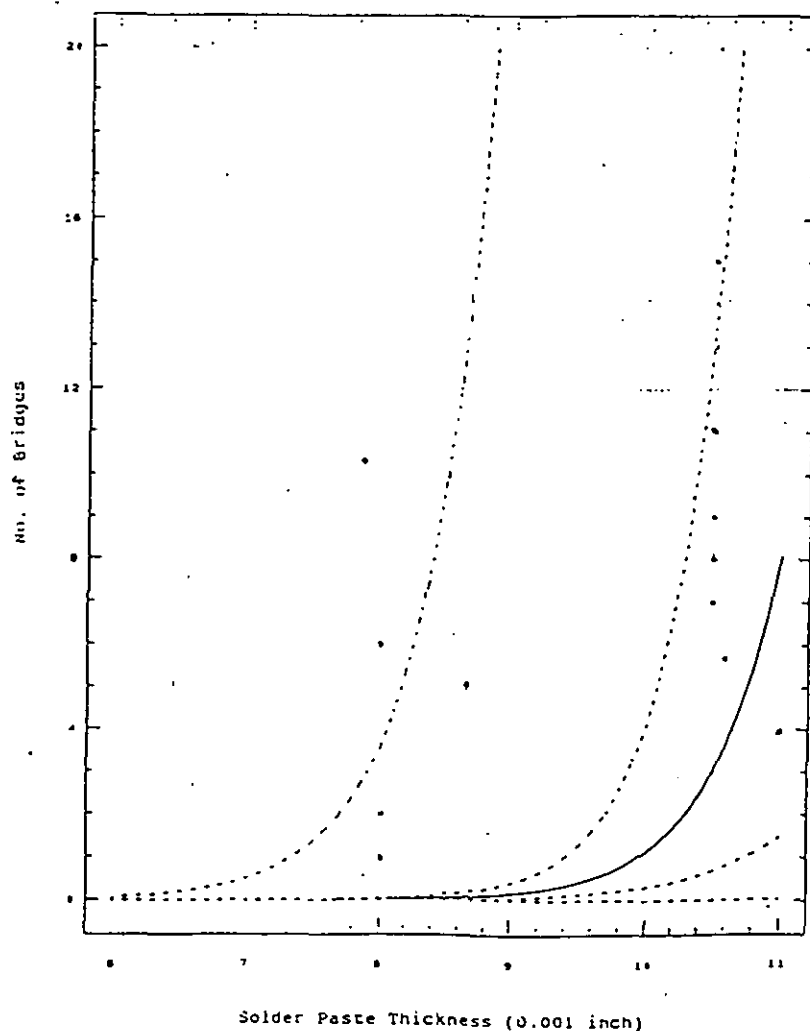


Fig 5.9 Solder bridge versus paste thickness, Design 4 (Conventional).

5.3.2 Component Misalignment Or/And Displacement

With Design 2, 3 and 4 (Quarter, Reduction and Conventional respectively) there were no observed misalignment errors as revealed in Table 5.6, 5.7, 5.8 and Figures 5.11-5.13.

Design 1, the Centre design, the regression analysis shows a negative linear correlation with misalignment faults as revealed in table 5.5 and Fig.5.10.

Table 5-5 Component misalignment versus paste thickness, Design 1 (Centre).

Parameter	Estimate	Standard Error	T Value	Prob. Level
Intercept	0.417343	0.228079	1.82982	0.07513
Slope	-0.0401832	0.0283306	-1.41837	0.16423

Regression Analysis — Linear model: $Y = a + bX$

Dependent Variable: Misalign.Centre

Independent Variable: Misalign.Thickness

Analysis of Variance

Source	Sum of Squares	Df	Mean Square	F-Ratio	Prob. Level
Model	0.1806438	1	0.1806438	2.011765	0.16423
Residual	3.412160	38	0.089794		
Lack of fit	0.4181568	2	0.2090784	2.513966	0.09506
Pure error	2.994003	36	0.083167		

Total (Corr.) 3.592804 39

Correlation Coefficient = -0.224231 R-Squared = 5.03 percent

Std. Error of Est. = 0.299656

Table 5-6 Component misalignment versus paste thickness, Design 2 (Quarter).

Parameter	Estimate	Standard Error	T Value	Prob. Level
Intercept	1E-3	0	9999.99	0.00000
Slope	0	0	9999.99	0.00000

Regression Analysis — Linear model: $Y = a + bX$

Dependent Variable: Misalign.Quarter

Independent Variable: Misalign.Thickness

Analysis of Variance

Source	Sum of Squares	Df	Mean Square	F-Ratio	Prob. Level
Model	0.0000	1	0.0000	9999.999	0.00000
Residual	0.000000	38	0.000000		

Total (Corr.) 0.000000 39

Correlation Coefficient = 1 R-Squared = 100.00 percent

5.3.3 Insufficient Solder (Solder Wicking)

With Design 3, Reduction in aperture length, there is very little correlation of the insufficient solder defect with stencil thickness as shown in regression Table 5.11 and Fig. 5.16. This shows the performance of the design is independent of paste thickness for the range of thicknesses explored. Designs 1, 2 and 4 (i.e. Centre, Quarter and Conventional respectively) show a correlation with the paste thickness. Design 1 has a positive linear correlation as revealed in table 5.9 and Fig. 5.14. Next, Design 2 shows a correlation that is multiplicative (Log) as revealed in table 5.10 and Fig. 5.15. Design 4, has an exponential correlation as shown in table 5.12 and Fig. 5.17.

Table 5-7 Component misalignment versus paste thickness, Design 3 (Reduction).

Parameter	Estimate	Standard Error	T Value	Prob. Level
Intercept	1E-3	0	9999.99	0.00000
Slope	0	0	9999.99	0.00000

Regression Analysis — Linear model: $Y = a + bX$

Dependent Variable: Misalign.Reduction

Independent Variable: Misalign.Thickness

Analysis of Variance

Source	Sum of Squares	Df	Mean Square	F-Ratio	Prob. Level
Model	0.0000	1	0.0000	9999.999	0.00000
Residual	0.000000	38	0.000000		

Total (Corr.) 0.000000 39

Correlation Coefficient = 1 R-Squared = 100.00 percent

Std. Error of Est. = 0

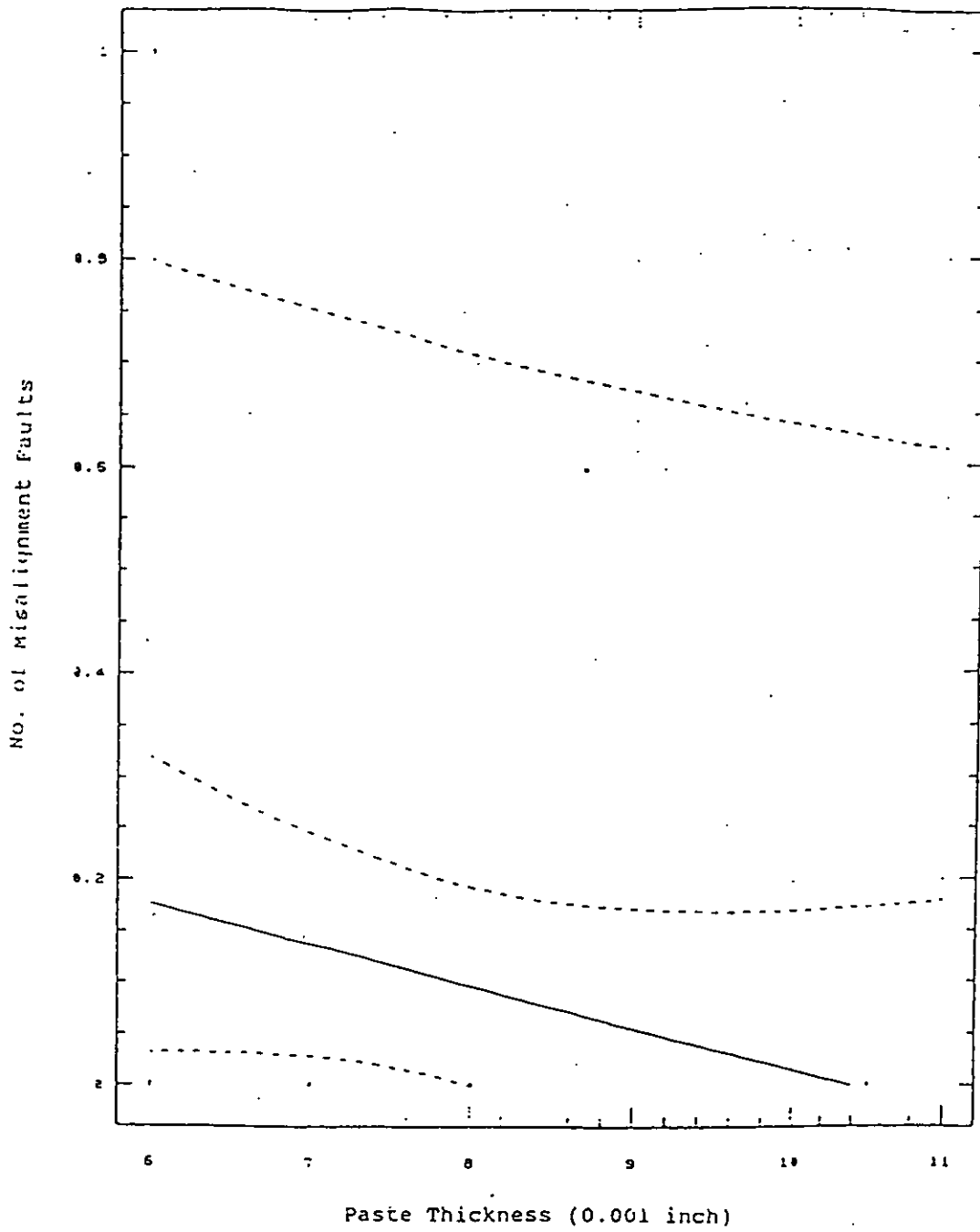


Fig 5.10 Component misalignment versus paste thickness, Design 1 (Centre).

Table 5-8 Component misalignment versus paste thickness, Design 4 (Conventional).

Parameter	Estimate	Standard Error	T Value	Prob. Level
Intercept	1E-3	0	9999.99	0.00000
Slope	0	0	9999.99	0.00000

Regression Analysis — Linear model: $Y = a + bX$
 Dependent Variable: Misalign.Convention
 Independent Variable: Misalign.Thickness

Analysis of Variance

Source	Sum of Squares	Df	Mean Square	F-Ratio	Prob. Level
Model	0.0000	1	0.0000	9999.999	0.00000
Residual	0.000000	38	0.000000		

Total (Corr.) 0.000000 39
 Correlation Coefficient = 1 R-Squared = 100.00 percent
 Std. Error of Est. = 0

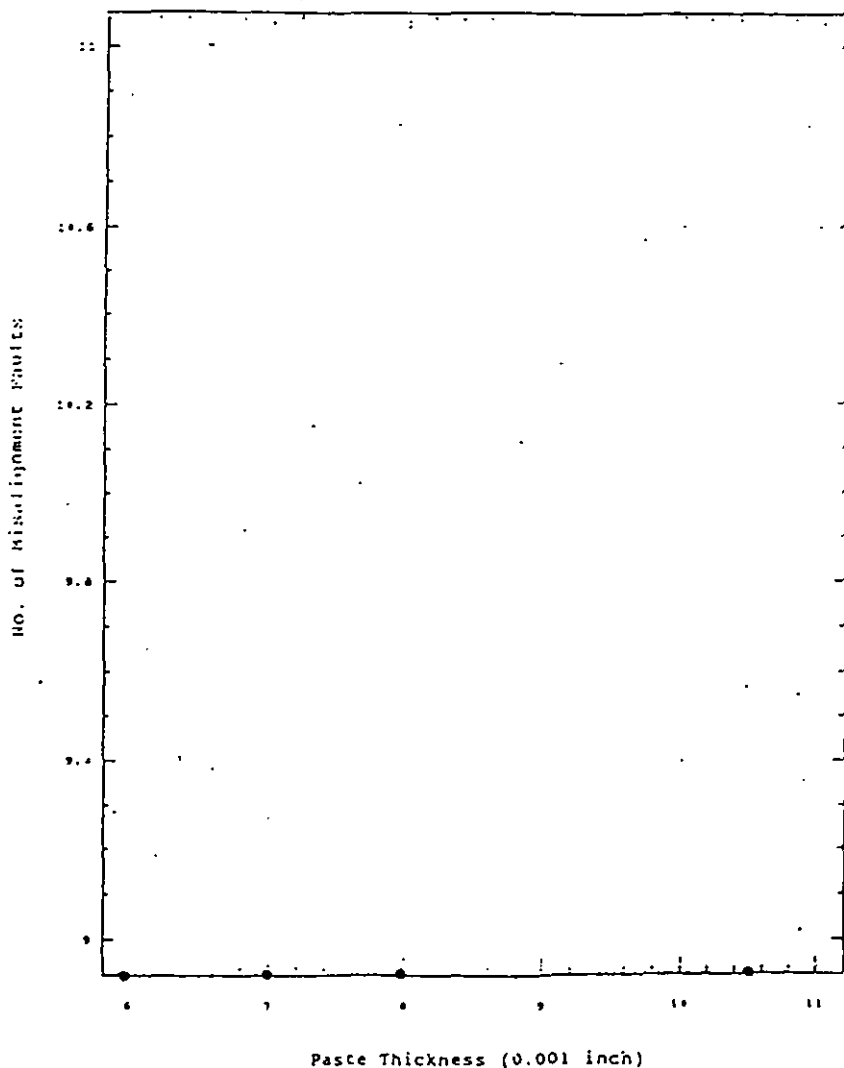


Fig 5.11 Component misalignment versus paste thickness, Design 2 (Quarter).

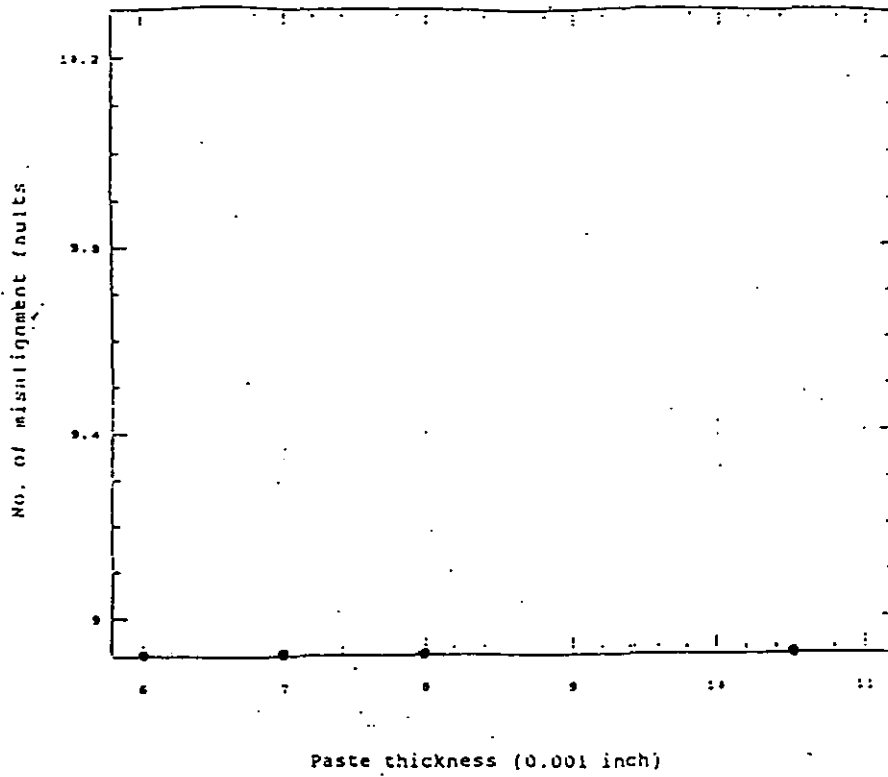


Fig 5.12 Component misalignment versus paste thickness, Design 3 (Reduction).

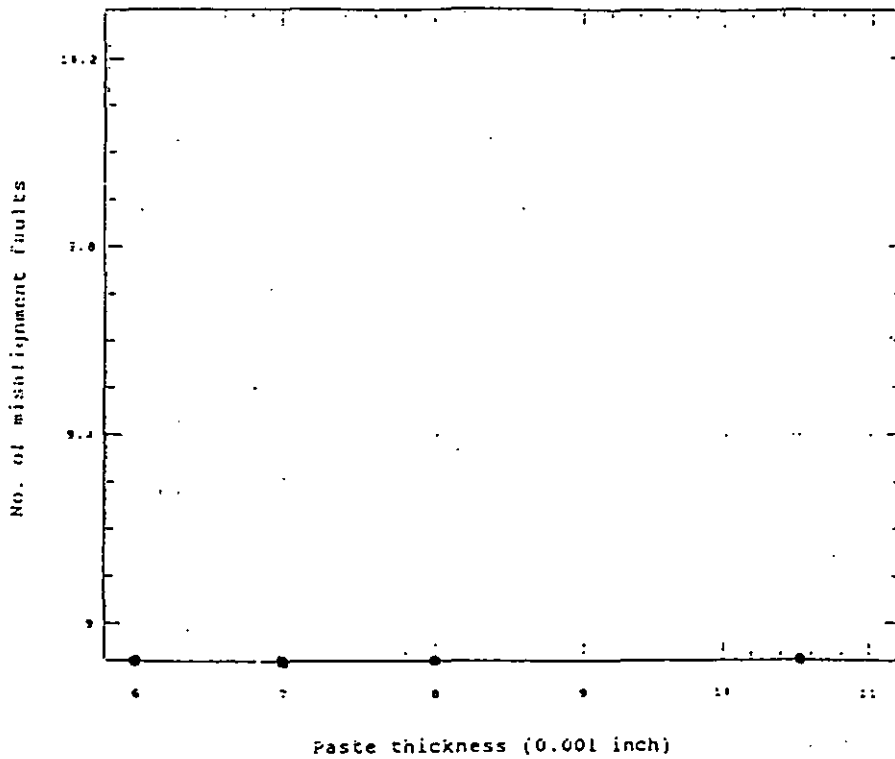


Fig.5.13 Component misalignment versus paste thickness, Design 4 (Conventional).

Table 5-9 Insufficient solder (solder wicking) versus paste thickness, Design 1-

(Centre).

Parameter	Estimate	Standard Error	T Value	Prob. Level
Intercept	-0.427063	0.358794	-1.19023	0.24132
Slope	0.108272	0.0445672	2.4294	0.01996

Regression Analysis — Linear model: $Y = a + bX$

Dependent Variable: Insuff.Centre

Independent Variable: Insuff.Thickness

Analysis of Variance

Source	Sum of Squares	Df	Mean Square	F-Ratio	Prob. Level
Model	1.3114792	1	1.3114792	5.901981	0.01996
Residual	8.443981	38	0.222210		
Lack of fit	1.9569740	2	0.9784870	5.430168	0.00869
Pure error	6.487007	36	0.180195		

Total (Corr.) 9.755460 39

Correlation Coefficient = 0.366654 R-Squared = 13.44 percent

Std. Error of Est. = 0.471392

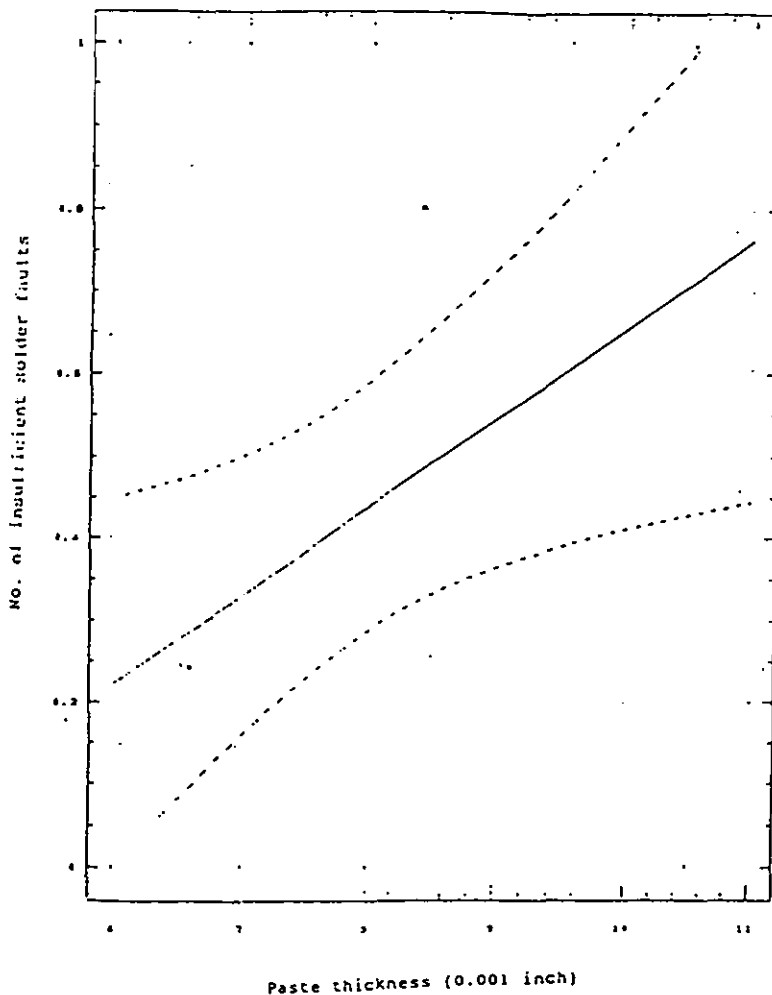


Fig 5.14 Insufficient solder (solder wicking) versus paste thickness, Design 1 (Centre).

Table 5-10 Insufficient solder (solder wicking) versus paste thickness, Design 2

(Quarter).

Parameter	Estimate	Standard Error	T Value	Prob. Level
Intercept*	3.84595	5.03645	0.763623	0.44981
Slope	-2.8981	2.45389	-1.18103	0.24493

*Note: The intercept is equal to Log a.

Regression Analysis — Multiplicative model: $Y = aX^b$

Dependent Variable: Insuff.Quarter

Independent Variable: Insuff.Thickness

Analysis of Variance

Source	Sum of Squares	Df	Mean Square	F-Ratio	Prob. Level
Model	14.191646	1	14.191646	1.39482	0.24493
Residual	386.63185	38	10.17452		
Lack of fit	52.612270	2	26.306135	2.33523	0.07187
Pure error	334.01958	36	9.27832		

Total (Corr.) 400.82350 39

Correlation Coefficient = -0.198165 R-Squared = 3.54 percent

Std. Error of Est. = 3.18975

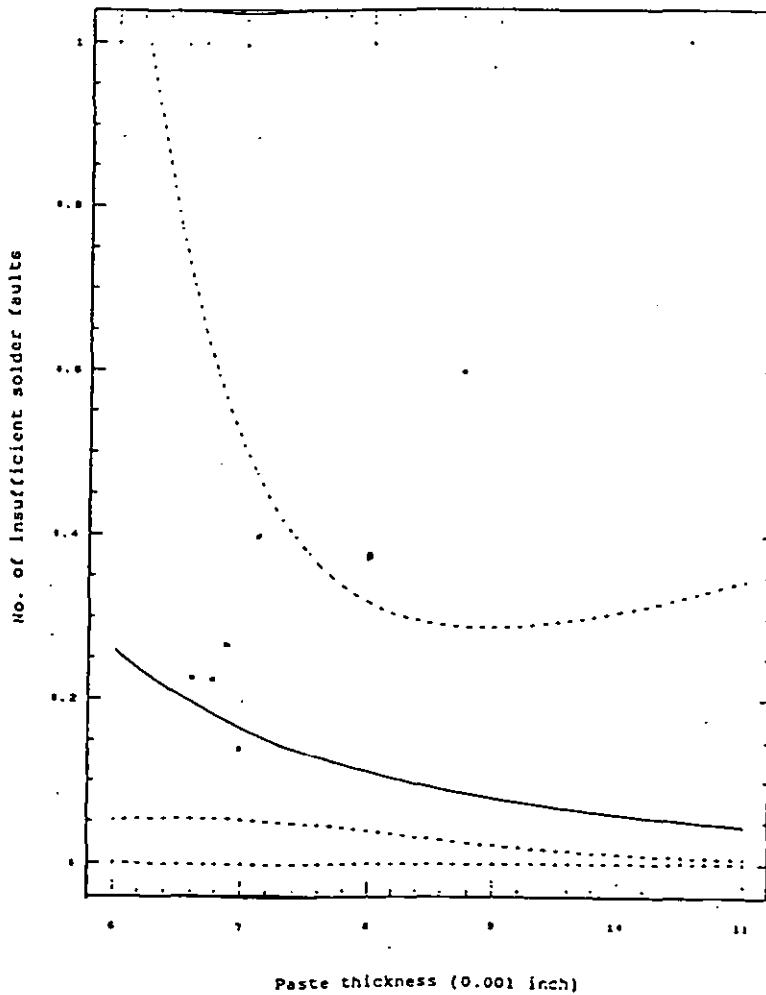


Fig 5.15 Insufficient solder (solder wicking) versus paste thickness, Design 2

(Quarter).

Table 5-11 Insufficient solder (solder wicking) versus paste thickness, Design 3

(Reduction).

Parameter	Estimate	Standard Error	T Value	Prob. Level
Intercept	0.119875	0.20535	0.583762	0.56283
Slope	-5.58101E-3	0.0255073	-0.2188	0.82798

Regression Analysis — Linear model: $Y = a + bX$

Dependent Variable: Insuff.Reduction

Independent Variable: Insuff.Thickness

Analysis of Variance

Source	Sum of Squares	Df	Mean Square	F-Ratio	Prob. Level
Model	0.0034836	1	0.0034846	0.047873	0.82798
Residual	2.765968	38	0.072789		
Lack of fit	0.2709656	2	0.1354828	1.954860	0.15633
Pure error	2.495003	36	0.069306		

Total (Corr.) 2.769453 39

Correlation Coefficient = -0.0354717 R-Squared = 0.13 percent

Std. Error of Est. = 0.269794

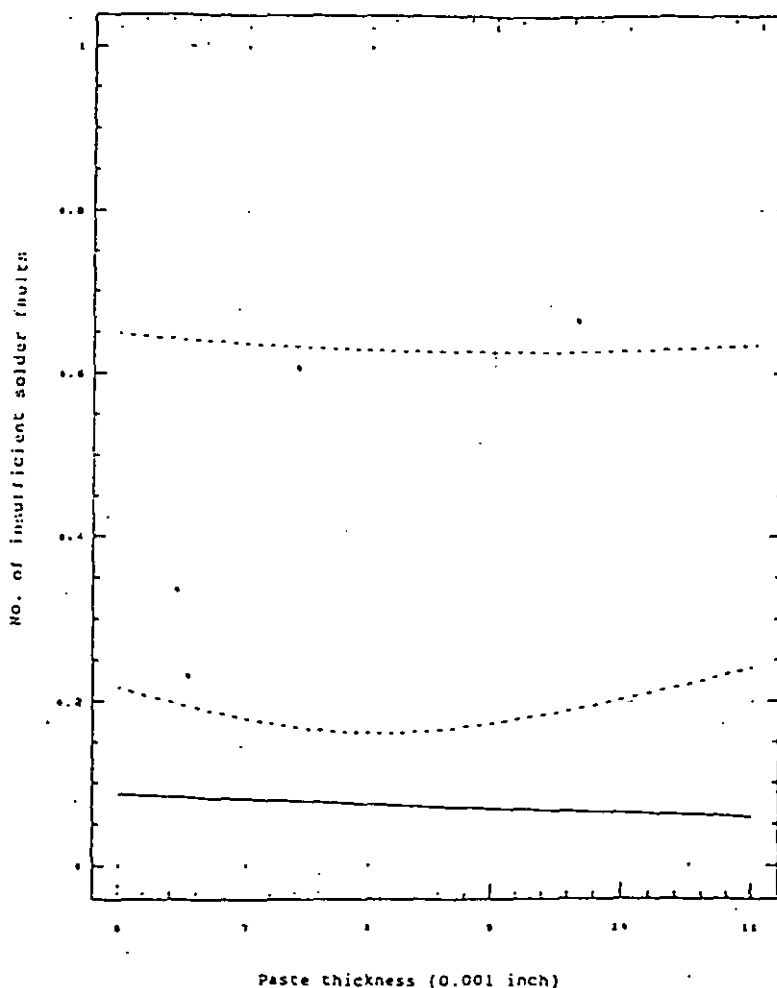


Fig 5.16 Insufficient solder (solder wicking) versus paste thickness, Design 3

(Reduction).

Table 5-12 Insufficient solder (solder wicking) versus paste thickness, Design 4 (Conventional).

Parameter	Estimate	Standard Error	T Value	Prob. Level
Intercept	-8.43228	3.55797	-2.36997	0.02297
Slope	0.898545	0.441949	2.03314	0.04907

Regression Analysis — Exponential model: $Y = \exp(a + bX)$

Dependent Variable: Insuff.Convention

Independent Variable: Insuff.Thickness

Analysis of Variance

Source	Sum of Squares	Df	Mean Square	F-Ratio	Prob. Level
Model	90.326012	1	90.326012	4.13366	0.04907
Residual	830.35055	38	21.85133		
Lack of fit	70.024182	2	35.012091	1.65776	0.20478
Pure error	760.32637	36	21.12018		

Total (Corr.) 920.67656 39

Correlation Coefficient = 0.313222 R-Squared = 9.81 percent

Std. Error of Est. = 4.67454

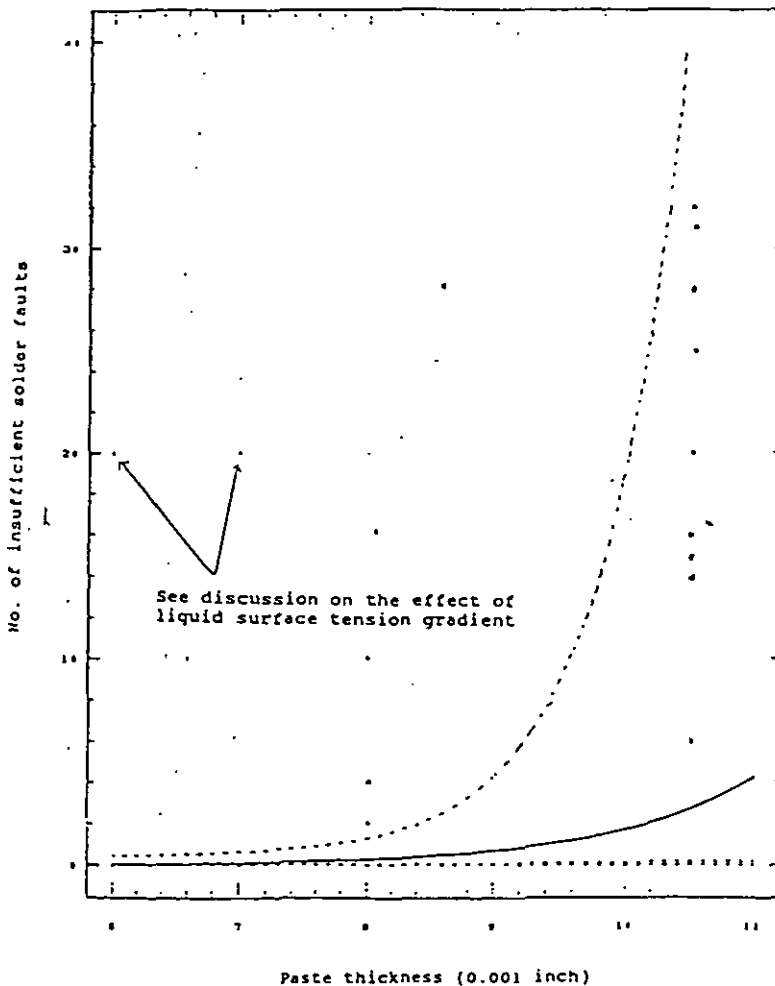


Fig 5.17 Insufficient solder (solder wicking) versus paste thickness, Design 4 (Conventional).

5.4 Discussion

5.4.1 Solder Bridges

From the results above we see that Designs 1, 2 and 3 reduce solder bridges. In contrast Design 4, the conventional design, shows an increase in bridges with increase in paste thickness. This shows the traditional design (i.e. without built-in separator or reduction in print size) is less attractive with respect to bridges. It should be observed that the formation of bridges can be reduced by using a smaller volume of solder. These modified designs potentially reduce the volume of solder on the pad by up to 20 to 25 percent which will necessarily reduce bridges. However, the variation of solder volume used in the present experiment has allowed the author to show that the modified stencil designs have a positive effect reducing bridges (and any consequent insufficient solder faults) at solder volumes that cause bridges with the conventional stencil design.

In the design of these experiments the intention was to use the revised screen apertures to modify both the macroscopic wetting driven flows and Marangoni convection driven surface tension effects. For pure liquids, as in the case of molten solder observed in this experiment, the surface tension forces are modified and spreading of molten solder is influenced by the curvature of the lead at the heel.

The thermally driven effects on surface tension and hence the action of the forces towards a vacant^{135, 136} region (the solder pad area without paste) are due to either a built in separator or reduction in stencil aperture design. This

phenomenon facilitates bridge breaking by serving as an added perturbation to the bridge surface while transporting a significant amount of solder towards the initially

empty area of the solder pad.

As the solder on the pads starts to spread during the solder reflow process, it draws away any solder that might cause a bridge. This acts to destabilize the equilibrium capillary surface action that forms the solder bridge defect as suggested by Singler⁷⁶.

5.4.2 Component Misalignment and Displacement

With respect to misalignment, Design 2,3 and 4 appear to be robust. Design 1 (separator located at the centre) has the worst performance due to the absence of paste adhesion in the middle of the pad resulting in component displacement and misalignment when the leads land on the pad. These errors can be corrected by an external vibration force in the final stage of the reflow zone of the oven as shown in chapter three.

5.4.3 Insufficient Solder (Solder Wicking)

Designs 1,2, and 4 (Centre, Quarter and Conventional respectively) show a correlation of the insufficient solder defect to the paste thickness for the following reasons. For Designs 1 and 2 the reason is obvious, the separator (0.010 inch gap) provides a challenge to the flux wetting and spreading capabilities. In these experiments R (rosin) flux was used where melting is completely completed before solder spreads to any significant extent. This results in an isolation of the quarter volume of solder left on the pad near the heel in design 2. For Design 1, the separator provides an isolation between the solder deposits located at the toe and heel of the pad, hence insufficient solder faults occurred.

Design 4(the Conventional design), table 5.12 and Fig. 5.17 show a correlation of

solder wicking and paste thickness increase¹⁰⁷. A previous investigation¹³⁷ (in chapter four) has studied the correlation between solder bridge and insufficient solder to show a direct linear, positive correlation of the two defects. When there is an increase in solder bridges there is a corresponding high probability of increase in the insufficient solder.

From the above results, it suggests the influence of liquid surface tension and Marangoni⁷⁵ driven flow, can have both positive and negative consequences in the conventional design (i.e. Design 4).

This weak surface motion seems to facilitate bridge breaking by serving as a disturbance to the bridge surface. Strong surface motions, however, can transport a significant amount of liquid along a pad often resulting in an inadequate amount of solder on pads^{75,76}. Ehrhard and Davis(1991)⁸⁶ have also shown the existence of surface tension can either retard or promote the rate of droplet spreading⁷⁵. For a situation where a bridge between two pads breaks asymmetrically as modeled by Whalley (1996)¹⁰⁷ more than half the bridge can flow towards the rightmost pad as observed by Singler^{76,138}. Should this action repeat itself along the pad row, then a situation similar to that of strong surface motion develops, in which the excess volume that is confined between the broken bridges cannot be dispersed even by complete wetting of the pads and a multiple pad bridge is formed^{107,138}. Also the pads adjacent to the multiple pad bridges have insufficient volume to wet completely, thus the conventional stencil design is the least desirable of all.

5.5 Conclusion

Design 3, reduced aperture length, is the most robust design, its performance is independent of paste thickness in all three defect cases i.e. bridging, component misalignment or displacement and solder wicking.

It is well known that, the problem of bridging becomes more serious as the lead pitch decreases. However, by controlling the flow of the wetting solder, bridgeless soldering can be accomplished. The modified print patterns described in Design 1,2 and 3 modified the surface tension driven flows during reflow soldering to effectively serve as bridge breaking mechanism that fulfilled the important aspects of the energy driven phenomena proposed by Singler (1994)⁷⁶, i.e. a reflow condition where the bridge is not stable and therefore does not form part of an equilibrium capillary surface.

This allows movement of liquid solder⁷⁶ such that should a bridge inadvertently form during the solder process or by smearing in the paste placement by a conventional stencil process the bridge breaking dynamics exhibited by the modified print process would draw away any solder that might cause the bridge. This chapter has unveiled the difficulty in using a traditional stencil design (i.e. without modification) to overcome the process faults of solder bridging and insufficient solder (wicking). Print modifications can provide a control over the flow of molten solder and help in reduction of such defects. High speed video experiments would help to verify this proposed phenomenology. It is also necessary to verify the reliability performance of the joints arising from the modified aperture. We now turn to explore the open faults.

Chapter Six

A Study of Solderability And Solder Spreading For SMT Open Joints

6.1 INTRODUCTION

“Open joint” is a term used to describe a gap that can occur between component

lead and a printed circuit (PCB) pad after solder reflow. Such open joints (Opens) are usually associated with "gull-wing" lead devices¹⁴³. There are three main reasons for this phenomenon: the first, most common, reason is that coplanarity errors prevent one or more leads contacting the solder paste when reflow takes place.

Secondly, the leads may heat up much more rapidly than the pads during reflow because of the greater thermal mass of the PCB^{66,137}, and flow based phenomena within single joints then can cause opens. Thirdly, SMT open joints can be associated with adjacent solder bridges, this phenomenon is rarely recognized by the SMT users, but has been discussed in detail in Refs. 107 and 137, and the author's earlier work (Ref.134). It will not be further discussed here.

The solution to the first case, apart from insisting on better coplanarity tolerances from the component suppliers, is to modify the lead shapes to compensate for the gap.

In the second case, due to thermally driven phenomena (see for an example Ref. 77) flux in the paste is attracted to the hottest area of the lead, in this case the heel. When the lead temperature has risen above the melting point of the paste alloy, the solder follows, leaving the pad barely wetted. Virtually all the solder can wick up the leads, leaving an insufficient amount to form a bond at the interface between the lead and pad, with the presence of lead coplanarity the open joint problem inevitably occurs. In this chapter potential solutions based on flux kinetics⁷⁵ and study of the design aspects of solderability may provide an avenue to solve elements of the problem caused by opens.

In this chapter, careful examination via empirical study of reflow solder joints was carried out on the family of "gull-wing" lead shapes typically used on SOIC (small outline integrated circuits) and QFP (quad flat pack) packages. In a further experiment, using rosin mildly activated (RMA) solder paste, the melting and spreading stages could be visually separated. Our challenge is to develop an understanding of the mechanisms that can limit open joints due to non-coplanar leads.

6.2. PHILOSOPHY OF THE EXPERIMENTAL PROGRAMME

Firstly, a solder spreading test is used to quantify the mobility of the fluxes with respect to heat applied. This understanding is critical in the paste selection process in order to select a material that is sufficiently robust against temperature changes. When the understanding of the characteristics of the fluxes (particularly when comparing rosin activated (RMA) with water-soluble fluxes) is established, we may be in a better position to combat the open joints problem due to solder wicking.

The next common problem that results open joints is lead non-coplanarity. The experiments conducted to explore this have two elements. The first of these elements is to study the effect of lead geometry design using a bond testing procedure. Secondly, using the known characteristics of the selected flux defined in solder spreading test, the effect of lead coplanarity was explored. These aim to allow modification of the lead shapes and the selection of a paste material to compensate for the gap present with coplanarity errors. The bond test procedure is used to quantify our findings. Each individual experimental method is described below followed by their results.

6.2.1 SOLDER SPREADING TEST

The Bell-Core Comb Test Pattern (TR-NWT-000078), 0.050 inch pitch; copper width, $W=0.025$ inch and length $L=1.2$ inch (fig 6.1) was used. For each flux type, a total of 3 comb test patterns were reflowed at peak temperatures of 213 deg C and 245 deg C respectively. The temperature profiles are then shown in figures reflowed at peak temperatures of 213 deg C and 245 deg C respectively. The temperature profiles are then shown in figures 6.1 and 6.2 . Prior to reflow, each comb pattern was deposited with solder paste in strip form across the bare copper trace as shown in fig 6.3

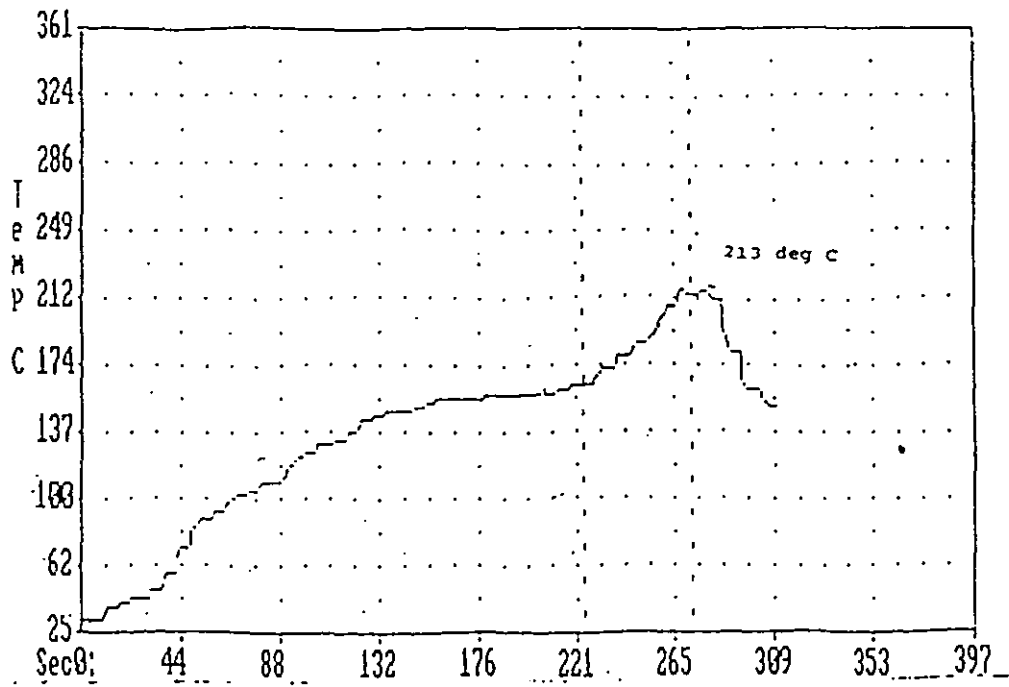


Fig 6.1 IR-reflow temperature profile at peak temperature 213 deg C

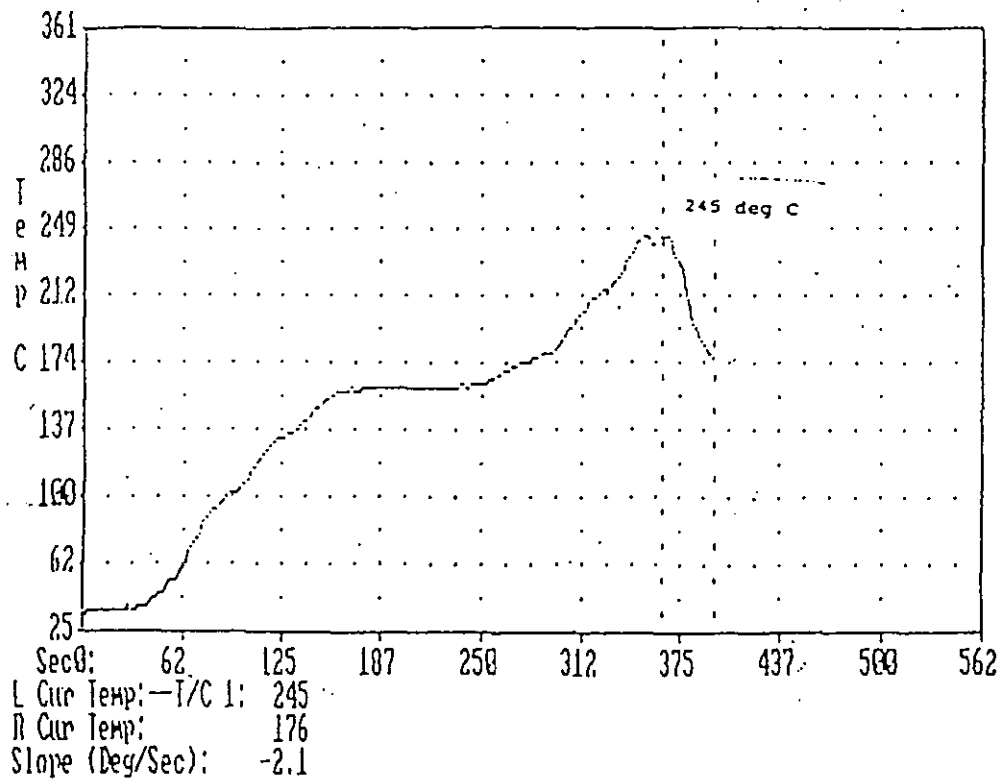


Fig 6.2 IR-reflow temperature profile at peak temperature 245 deg C

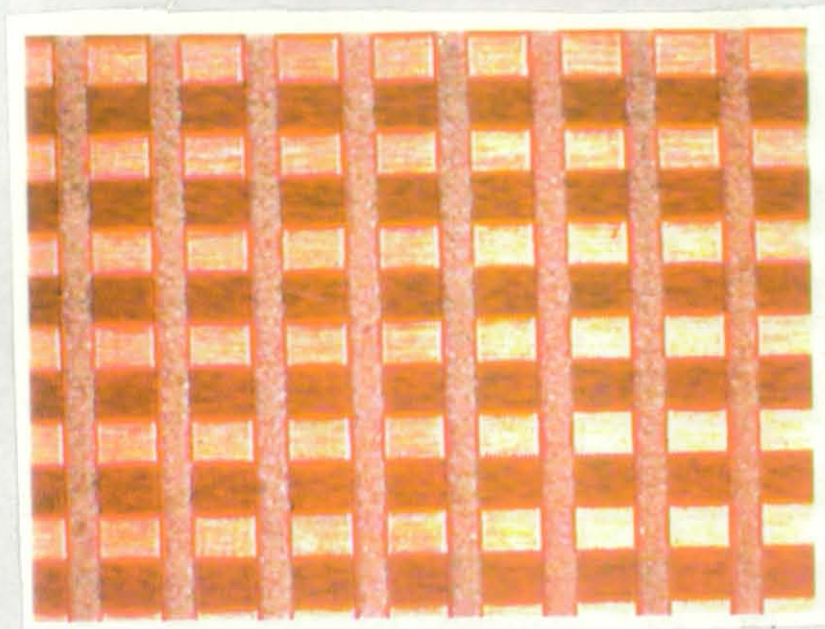


Fig.6.3 Comb Pattern Printed With Solder Paste Prior To Reflow

6.2.2 SOLDER PASTE TYPE

Three types of no-clean (i.e. rosin mildly activated, RMA) pastes and a water-soluble (i.e. Organic acid flux, OA) paste were evaluated during the study. The no-clean pastes are Kester R244 (K1), Kester R246S (K2) and Alpha 390DH3 (A1). They are blended with different activators, K1 is less active (as evidenced in the following spreading test) than K2 and A1 although they are of similar type i.e. rosin mildly activated (RMA). The water-soluble paste is known as Kester 587SA2 (K3). K & A above denote the manufacturers Kester and Alpha respectively.

6.2.3 LEAD GEOMETRY DESIGN AND BOND TEST PROCEDURE

The generic term “gull-wing”, encompasses a family of lead shapes. A commercially available gull-wing lead usually has a dihedral angle that is either positive (less-common) or negative. The outward L design is most commonly used. In this investigation, positive dihedral geometry and outward L are investigated for their robustness against lack of coplanarity, and influence on heat transfer during reflow.

A vertical pull test on the leads using the Tweezer Pull Testing procedure was used to quantify the results of both the above parameters. This test is applied to test QFP and SOIC solder bond peel force. In this instance, the lead is cut, and a tweezer on the bond tester grips the lead attached to the pad bonded. The necessary force to pull that bond apart is then determined.

6.2.4 LEAD COPLANARITY TEST

Both geometry bond and lead coplanarity tests were conducted on established PCBA models namely "A" (sound card) and "B" (CD-ROM card) respectively, while observations were on the QFPs (quad flat pack) 100 pin, 0.025 inch pitch devices. The lead coplanarity test was performed on the QFP 100 pin device on model "B", the device under test (DUT) was deliberately formed to a 0.005 inch coplanarity error at the centre and extreme corner leads of all sides of the QFP (quad flat pack) as shown later in fig.6.4. This value is known to be too large for fine pitch technology, where a maximum error of 0.003 incoplanarity is presently acceptable for assembly in the SMT industry¹⁴¹. In this experiment the device under test (DUT) was placed on the wet paste using a pick and place machine, and reflowed through the convection oven. Inspection was carried after reflow on the pre-assigned non-coplanar leads as mentioned above.

Boards were screen printed using the reduced aperture presented in Fig 5.4.

Reflow Conditions

The reflow conditions are set up according to the paste suppliers recommendations.

Preheat:

The heat-transfer process begins as the PCB assembly enters the oven tunnel at ambient temperature. To reduce the risk of component thermal shock and PCB delamination, a heating rate of less than 4 deg C per second for the first 100 degrees of preheat was used. A soak period is initiated upon reaching 100 to 120 degrees C (with RMA fluxes), the board temperature is maintained for 180 to 200 seconds to allow energy to transfer throughout the assembly. During the preheat stage, activators initiate scrubbing and some solvents begin to evaporate, flux activators may begin oxide reduction at this stage.

Preflow:

As the temperature of the interconnections is brought to just below the solder melting point, fluxes are fully activated and wetting begins. The temperature range and duration of this stage can vary

according to the paste manufacturer's formulation and recommendation. However, in this investigation the RMA fluxes become fully activated in a reflow soak at a temperature between 150 degrees C and 170 degrees C. This phase typically lasts for one minute but may vary according to individual manufacturer's formulations.

Reflow:

As the solder paste temperature exceeds the solder alloy's melting point and the former material becomes molten, the assembly enters the reflow stage. Both Kester R244 and Alpha 390 DH3 are 63/37 eutectic solder (the most commonly used alloy in SMT) and the molten stage occurs at 183 degree C. During this stage, all solderable portions of the assembly reach their desired peak temperature. Both Kester and Alpha Metal recommend bringing the interconnect temperature about 15 degrees C to 25 degrees C above the alloy melting point to achieve full liquidous, ensure good solder reflow and aid fillet formation. The amount of time a solderable interconnect remains above the melting point of the solder is called the "dwell at liquidous". This period extends through reflow and into cool-down until the solder reaches solidus. This dwell was kept between 20 seconds to 50 seconds in both experiments, care was taken to minimize the temperature

exposure of the assembly.

Cool-down :

After the assembly reaches peak temperature it begins to cool, eventually dipping below the point at which the solder solidifies. Cooling was accelerated using fans at the exit of the oven. the cooling rate was kept below 4 degree C per second in order to avoid thermal shock.

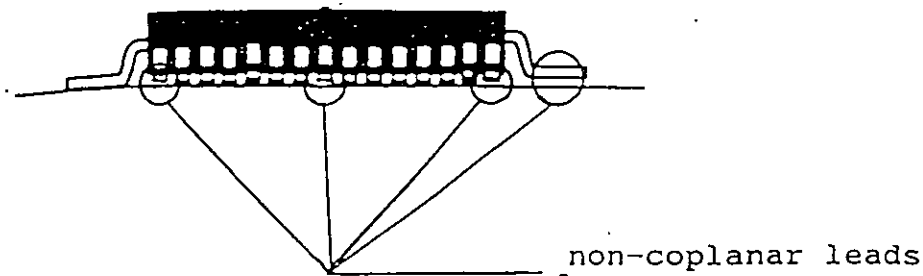


Fig. 6.4 Pre-assigned non-coplanar leads at centre and two extreme corners of the QFP (quad-flat-pack).

6.3 RESULTS AND ANALYSIS

6.3.1 SOLDER SPREADING TEST

Table 6-1 summarises the results of the spreading test. These record the number of unions of more than three solder droplets on the test

coupons after reflow. This method was adopted because in high activity pastes, solder tends to spread further across the copper strips and make an union (adhere) with adjacent solder droplets.

Flux Types		K1	K2	K3	A1
Temp	213	31	28	2	66
deg.C	245	40	107	1	94

K1 - Kester R244 (RMA) K2 - Kester 246S (RMA)

K3 - Kester 587 SA (OA) A1 - Alpha 390 DH3 (RMA)

Table-6-1 Number of Unions Observed In Spreading Test On Comb Pattern

The categorical data analysis (Ref. 146) using the chi-squared test for contingency table at 95 percent confidence level, revealed the following:

Chi-Squared	D.F	Significance
17.0188	3	7.00471E ⁻⁴

The high value of chi-squared and the small significance level

suggest that the fluxes make a significant difference in the level of performance in terms of solder spreading and wetting. Figure 6.5 to 6.12 show the test coupons themselves, showing particularly the effect of using RMA fluxes.

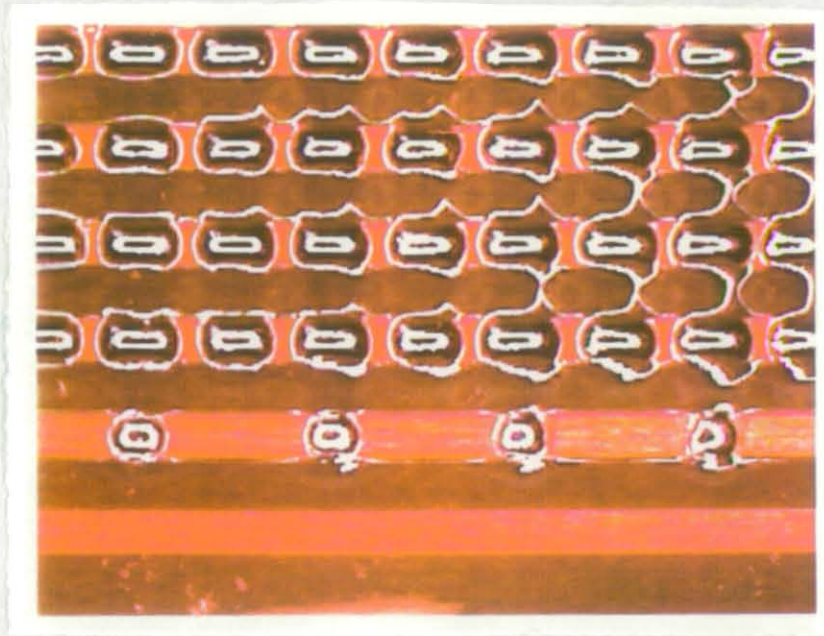


Fig. 6.5 K1 reflow at 213 deg C

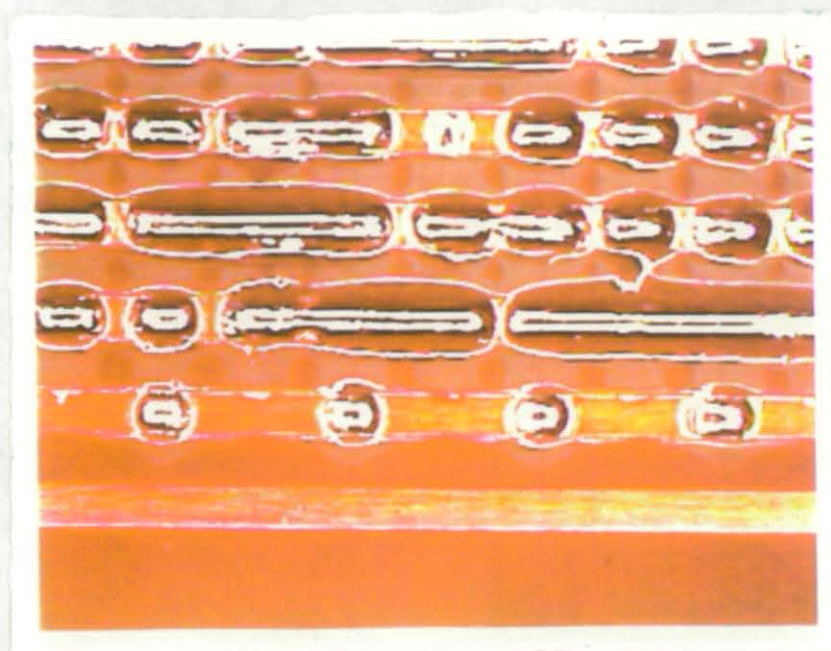


Fig. 6.6 K1 reflow at 245 deg C

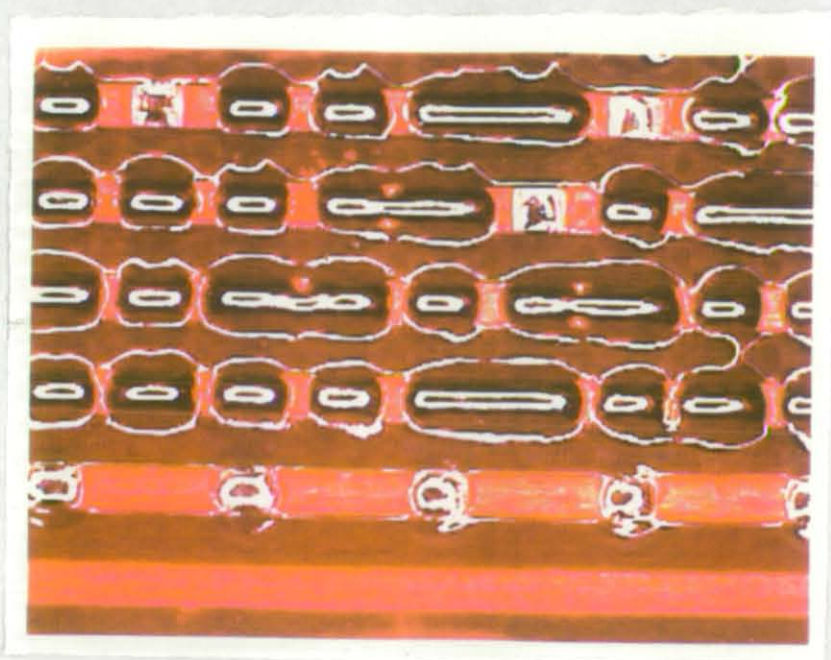


Fig.6.7 K2 reflow at 213 deg C

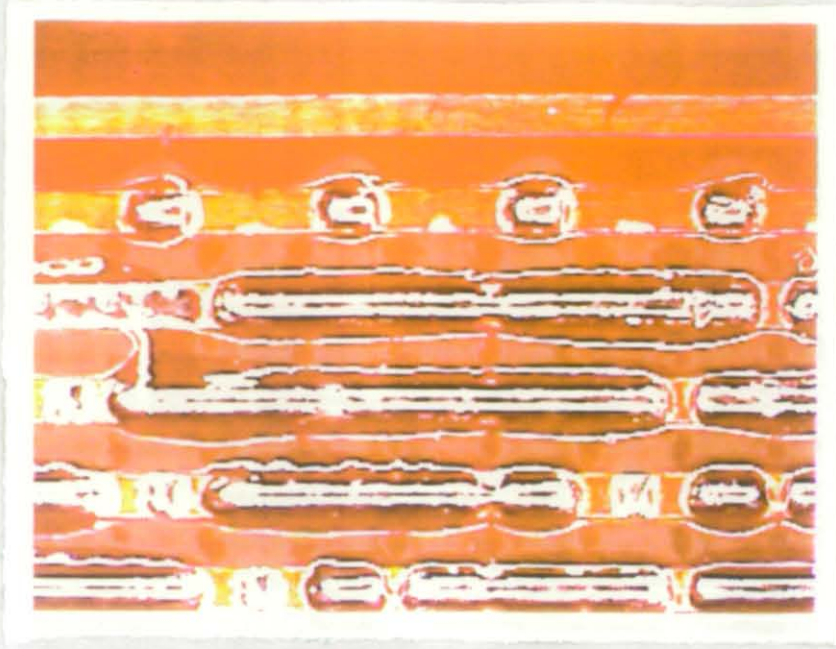


Fig.6.8 K2 reflow at 245 deg C



Fig. 6.9 K3 reflow at 213 deg C

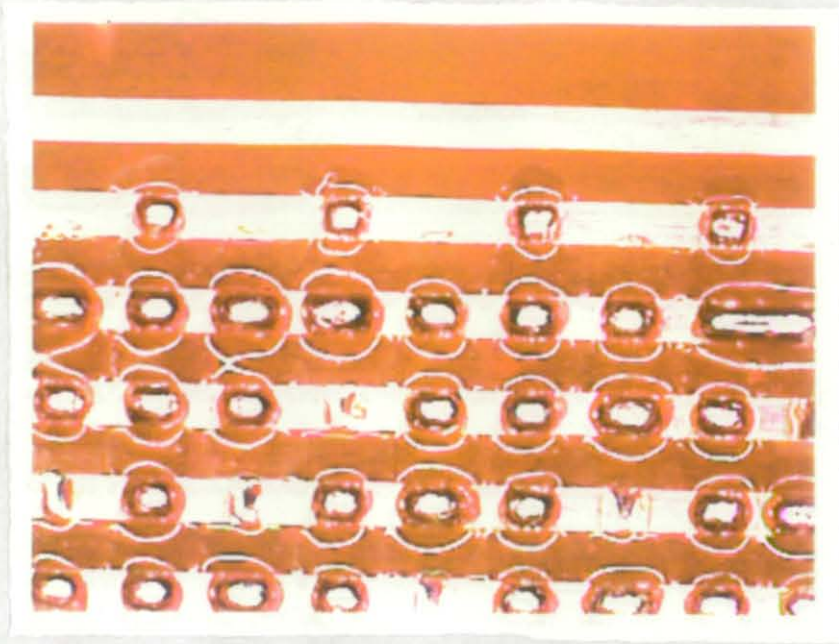


Fig. 6.10 K3 reflow at 245 deg C

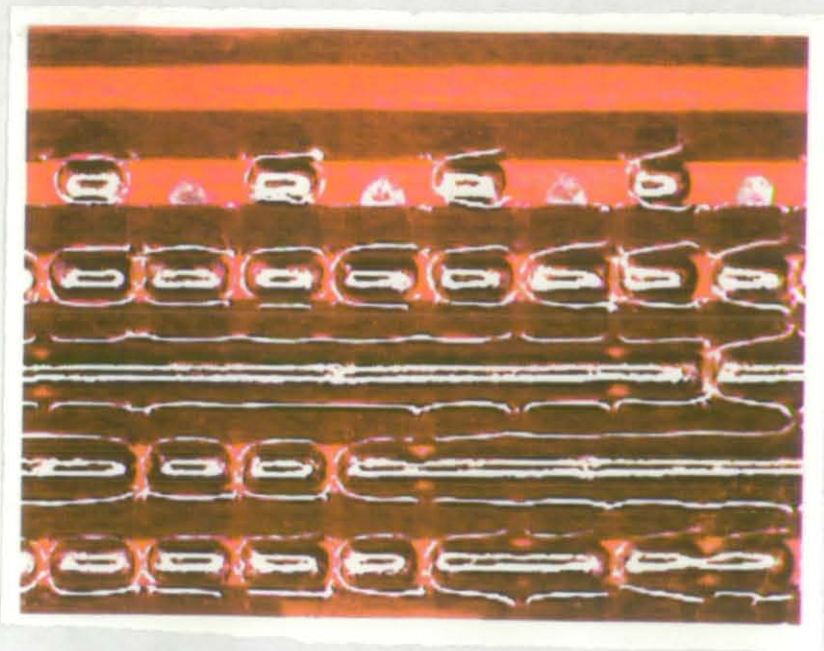


Fig. 6.11 A1 reflow at 213 deg C

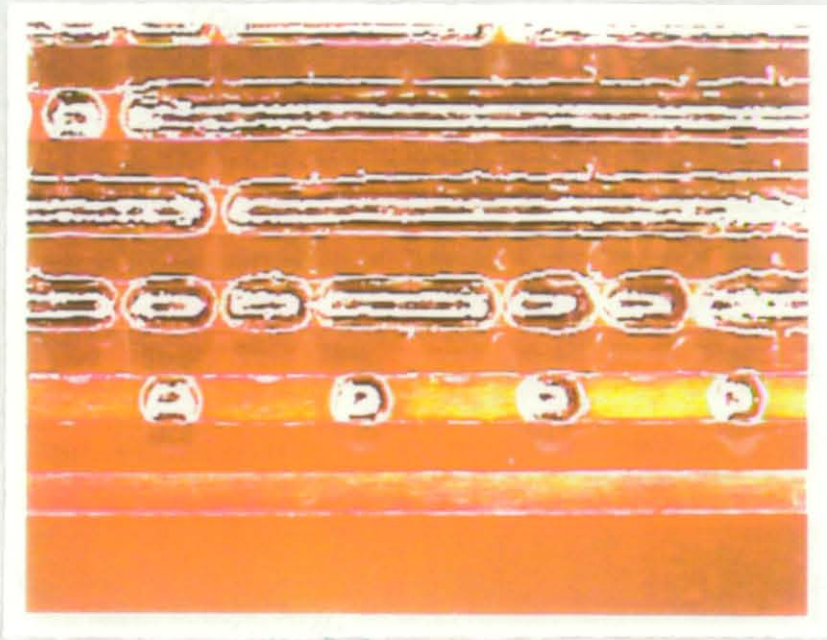


Fig. 6.12 A2 reflow at 245 deg C

6.3.2 BOND TESTING WITH RESPECT TO SOLDER PASTES

Lead Pull tests were conducted after reflow on both Kester and Alpha pastes, in both cases the RMA flux was used and the results are as follows:

Table 6-2

Two-Sample analysis on pull strength test

	Kester (K1)	Alpha (A1)	Pooled
Sample statistics	R244	390DH3	
Number of observations	41	46	87
Average (lbf)	3.00976	3.95217	3.508
Variance	0.163402	0.33144	0.252
Std. Deviation	0.404231	0.575708	0.502
Median	3	4	3.4

Conf. Interval for Difference in means: 95 percent

Hypothesis Test for Ho: Different = 0 Computed t-statistic = -8.734

Vs Alternate: Not Equal

Sig. Level = 2.60136E-7

at Alpha Risk = 0.05

so reject Ho.

The significance (sig.) level value measures whether the t-statistic is significantly greater than 1, small significance levels (less than 0.05 for most practical applications) indicates that there is a difference in pull test results due to the difference in fluxing conditions.

6.3.3 BOND TESTING WITH RESPECT TO LEAD GEOMETRIES

The lead shape of the SOIC and QFP were specially formed with a positive dihedral angle at about 40 degrees as shown in 6.4. The maximum dihedral angle that is specified currently is 0 to 10 degrees. This modify dihedral angle was anticipated to change the wetting behaviour significantly to reduce open joints. The experiment was carried out on fresh dummy QFPs and recycled SOIC and QFP devices. Two types of fluxes (both Rosin Mildly Activated, RMA) namely Kester and Alpha used in the evaluations.

Analysis

The One-Way Analysis of Variance (ANOVA) procedure adopted here analyzes the effect of positive dihedral gull-wing lead angle on bond strength (dependent variable). Also, a widely used procedure for comparing all pairs of means - the multiple range test developed by Duncan (1955), is also included in the analysis.

Table 6-3 One-Way ANOVA

Analysis of Variance					
Source of variation	Sum of square	d.f	Mean Square	F-ratio	Sig.Level
Between groups	75.083	7	10.726	16.66	0.0000
Within groups	36.928	56	0.660		
Total (corrected)	112.012	63			

0 missing values have been excluded

The high F-ratio (greater than 1) and small value of significance level (less than 0.05) indicates that the respond variable i.e bond strength is significantly influenced by the classification factor i.e gull-wing's dihedral angle.

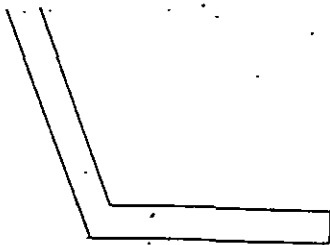


Fig. 6.13 Gull-Wing Outward L

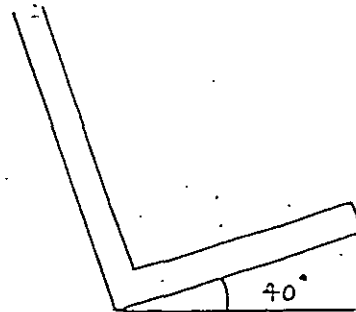


Fig. 6.14 Gull-Wing Outward L (with positive dihedral)

Duncan Multiple Range Test¹³

Method: 99 percent confident interval.

Level	Count	Average	Homogenous Groups
Kester QFP (F)	8	2.96	*
Kester QFP (R)	8	3.59	**
Alpha QFP (R)	8	3.79	**
Alpha QFP (F)	8	4.43	*
Alpha SOIC (R)	8	5.46	*
Kester SOIC (R)	8	5.56	*

F denotes fresh and R denotes recycled

Table 6-4. Test matrix for lead shapes and solder paste types.

Description	Lead Geometry Designs	
	Outward L	Outward L (Positive Dihedral)
Kester QFP (fresh)	yes	-
Kester QFP (recycle)	yes	-
Kester SOIC (recycle)	-	yes
Alpha QFP (fresh)	yes	-
Alpha QFP (recycle)	yes	-
Alpha SOIC (recycle)	-	yes

In comparing all pairs of means, the multiple range test revealed that gull-wing lead formed with dihedral angle yielded a much higher bond strength (i.e. 5.46 to 5.56 lbf) than the traditional outward-L, regardless of solder paste type and/or whether ICs are fresh or recycled.

6.3.4 LEAD COPLANARITY TEST

In this experiment, the QFP 100 of model B (CD-ROM card) was examined after reflow. The QFP's pin location at 1, 13, 30, 31, 41, 50, 51, 67, 80, 81, 90 and 100 were deformed to simulate the non-coplanar lead problem. The results after IR-reflow are follows:

Kester R244 (K1) - Examination of all the joints with a test probe showed that the joints were intact and soldered (fig.6.15a-e).

Alpha 390DH3 (A1) - All pins remain lifted i.e. Open circuit (fig.6.16a-e)



Fig. 6.15a-d, Lead Coplanarity Test for Solder Paste K1

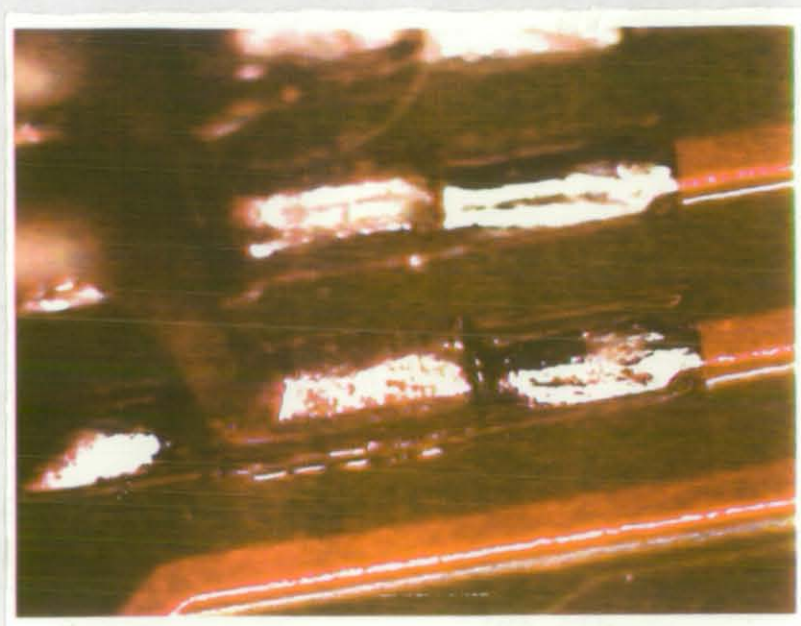


Fig. 6.15e, Close up view of Lead Coplanarity Test for Paste K1



Fig. 6.16a-d, Lead Coplanarity Test for Solder Paste Al



Fig. 6.16e, Close Up View of Lead Coplanarity Test For Paste Al

6.4 Discussions and Recommendations

6.4.1 SOLDER SPREADING

From the spreading test on the comb patterns, we observed Kester R244 (K1, no clean RMA) and 587SA2 (K3, water-soluble OA) were robust against temperature change for solder spreading and that the kinetics of the moving contact line were limited and hence the extent of solder spreading. This in turn, suggested that potentially the above fluxes are capable of providing a delayed wetting action. Understanding of this mechanism is deemed critical in paste selection in order to reduce open joints and insufficient solder (wicking). This finding is significant, if we examined the thermal model^{66,136} as follows. The heat distribution of a gull-wing lead is that the heel of the lead tends to heat up much more quickly than the toe during IR-reflow. As a result, a significant amount of solder can be attracted to the heel, thus leaving a gap between the pad and the lead. During the tests presented here, Kester R244 (K1) appeared to be less active than Kester R246 (K2) and Alpha 390 DH3 (A1). This has a major effect on both the bond strengths and lead coplanarity faults as discussed in the following sections.

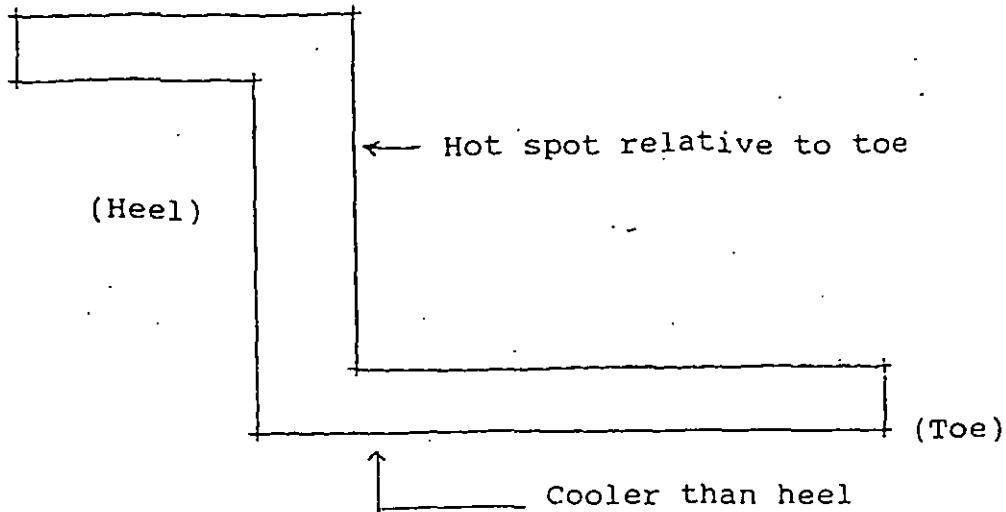


Fig. 6.17 Thermal Distribution of Gull-Wing During Reflow

In this experiment, it is interesting to observe wetting with the water-soluble flux (OA, organic acid) is insensitive to temperature changes (as evident in fig. 6.9 & 6.10). With the OA flux, melting is clearly completed before the solder spreads to any significant extent leaving sufficient solder on the pad.

6.4.2 BOND TEST WITH RESPECT TO SOLDER PASTES

Two-Sample analysis for the bonding test between Kester R244 (K1) & Alpha 390DH3 (A1) on the actual production boards revealed a higher pull strength achieved by Alpha 390DH3 (A1), typically 1 lbf above Kester R244 (K1) perhaps due to higher flux

activity increasing the wetting action. This phenomenon is evident in the solder spreading test, where Alpha 390 DH3 has 107 solder droplets unions at 245 degree C (peak) compared to Kester R244 which has less (i.e. 40) unions. Hence, we can deduce higher flux activity will result in greater bonding strength between the leads and the pad under the condition that the leads are free from coplanarity problems and that the geometry of the joints is the same.

6.4.3 THE INTERRELATIONS OF BOND STRENGTH, SOLDER FILLETS, LEAD GEOMETRIES AND SOLDER SPREADING

As component pitches become finer and finer, the requirement for easily solderable surfaces is a key issue. The smaller the solder fillet volumes, the more important the influence of lead geometry interfacial and surface properties of the joint on strength and fatigue performance.

In this work the Vertical Pull Test as used in the semi-conductor industry has been used to provide an indication of the integrity of the bonds between the solder pad and the lead. The test has demonstrated the significant differences in strength for the

experiments described here. These variations may be due to macroscopic joint geometry variations (for example when comparing the modified dihedral angle joints with conventional gull-wings), microscopic variations such as fillet geometry differences and microstructural variations such as intermetallic formation at the lead interface.

From micro-sections of joints produced, fillet shape is shown to have a large effect on the strength in the pull test. Both the toe and heel fillets vary with lead shapes i.e. either traditional outward-L or one with dihedral angle. It is observed that the gullwing lead with dihedral angle has a greater tendency to form concave fillet - the process has transformed from lead surface to point soldering. In general, the concave fillets are shown to have consistently higher fatigue lives than convex fillets with similar radii ¹⁴⁵. Also the pull strength for leads with the modify dihedral angle is typically 1 to 2 lbf higher as seen in the pull test experiment.

Solder spreading has a significant effect on joint fillet formation. As the liquid metal (molten solder) on the pads begin to wet the leads, there is a change in interfacial energy due to the changes in the interfacial areas.¹³⁸ The wetting motions typically serve to

decrease the potential energy of the liquid on the lead. In the experiments reported here, it is our intention to control this rate of reduction of potential energy using the results of solder spreading test which shows that some pastes provide delayed wetting. The objective is therefore to reduce the speed of the wetting action in order to minimize the rush of solder to the heel of the lead. Also, the leads with the dihedral angle reduce the thermal mass of the pad. As the toe of the lead is not in contact with the pad. This reduces the thermal demand of the pad and allows pad to heat up more quickly to a temperature similar to that of the lead. Hence, there will be sufficient solder on the joint to form the solder fillets even if it is hoped in the presence of coplanarity errors.

6.4.4 BOND TESTING WITH RESPECT TO LEAD SHAPES

The result of bond testing reported in Sec. 6.3.3 revealed the significance of gull-wing leads with increased dihedral angles and demonstrated the importance of design for solderability. The average pull strength ranges from 4.9 lbf to 5.3 lbf in contrast to the traditional outward L with an average value of 3 lbf to 4 lbf. The key feature of the modified gull-wing is that it has a dihedral angle (positive) which is less sensitive to lack of coplanarity, and that is more likely to penetrate solder paste deposits. This promotes

an improved wetting action during the reflow stage, and more importantly it can avoid some of the floating phenomenon associated with solid-liquid surface tensions observed by Boettinger, Handwerker, Kattner⁷⁵ and Whalley, Conway, Kalantry,¹⁴² which occur during lead insertion through the molten solder because the modified lead shape allows lead penetration and submergence into the wet paste. This enables the paste to go round the lead prior to reflow, as opposed to the traditional outward-L design which rests on top of the paste.

6.4.5 LEAD COPLANARITY TEST

As a consequence of the observations made in the solder spreading experiment, this test was carried out to ascertain effect of flux activity on the lead coplanarity problem. As described in Sec.6.2.4, the device under test (DUT) i.e QFP 100 pin was deliberately formed to 0.005 inch coplanarity, which is typically too large for successful reflowing in present fine pitch technology.

Kester R244 (K1), which appeared to be less active in solder spreading and bond tests experiment, is capable of providing a delayed wetting action, giving sufficient time for homogeneous

heating between the heel and the pad. This resulted in reduced opens as evidenced in Sec. 6.3.4, fig. 6.15a-e and proved to be less sensitive to lead coplanarity problems and solder wicking. Fig. 6.15e (a close up view of the joint after reflow using Kester R244) shows clear evidence of the solder fillet following the lead contour, despite the 0.005 inch coplanarity gap. Fig. 16e (a close up view of the joint after reflow using Alpha 390 DH3) shows that the gap remains.

6.4.6 MICROSECTION OF BONDED AREA

The appearance of lead joint with dihedral angle and its cross-section are shown in Figs.6.18 & 6.19 respectively. It can be seen that the solder joint conforms well to IPC-601B workmanship standard (The Institute for Interconnection and Packaging Electronic Circuits). There are sufficient solder fillets at the toe and heel of the lead making it a good joint.

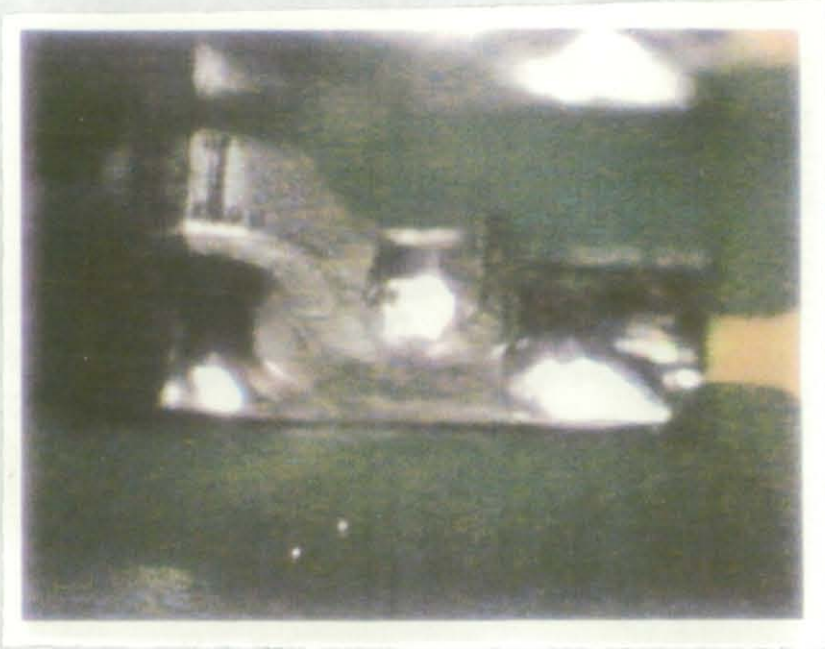


Fig. 6.18 Solder Joint of Gull-Wing Lead With Dihedral Angle

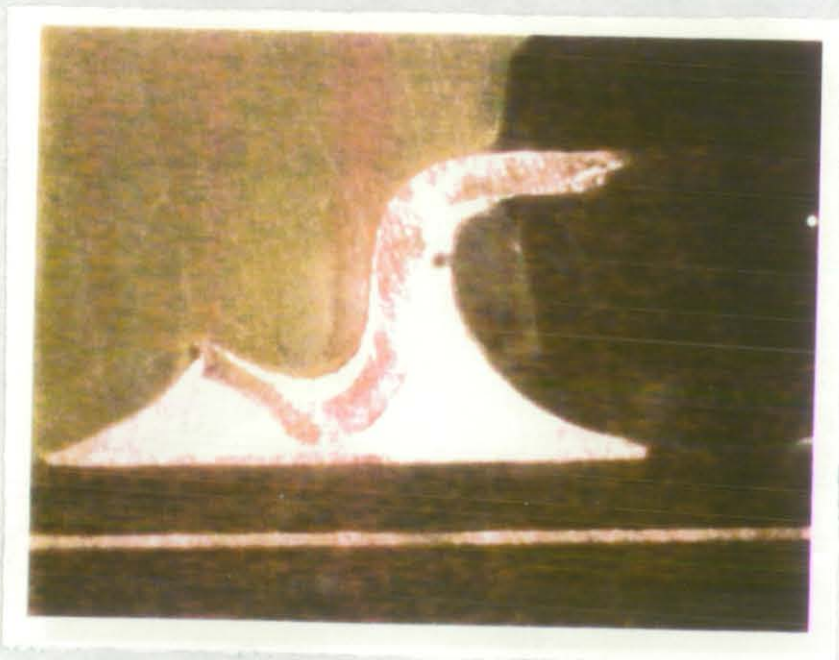


Fig. 6.19 Cross-Section of Gull-Wing Lead Bonded Area

Figures 6.20 and 6.21 show a solder joint with a coplanarity defect and its cross-section results produced with Kester R244, the wetting action of the flux on the tin-lead coating of the lead sharply reduces, inhibits wicking of both the flux and, therefore, the solder. In spite of the presence of the lead coplanarity problem prior to reflow, the delayed wetting action of the flux allow more time for the pads to heat up to a temperature similar to that of the leads so that much of the molten solder remains at the lead/pad interface to compensate for the gap (as seen in figures 6.20 and 6.21) and eliminate the risk of an open joint.

Figures 6.22 and 6.23 show the microsection results of an outward-L lead joint produced with Kester 587SA2 water soluble flux. Unlike the RMA flux shown in the solder spreading test, this has a much lower mobility of flow, because the water soluble flux restricts movement of contact line which reduces the solder wicking action and leaves sufficient amount of solder on the pad.

Figures 6.24 and 6.25 show results of attempting to solve a coplanarity error with Alpha Metal 390DH3 (RMA with more aggressive activators). The gap on the lead/solder interface remains and causes an open joint. This may be due to the much more

aggressive activator used in 390DH3. This increases the flow of the molten solder to cover the entire pad quickly (the pad length is longer than the toe of the lead) leaving insufficient solder on the pad to compensate for the gap. This rapid wetting phenomena is also shown in solder spreading test.



Fig. 6.20 Lead Joint With Coplanarity Defect After Reflow Using Kester R244



Fig. 6.21 Cross-Section of Lead Joint With Coplanarity Defect Using Kester R244

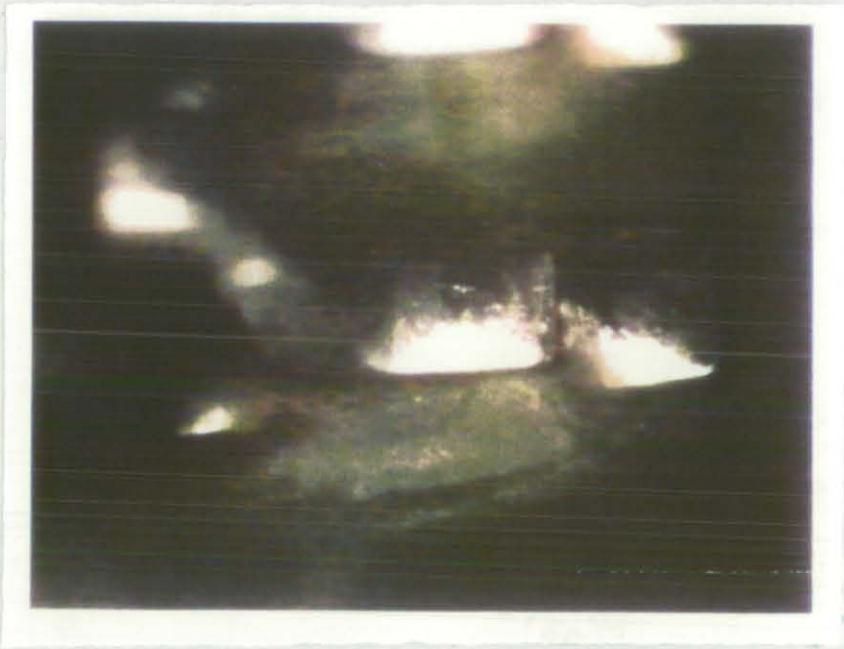


Fig. 6.22 Lead Joint Of Outward-L Using Kester 587SA Water-Soluble Flux

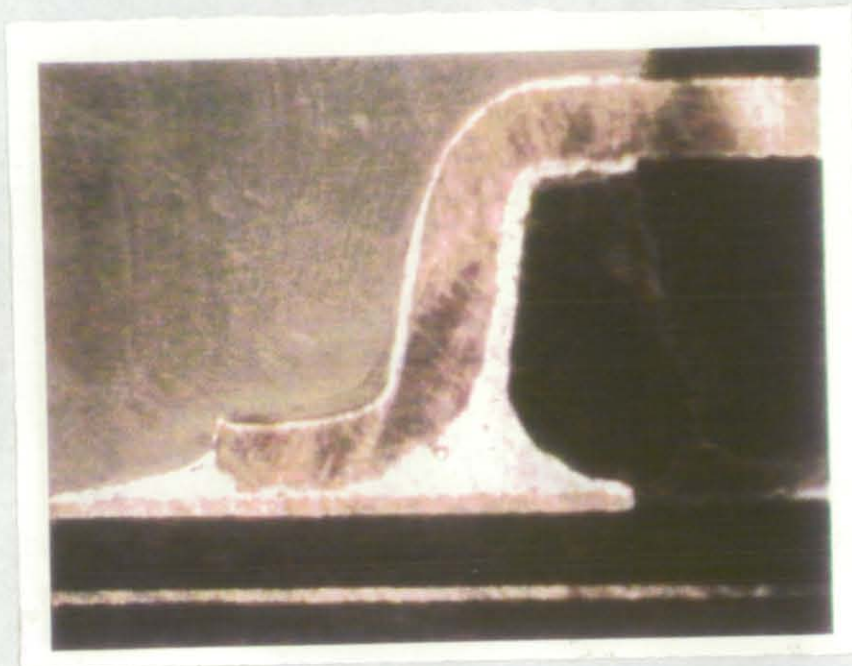


Fig. 6.23 Cross-Section Of Outward-L Lead Joint Using Kester 587SA
Water-Soluble Flux

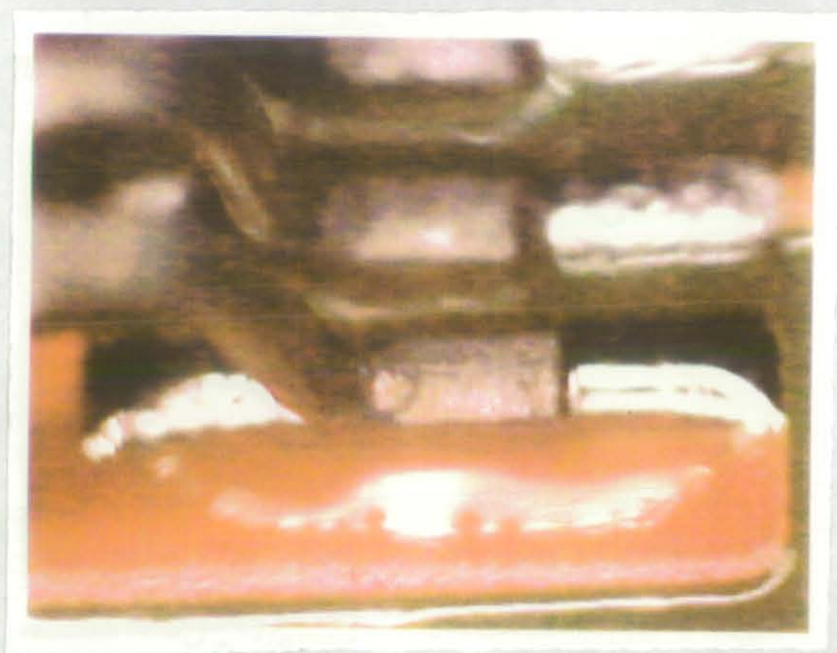


Fig. 6.24 Lead Joint Of Outward-L Using Alpha Metal A390DH3
RMA Flux



Fig. 6.25 Cross-Section Of Outward-L Lead Joint Using Alpha Metal
A390DH3 RMA Flux

6.5 CONCLUSION

Open joints are becoming a serious problem with fine leads. The primary causes are a lack of coplanarity and solder wicking. The lack of coplanarity indicates that some of the leads are above the pads allowing an open joint. Wicking may cause open joints if

enough solder is wicked up the lead to remove the required solder from the joint. To address these problems, alternate dihedral geometries for lead shape design are recommended as they are less sensitive to lack of coplanarity and more likely to penetrate solder deposits, improve thermal transfer from the lead to the solder paste (as the leads are embedded in the paste) and thus promote ease of soldering.

The worst effect of poor solderability is an open solder joint, which results when there is too much space between the device lead tip and its pad on the PCB. This commonly occurs with solder wicking^{134,137}, i.e. the solder climbs up the lead, creating an open joint. The experiment described here on solder spreading has indicated the importance of this phenomenon on the incidence of flow driven open joints.

In the case of solder wicking, the flux in the paste is attracted to the hottest area - the heel of the lead. When the lead temperature has risen above the melting point of the paste alloy i.e. 183 degree C, the solder follows, thus leaving the pad with very little solder. This phenomena is particularly significant for Rosin Mildly Activated flux (RMA) but not water soluble (OA) flux, as the latter is less

mobile than the former as revealed in the solder spreading test. Fluxes with delayed wetting actions seem less likely to lead to wicking and are more tolerant of coplanarity errors. Further work is necessary to establish the effect of fillet geometry and intermetallic formation on observed bond strength particularly in fatigue.

Due to the complexities of the packaging of IC's device vendors cannot be expected to eliminate coplanarity problems. However preforming lead geometries with an increased positive dihedral angle may avoid solder joints due to coplanarity problems. The key here is a fundamental change in soldering methodology i.e. from traditional lead surface towards point soldering. This fundamental change is proved to be forthcoming for example solder ball reflow in Ball Grid Array (BGA) and Direct Chip Attach (DCA) packages. The traditional outward-L lead in quad flat pack (QFP) package has yielded defect levels significantly higher than BGA package, typically 6000 ppm for a QFP of 0.4 mm pitch versus 0.5 to 0.3 ppm in BGA¹⁶. The microsection results show no abnormality in the joint structure formed by the modified methods. The joints produced proved to have greater joint strength than the traditional outward-L in the vertical pull test. The cross-section results shown here have supported the theoretical consideration that led to the work in this chapter and have contributed to our understanding of open formation in solder joining and necessary actions for process improvement.

Chapter Seven

Conclusions

7.0 Introduction

This thesis has focused on the successful formation of the solder joints. The empirical work presented in this thesis helped to define a number of key stencil aperture, screen printing, soldering and package lead design parameters in support of the reduction of manufacturing problems. The thesis has also investigated four major types of soldering defects. Methods of statistical analysis have been used to set up a practical experimental scheme, in which the number of experiments is relatively small to explore the significance of the parameters. Significant insights have been obtained from the analysis of the experimental results. The results show that successful soldering depends strongly on the understanding of the science of fluid and surface physics, including phenomena driven by liquid surface tension gradients, solder spreading and the thermodynamics of wetting. These are the major factors determining the solder joint quality (assuming that the soldering parameters are within the boundaries conventionally applied in industry). Because of the quality levels demanded, improvement in the reduction of the number of soldering defects can be achieved only by careful consideration of the present analytical models combined with rigorous empirical work. This approach can lead to many improvements in the SMT processes. The following sections summarises solutions to the most common soldering defects that arise from the understanding generated in this

research. This chapter summarises the contribution of the thesis to the reduction of solder faults and the basis of each innovation and closes with a discussion of further work.

7.1 The Solder Bridge Problem

In recent years, many researchers have constructed mathematical computational models of solder bridges i.e. either one or multiple - pad bridges^{76,93,94,107,125,138}. These efforts sought by computational means or mathematical search for a local optimal point, to provide guidelines on which board and joint layout could be based to design against solder bridging. However, these models have many underlying assumptions that over-simplifying the problem, for example the widths of pad and lead are chosen to be equal^{93,94}. This assumption inevitably weakens the proposed solutions and they therefore may not be sufficient robust in a mass production environment. However, the understanding from these models in combinations with experiments carried out in real production situations has led to the innovation described in Chapter 5, Section 5.2. This print process modification by stencil aperture redesign allows a much wider process window both in the pre-reflow processes of print setup and placement tolerance and makes the screen printing process less critical to the formation of the solder joint. This practical contribution is firmly grounded in the application of a scientific understanding of fluid and surface physics relevant to bridging phenomenon. The capillary pressure gradient resulting from the modified screened solder deposit drives bridge liquid away from the neck of the lead towards lower pressure regions at the pad. This mechanism causes bridges to snap or become unstable and thus reduces the incidence of bridges.

7.2 The Insufficient Solder Problem

In this thesis, an effort has been made to correct a misconception held by SMT users with respect to the solder bridge and insufficient solder process faults are events that are mutually exclusive and that they therefore can be controlled by adjusting screen printing process parameters alone to change the volume of solder paste applied. Careful observation during the initial experiments described in Chapter 3, showed the volume of solder forming a bridge is typically drawn from adjacent leads or its own lead and as a result solder bridges and insufficient solder faults occur concurrently. This observation was further confirmed by Whalley's computational model¹⁰⁷ and quantified by the detailed empirical work described in Chapter Four. The regression models presented in this chapter suggest that the solder bridge and insufficient solder (wicking) faults are strongly correlated. This new understanding of the defect origin, supported the formulation of guidelines for stencil design to avoid solder bridging by reducing the length of stencil aperture relative to the length of pad, as has been presented in Chapter Five.

This design is successful because the modified force patterns due to surface tension and the liquid surface tension gradients (Marangoni motion) facilitate bridge breaking by serving as added perturbations to the bridge surface when in unstable condition and prevent it from forming a permanent defect. This in turn prevents the formation of a correlated insufficient solder fault by allowing optimise paste deposition.

7.3 The Open Circuit Joints Problem

“Open joint” is a term used to describe the gap that can occur between a component lead and a printed circuit board (PCB) pad after solder reflow. It is commonly found both in the laboratory (Singer, 1994)¹²⁵ and in the mass production environment. Wicking of solder away from the joint can lead to open joints. The consequences of wicking are perhaps most severe when wicking occurs at a joint which are not coplanar with other leads. In this situation an open joint is a distinct possibility.

In Chapter Six, the characteristics of solder wicking phenomena for both water-soluble (i.e. organic acid flux, OA) and no-clean (i.e. rosin mildly activated, RMA) pastes were investigated. Wicking was found to be particularly significant with rosin mildly activated flux (RMA) but not for water soluble (OA) flux, i.e. the solder spreading test reported in Chapter Six, Section 6.2.1 shows that the reflowing solder travels less far and more slowly in the case of OA flux. No-clean fluxes therefore exhibit a delayed wetting action i.e. the movement of the reflowing solder takes place more slowly and is seen to be less likely to lead to wicking faults and thus is more tolerant of coplanarity errors. The theory behind this observation / development is based in the dynamics of the wetting process. The work that has been carried out, for example Whalley and Conway (1996)¹⁵⁴, Moon et al (1996)¹⁵⁵ and Singler et al (1996)¹⁵⁶, is considering the dynamics of single phase system (for example the motion due to solder surface tension in the presence of flux) does not accurately describe the process. These experiments, together with those of Conway indicate the importance of considering both the dynamics of the solder system and the flux system when attempting to describe the final geometry of

solder joints. This delayed wetting action inhibits wicking of both the flux and therefore, the 63/37 tin-lead solder. It allows sufficient amount of solder to stay on the pad to form a bond at the interface between the lead and pad.

7.4 The Lead Coplanarity Problem

As a result of the complexities of packaging IC devices, and the multi-machine environments within SMT assemblers it is difficult for package vendors and users to eliminate coplanarity problems at source. However on site modification of gull-wing lead geometries to produce a positive dihedral angle as presented in Chapter Six, Section 6.3.3 may solve the long-standing problem of the successful soldering of leads that lack coplanarity. The main feature of this modification is a fundamental change in the soldering process towards point soldering.

7.5 The Component Lead Misalignment Problem

This problem was found to be significant during the survey of the performance of Singapore-Based SMT plants described in Chapter Three. Various techniques to correct misalignment of chip component with respect to solder pad geometry have been discussed by Kress and Warwick(1985)¹³², Singler(1994)⁷⁶ and Ellis and Masada(1990)¹³⁸.

This thesis however indicates the application of a novel vibration technique to correct this fault for QFPs. An electrically operated vibrator was installed at the exit of the reflow oven triggered by a board exiting from the oven. This additional external vibration force helped to overcome the mass of the Quad Flat Pack packages and supported their self-centering. The evaluation in Chapter Three clearly shows the effectiveness of the use of

vibration to remedy the QFP misalignment problem seen in IR solder reflow.

7.6 Summary

This thesis has demonstrated the importance of understanding the origins of process defects in order to allow the achievement of world-class quality levels. The scientifically guided empirical approach of this work has contributed towards an understanding of defects origins in SMT. The innovations from this understanding have led to increased process robustness when compared to methods presently widely used in SMT mass production environments. The empirical approach of this thesis is in contrast to analytical modelling approaches used by many academic workers which typically require a significant number of simplifying assumptions. The work in this thesis has however been informed by the results of these approaches. The combination of the broad understanding from the models with deep empirical knowledge has led to many improvements which can be applied in the mass production environment.

7.7 Suggestions for further work

There are two main areas that can be identified for further work.

7.7.1 Further investigations into wettability from a physicochemical process perspective.

In modern interconnect technologies, there are a variety of surfaces and liquids simultaneously involved. There are often multiple metal and organic species present at a particular joint site creating a very complex physicochemical environment. The interactions which occur in the liquid state can significantly influence the structural

properties of the solder joint and ultimately its performance and reliability in the fluid.

Two fundamental physicochemical processes at the solder-substrate interface have been identified to date (Singler, 1994)⁷⁶:

1. dissolution of the substrate material, and
2. formation of an intermetallic layer between the substrate and the liquid solder (ultimately the bond between the two materials.)

It is necessary to further understand the interaction between these well understood metallurgical processes, presently inadequately described fluxing processes and joint geometry, both finally and dynamically during the formation of the solder joints.

7.7.2 There has been little research into the properties of liquid metal surfaces such as solder in the presence of oxidizing or "inert" gases. There is certainly a difference between the behaviour of a surface in the N₂ (nitrogen) soldering process and the current conventional processes. While it is well known that the solder surface tension is lowered by oxidation and that this enhances wetting generally^{88,101} other characteristics of the oxidized surface are likely to retard wetting. There is however no experimental evidence quantifying this effect. If the ultimate goal is understanding wettability at a fundamental level to advance the understanding of solderability, it is clear that this aspect of research work will be most useful and warrant a better justification for a N₂ soldering process.

Appendix A

Factorial Design

A.1 Measuring the effects of variables:

Experiments are frequently performed to measure the effects of one or more variables on a response. Factorial designs are extremely useful for this purpose and in this research, especially two-level factorial designs¹⁴⁷. The technique has been applied to a wide range of processes, including electronics assembly and soldering processes.

A.2 Factorial Designs At Two Levels (Box, Hunter & Hunter, 1978)

To perform a general factorial design, an investigator selects a fixed number of “levels” for each of a number of variables (factors) and then runs experiments with all possible combinations. If there are l_1 levels for the first variable, l_2 for the second, and l_k for the k th, the complete arrangement of $l_1 \times l_2 \times \dots \times l_k$ experimental runs is called an $l_1 \times l_2 \times l_3 \times \dots \times l_k$ factorial design. For example, a $2 \times 3 \times 5$ factorial design requires $2 \times 3 \times 5 = 30$ runs, and a $2 \times 2 \times 2 = 2^3$ factorial design 8 runs.

Of particular importance for our purpose in this research are the “two-level” factorial designs in which each variable occurs at just two levels. Such designs are especially useful at the exploratory

stage of an investigation, when not very much is known about a system and the model is still to be identified. The initial two-level pattern can be a first building block in developing structures of many different sorts. A model identification technique of great value that may be used in association with this type of design is the plotting of coefficients on normal probability paper^{147,148}. In general, a 2^k factorial design consists of all the 2^k runs (points) with levels¹⁴⁷.

$$(X_1, X_2, \dots, X_k) = (\pm 1, \pm 1, \dots, \pm 1)$$

Where every possible combination of \pm signs is selected in turn.

Geometrically the design consists of the vertices of a hypercube in K dimensions. For purposes of analysis, it is convenient to list the runs in standard order, not in the order (usually randomized) in which they were made. This standard order is obtained by writing alternate $-$ and $+$ signs in the column headed X_1 , alternate pairs $--$, $++$, in the X_2 column, alternate fours $----$, $++++$, in the X_3 , and so on.

A.3 Analysis of the Factorial Design

The main effect of a given variable as defined by Yates (1937)¹⁴⁹ is the average difference in the level of response as one moves from the low to the high level of that variable. A mathematical model (Chatfield, 1970)¹⁴⁶ for a factorial experiment will be discussed, after which the factor effects can be estimated. Then these effects will be tested to see if they are significantly large.

Suppose that factor A is investigated at r levels and factor B at c levels and that the experiment is replicated at n times. The following model is proposed to describe this situation.

$$X_{ijk} = \mu + A_i + B_j + (AxB)_{ij} + \varepsilon_{ijk}$$

$$(i=1, \dots, r \quad j=1, \dots, c \quad k=1, \dots, n),$$

where μ = over-all average,

A_i = effect of A at i th level,

B_j = effect of B at j th level,

$(AxB)_{ij}$ = joint influence of A at i th level and B at j th level ; that is the interaction effect.

ε_{ijk} = random error.

Since μ is the over-all average it can be shown that

$$\sum_i A_i = \sum_j B_j = 0.$$

It can also be shown that

$$\sum_j (AxB)_{ij} = 0 \text{ (for all } i \text{) and}$$

$$\sum_i (AxB)_{ij} = 0 \text{ (for all } j \text{)}$$

It is again convenient to assume that the errors are normally distributed with mean zero and constant variance σ^2 , and successive errors are independent. The data can be tabulated in the following way.

Table A-1

		Factor B			Row total	Row average
		Level 1	Level 2 Level c			
Factor A	Level 1	$x_{111} \dots x_{11n}$	$x_{121} \dots x_{12n}$	$x_{1c1} \dots x_{1cn}$	T_1	x_1
	Level 2	$x_{211} \dots x_{21n}$	$x_{221} \dots x_{22n}$	$x_{2c1} \dots x_{2cn}$	T_2	x_2
	Level r	$x_{r11} \dots x_{r1n}$	$x_{r21} \dots x_{r2n}$	$x_{rc1} \dots x_{rcn}$	T_r	x_r
	Column total	T_1	T_2	T_c		
	Column average	x_1	x_2	x_c		

The following quantities are calculated as shown:

$$x_i = \frac{T_i}{nc} \quad x_j = \frac{T_j}{nr}$$

$$T = \sum_i T_i = \sum_j T_j$$

$$x = \frac{T}{nrc}$$

T_{ij} = (sum of observations in (i,j)th cell),

$$x_{ij} = (\text{average observation in (i,j)th cell}) = \frac{T_{ij}}{n}$$

It can be shown that the best unbiased estimates of the model

parameters are given by:

$$\mu = x.$$

$$A_i = x_i - x \quad \beta_j = x_j - x.$$

$$(AxB)_{ij} = x_{ij} - x_i - x_j + x.$$

The next step is to test the main effects of the two factors and the interaction effect to see if any of them are significantly large. The best way of doing this is by an analysis of variance. The total sum of squares, $\sum(x_{ijk} - \bar{x})^2$, is partitioned into four components. Two of these components, the row sum of squares and the column sum of squares, have the same value. In addition the interaction sum of squares is calculated. The required formulae are given below.

Table A-2

Two-factor ANOVA with interaction.

Source	Sum of square	d.f	E(mean square)
Main effect A (rows)	$nc \sum_i (x_i - \bar{x})^2$	r-1	$\sigma^2 + nc \sum \frac{A_i^2}{r-1}$
Main effect B (columns)	$nr \sum_j (x_j - \bar{x})^2$	c-1	$\sigma^2 + nr \sum \frac{\beta_j^2}{c-1}$
Interaction	$n \sum_{i,j} (x_{ij} - x_i - x_j + \bar{x})^2$	(r-1)(c-1)	$\sigma^2 + n \sum \frac{(AxB)_{ij}^2}{(r-1)(c-1)}$
Residual	$\sum_{i,j,k} (x_{ijk} - x_{ij})^2$	rc(n-1)	σ^2
Total	$\sum_{i,j,k} (x_{ijk} - \bar{x})^2$	rcn-1	

The observed mean squares of the different effects are obtained by

dividing the appropriate sum of squares by the appropriate number of degrees of freedom. The expected values of these mean squares are shown above. It is clear from these quantities that the A, B , and interaction mean squares should be compared with the residual mean square by means of an F -test. For example, to test the hypothesis

$$H_{01}: \text{all } A_i = 0,$$

$$\text{calculate } F = \frac{\text{A mean square}}{\text{Residual mean square}}$$

If this exceeds $F_{0.05, r-1, re(n-1)}$, then H_{01} is rejected at the 5 per cent level. A similar procedure is adopted to test the hypotheses

$$H_{02}: \text{all } B_j = 0 \quad H_{03}: \text{all } (A \times B)_{ij} = 0.$$

We will not attempt to derive the algebraic quantities shown in table A-2. However it is worth stressing that the total sum of squares is equal to the sum of other sums of squares. Similarly the total number of degrees of freedom is equal to the sum of constituent degrees of freedom.

The computation proceeds as follows. Calculate the row totals, the column totals, the individual cell totals and the over-all total. Also calculate $\sum_{i,j,k} x_{ijk}^2$ and the correction factor T^2/nrc .

$$\text{Total corrected sum of squares} = \sum (x_{ijk} - \bar{x})^2 = \sum x_{ijk}^2 - \frac{T^2}{nrc}$$

$$\text{Row sum of squares} = nc \sum_{i=1}^r (x_i - \bar{x})^2 = \frac{\sum_{i=1}^r T_i^2}{nc} - \frac{T^2}{nrc}$$

$$\text{Column sum of squares} = nr \sum_{j=1}^c (x_j - \bar{x})^2 = \frac{\sum_{j=1}^c T_j^2}{nr} - \frac{T^2}{nrc}$$

$$\text{Residual sum of squares} = \sum (x_{ijk} - x_{ij})^2 = \sum x_{ijk}^2 - \frac{\sum_{i,j} T_{ij}^2}{n}$$

The interaction sum of squares can then be obtained by subtraction.

Appendix B

One-way Analysis of Variance (ANOVA) and Duncan's

Multiple Range Test¹⁴⁴

B.1 One-Way Analysis of Variance (ANOVA)

This section describes a method of testing the hypothesis that there is no difference between a number of treatments. The total variation of the observations is partitioned into two components, one measuring the variability between the group means, x_1, x_2, \dots, x_c and the other measuring variation within each group. These two components are compared by means of an F -test.

The procedure of comparing different components of variation is called the analysis of variance. In the above situation the observations are divided into mutually exclusive categories and this is called a one-way classification. We then have a *one-way analysis of variance*. It is a little more complicated than the range test but is often more efficient and has the advantage that a similar technique can be applied to more complex situations where the observations are classified by two or more criteria.

We have already seen that the combined estimate of σ^2 from the variation within groups is given by

$$S^2 = \sum_{i=1}^c \frac{s_i^2}{c} = \sum_{i=1}^c \sum_{j=1}^n \frac{(x_{ij} - x_i)^2}{c(n-1)}$$

and this is based on $c(n - 1)$ degrees of freedom.

We now look at the variation between groups. The observed variance of the treatment means is given by

$$\sum_{i=1}^c \frac{(x_i - \bar{x})^2}{c-1}$$

If the null hypothesis is true, this is estimate of σ^2/n , since the standard error of the treatments means will be σ / \sqrt{n} . Thus

$$S_B^2 = n \sum_{i=1}^c \frac{(x_i - \bar{x})^2}{c-1}$$

is an estimate of σ^2 based on $c - 1$ degrees of freedom.

If H_0 is true both s^2 and S_B^2 are estimates of σ^2 and the ratio $F = \frac{S_B^2}{S^2}$ will follow an F-distribution with $c - 1$ and $c(n - 1)$ degrees of freedom. On the other hand, if H_0 is not true, s^2 will still be an estimate of σ^2 but S_B^2 will be increased by the treatment of differences and so the F-ratio may be significantly large. In this case, we reject H_0 and conclude that there is evidence of a difference between the treatment effects.

The usual way to obtain the F-ratio is to calculate the following quantities and enter them in what is called an analysis of variance (ANOVA) table.

Table B-1

One-way ANOVA

Source of variation	Sum of squares	d.f	Mean square
Between groups (between treatments)	$n \sum_{i=1}^c (x_i - \bar{x})^2$	c-1	S_b^2
Within groups (residual variation)	$\sum_{i=1}^c \sum_{j=1}^n (x_{ij} - x_i)^2$	c(n-1)	S^2
Total variation	$\sum_{i=1}^c \sum_{j=1}^n (x_{ij} - \bar{x})^2$	cn-1	

The two mean squares s and s^2 , are obtained by dividing the appropriate sum of squares by the appropriate number of degrees of freedom.

An important feature of the ANOVA table is that the total sum of squares is equal to the sum of the between-group and within-group sum of squares. This can be shown as follows. We have

$$x_{ij} - \bar{x} = (x_{ij} - x_i) + (x_i - \bar{x})$$

Squaring both sides and summing over all values of i and j , we find

$$\sum_{i,j} (x_{ij} - \bar{x})^2 = \sum_{ij} (x_{ij} - x_i)^2 + \sum_{i,j} (x_i - \bar{x})^2 + 2 \sum_{i,j} (x_{ij} - x_i)(x_i - \bar{x}).$$

However the sum of the cross product terms is zero since

$$\sum_{i=1}^c \sum_{j=1}^n (x_{ij} - x_i)(x_i - \bar{x}) = \sum_{i=1}^c \{(x_i - \bar{x}) \sum_{j=1}^n (x_{ij} - x_i)\}$$

and $\sum_{j=1}^n (x_{ij} - x_i) = 0$ for each i .

$$\text{Also } \sum_{i=1}^c \sum_{j=1}^n (x_i - x)^2 = n \sum_{i=1}^c (x_i - x)^2$$

and we have the required result.

Another important feature of the ANOVA table is that the total number of degrees of freedom is equal to the sum of the between group and within group degrees of freedom. The actual computation proceeds as follows.

Firstly calculate the group totals T_i ($i = 1$ to c) and the over-all total

T . Hence find the group means \bar{x}_i ($i = 1$ to c) and the over-all mean \bar{x} .

Also calculate $\sum_{i,j} x_{ij}^2$, which is sometimes called the total uncorrected sum of squares. Secondly calculate the total sum of squares (sometimes called the total corrected sum of squares) which is given by

$$\sum_{i,j} (x_{ij} - x)^2 = \sum_{i,j} x_{ij}^2 - cnx^2 = \sum_{i,j} x_{ij}^2 \frac{T^2}{cn}.$$

The quantity cnx^2 or T^2/cn is sometimes called the correction factor.

Thirdly calculate the between group sum of squares which is given

by

$$n \sum_{i=1}^c (x_i - x)^2 = n \sum_{i=1}^c x_i^2 - cnx^2 = \frac{1}{n} \sum_{i=1}^c T_i^2 - \frac{T^2}{cn}$$

Note that the same correction factor is present. Lastly the residual sum of squares can be obtained by subtraction.

B.2 Follow-up Study of The Treatment Means By Duncan's Multiple Range Test [Duncan,1955].

A widely used procedure for comparing all pairs of means is the multiple range test developed by Duncan (1955)¹⁴⁴. To apply Duncan's multiple range test for equal sample sizes, the treatment averages are arranged in ascending order, and the standard error of

each average is determined as: $S_{y_i} = \sqrt{\frac{MSE}{\eta}}$

For unequal sample size, replace in the above equation by the

harmonic mean η_h of the η_i , where $\eta_h = \frac{a}{\sum_{i=1}^a (1/n_i)}$.

Note that if $n_1 = n_2 = \dots = n_a$, then $\eta_h = n$. From Duncan's table of significant ranges, obtain the values $r_\alpha(p, f)$ for $p = 2, 3, \dots, a$, where α is the significant level and f is the number of degrees of freedom for error. Convert these ranges into a set of $a - 1$ least significant ranges (e.g., R_p) for $p = 2, 3, \dots, a$ by calculating

$$R_p = r_\alpha(p, f) S_{y_i} \quad \text{for } p = 2, 3, \dots, a.$$

Then, the observed differences between means are tested, beginning with largest versus smallest, which would be compared with the least significant range R_a . Next, the difference of the largest and the second smallest is computed and compared with the least significant range R_{a-1} . These comparisons are continued until all

means have been compared with the largest mean. Finally, the difference of the second largest mean and the smallest mean is computed and compared against the least significant range R_{a-1} . This process is continued until the differences of all possible $a(a - 1)/2$ pairs of means have been considered. If an observed difference is greater than the corresponding least significant range, then we conclude that the pair of means in question is significantly different. To prevent contradictions, no differences between a pair of means are considered if the two means involved fall between two other means that do not differ significantly.

Duncan's test requires a greater observed difference to detect significantly difference pairs of means as the number of means included in the group increases. For two means, the critical value R_2 will always exactly equal the LSD value from the t test. The values $r_\alpha(p, f)$ in Duncan's table are chosen so that a specified protection level is obtained. That is, when two means that are p steps apart are compared, The protection level is $(1 - \alpha)^{p-1}$, where α is the level of significance specified for two adjacent means. Thus, the error rate is $1 - (1 - \alpha)^{p-1}$ of reporting at least one incorrect significant difference between two means when the group size is p .

Generally, if the protection level is α , then tests on means have a significance level that is greater than or equal to α . Consequently,

Duncan's procedure is quite powerful; that is, it is very effective at detecting differences between means when real differences exist.

For this reason, Duncan's multiple range test is very popular.

Appendix C

Regression Analysis

C.1 Simple Linear Regression (Montgomery, 1991) ¹⁵⁰

To determine the relationship between a simple regressor variable x and a response variable y . The regressor variable x is usually assumed to be a continuous variable that is controllable by the experimenter. Then if the experiment is designed, we choose the values of x and observe the corresponding value of y .

Suppose the true relationship between x and y is a straight line, and that the observation y at each level of x is a random variable. Now the expected value of y for each value of x is

$$E(y/x) = \beta_0 + \beta_1 x \quad \text{c-1}$$

where the parameters of the straight line β_1 and β_2 are unknown constants. We assume that each observation y can be described by the model

$$y = \beta_0 + \beta_1 x + \varepsilon \quad \text{c-2}$$

where ε is a random error with mean zero and variance σ^2 . The $\{\varepsilon\}$ are also assumed to be uncorrelated random variables. The regression model (Equation c-2) involving only a single regressor variable x is often called the *simple linear regression model*.

If we have n pairs of data $(y_1, x_1), (y_2, x_2), \dots, (y_n, x_n)$, we may estimate the model parameters β_0 and β_1 by least squares. By

Equation C-2, we may write

$$y_i = \beta_o + \beta_1 x_i + \varepsilon_i \quad i=1,2,3,\dots,n$$

and the least squares function is

$$L = \sum_{i=1}^n \varepsilon_i^2 = \sum_{i=1}^n (y_i + \beta_o + \beta_1 x_i)^2 \quad \text{c-3}$$

Minimizing the least squares function is simplified if we rewrite the

model, equation C-2, as

$$y = \beta'_o + \beta_1(x_i - x) + \varepsilon \quad \text{c-4}$$

where $x = \left(\frac{1}{n}\right) \sum_{i=1}^n x_i$ and $\beta'_o = \beta_o + \beta_1 x$. In equation C-4 we have simply corrected the regressor variable for its average, resulting in a

transformation on the intercept. Equation C-4 is frequently called

the transformed simple linear regression model or, more simply, the

transformed model. In addition to simplifying the estimation

problem, use of the transformed model allows other inference tasks

to be performed more easily. By employing the transformed model, the

least squares function becomes

$$L = \sum_{i=1}^n [y_i - \beta'_o - \beta_1(x_i - x)]^2 \quad \text{c-5}$$

The least squares estimators of β'_o and β_1 , say $\hat{\beta}'_o$ and $\hat{\beta}_1$, must satisfy

$$\frac{\partial L}{\partial \beta'_o, \beta_1} = -2 \sum_{i=1}^n (y_i - \beta'_o - \beta_1(x_i - x)) = 0$$

$$\frac{\partial L}{\partial \beta_1, \beta_o, \beta_1} = -2 \sum_{i=1}^n [y_i - \beta'_o - \beta_1(x_i - x)](x_i - x) = 0$$

Simplifying these two equations yields

$$n\beta'_0 = \sum_{i=1}^n y_i \quad \text{c-6}$$

$$\beta_1 \sum_{i=1}^n (x_i - \bar{x})^2 = \sum_{i=1}^n y_i (x_i - \bar{x})$$

Equations C-6 are called the least squares normal equations. Their

solutions are $\beta'_0 = \frac{1}{n} \sum_{i=1}^n y_i = \bar{y}$ c-7

$$\beta_1 = \frac{\sum_{i=1}^n y_i (x_i - \bar{x})}{\sum_{i=1}^n (x_i - \bar{x})^2} \quad \text{c-8}$$

Thus, β'_0 and β_1 are the least squares estimators of the intercept and slope, respectively.

The fitted simple linear regression model is

$$y = \beta'_0 + \beta_1(x_i - \bar{x}) \quad \text{c-9}$$

If we wish to present our results in terms of the original intercept, β_0 ,

then $\beta_0 = \beta'_0 + \beta_1 \bar{x}$

and the fitted model is $y = \beta_0 + \beta_1 x$ c-10

Rotationally, it is convenient to give special symbols to the numerator and denominator of Equation C-8. That is, let

$$S_{xx} = \sum_{i=1}^n (x_i - \bar{x})^2 = \sum_{i=1}^n x_i^2 - \frac{\left(\sum_{i=1}^n x_i\right)^2}{n} \quad \text{c-11}$$

and

$$S_{xy} = \sum_{i=1}^n y_i(x_i - \bar{x}) = \sum_{i=1}^n x_i y_i - \frac{\left(\sum_{i=1}^n x_i\right)\left(\sum_{i=1}^n y_i\right)}{n} \quad \text{c-12}$$

We call S_{xx} the corrected sum of squares of x and S_{xy} the corrected sum of the cross-products of x and y . The extreme right-hand sides of Equations C-11 and C-12 are the usual computational formulas. Using this new notation, the least squares estimator of the slope is

$$\beta_1 = \frac{S_{xy}}{S_{xx}} \quad \text{c-13}$$

estimators. consider first β_1 . The expected value of B_1 is

$$\begin{aligned} E(\beta_1) &= E\left(\frac{S_{xy}}{S_{xx}}\right) = \frac{1}{S_{xx}} E\left[\sum_{i=1}^n y_i(x_i - \bar{x})\right] = \frac{1}{S_{xx}} E\left[\sum_{i=1}^n (\beta_0 + \beta_1(x_i - \bar{x}) + \varepsilon_i)(x_i - \bar{x})\right] \\ &= \frac{1}{S_{xx}} \left\{ E\left[\beta_0 \sum_{i=1}^n (x_i - \bar{x})\right] + E\left[\beta_1 \sum_{i=1}^n (x_i - \bar{x})^2\right] + E\left[\sum_{i=1}^n \varepsilon_i (x_i - \bar{x})\right] \right\} = \frac{1}{S_{xx}} \beta_1 S_{xx} = \beta_1 \end{aligned}$$

since $\sum_{j=1}^n (x_j - \bar{x}) = 0$, and by assumption $E(\varepsilon_j) = 0$. Thus, β_1 is an

unbiased estimator of the true slope β_1 . Now consider the variance of

$$\beta_1. \text{ Since we have assumed that } V(\varepsilon_j) = \sigma^2, \text{ it follows that } V(y_i) = \sigma^2, \text{ and } V(\beta_1) = V\left(\frac{S_{xy}}{S_{xx}}\right) = \frac{1}{S_{xx}^2} V\left(\sum_{j=1}^n y_j(x_j - \bar{x})\right) \quad \text{(C14)}$$

The random variable y_i are uncorrelated because the ε_i are

uncorrelated. Therefore, the variance of the sum in equation C-14 is

just the sum of the variance of each term in the sum, say $V[y_i(x_i - \bar{x})]$

$$\text{, is } \sigma^2 (x_i - \bar{x})^2. \text{ Thus, } V(\beta_1) = \frac{1}{S_{xx}^2} \sigma^2 \sum_{i=1}^n (x_i - \bar{x})^2 = \frac{\sigma^2}{S_{xx}} \quad \text{(C15)}$$

By using a similar approach, we can show that $E(\beta_0') = \beta_0'$

$$V(\beta_0') = \frac{\sigma^2}{n} \quad (\text{C16}) \quad \text{and} \quad E(\beta_0) = \beta_0 \quad V(\beta_0) = \sigma^2 \left[\frac{1}{n} + \frac{\chi^2}{S_{xx}} - \right] \quad (\text{C17})$$

To find $V(\beta_0)$, we must make use of the result $\text{Cov}(\beta_0', \beta_1) = 0$.

However, the covariance of β_0 and β_1 is not zero; in fact,

$\text{Cov}(\beta_0, \beta_1) = -\sigma^2 \chi / S_{xx}$. Note that β_0' and β_0 are unbiased estimators of β_0' and β_0 respectively.

It is necessary to obtain an estimate of σ^2 . This estimate may be obtained from the residuals $e_i = y_i - \hat{y}_i$. The sum of the squares of the residuals, or the error sum of squares, would be

$$SS_E = \sum_{i=1}^n e_i^2 = \sum_{i=1}^n (y_i - \hat{y}_i)^2 \quad \text{c-18}$$

A more convenient computing formula for SS_E may be found by substituting the estimated model $\hat{y}_i = \bar{y} + \beta_1(\chi_i - \chi)$ into Equation C-18 and simplifying as follows:

$$\begin{aligned} SS_E &= \sum_{i=1}^n [y_i - \bar{y} - \beta_1(\chi_i - \chi)]^2 \\ &= \sum_{i=1}^n [y_i^2 + \bar{y}^2 + \beta_1^2(\chi_i - \chi)^2 - 2y_i\bar{y} - 2\beta_1 y_i(\chi_i - \chi) - 2\beta_1 \bar{y}(\chi_i - \chi)] \\ &= \sum_{i=1}^n y_i^2 + n\bar{y}^2 + \beta_1^2 S_{xx} - 2\bar{y} \sum_{i=1}^n y_i - 2\beta_1 S_{xy} - 2\beta_1 \bar{y} \sum_{i=1}^n (\chi_i - \chi) \end{aligned} \quad \text{c-19}$$

The last term in Equation C-19 is zero, $2\bar{y} \sum_{i=1}^n y_i = 2n\bar{y}^2$, and

$\beta_1^2 S_{xx} = \beta_1 (S_{xy} / S_{xx}) S_{xx} = \beta_1 S_{xy}$. Therefore Equation C-19 becomes

$$SS_E = \sum_{i=1}^n y_i^2 - ny^2 - \beta_1 S_{xy}$$

But $\sum_{i=1}^n y_i^2 - ny^2 = \sum_{i=1}^n (y_i - y)^2 \equiv S_{yy}$, say, which is just the corrected

sum of squares of the y 's. so we may write SS_E as

$$SS_E = S_{yy} - \beta_1 S_{xy}$$

By taking expectation of SS_E , we may show that $E(SS_E) = (n - 2)\sigma^2$.

Therefore, $\sigma^2 = \frac{SS_E}{n - 2} \equiv MS_E$

is an unbiased estimator of σ^2 . Note that MS_E is the error or residual

mean square.

Appendix D

The relationship between the normal, χ^2 , t and F-distributions¹⁴⁶

The χ^2 distribution

If X is $N(0,1)$ then the random variable $Y = X^2$ is said to be a χ^2

random variable with one degree of freedom. In the general case, if

X_1, X_2, \dots, X_n are independent $N(0,1)$, then $Y = \sum_{i=1}^n X_i^2$ is said to be

a χ^2 random variable with n degrees of freedom. Thus, if $X_1, X_2, \dots,$

X_n are independent $N(\mu, \sigma^2)$, then

$$Y = \sum_{i=1}^n \left(\frac{x_i - \mu}{\sigma} \right)^2$$

is also a χ^2 random variable with n degrees of freedom.

This distribution is useful in many situation including the following; if

x_1, \dots, x_n is a random sample size n from $N(\mu, \sigma^2)$, where μ is

unknown, then the sampling distribution of

$$\sum_{i=1}^n \left(\frac{x_i - \bar{x}}{\sigma} \right)^2 = \frac{(n-1)s^2}{\sigma^2}$$

is χ^2 with $(n-1)$ degrees of freedom. One degrees of freedom is 'lost'

by substituting \bar{x} for μ , as this places one linear constraint on the

values of $(x_i - \bar{x})$.

The p.d.f. of a χ^2 distribution with v.d.f. is given by

$$f(y) = \begin{cases} \frac{y^{(v-2)/2} e^{-(y/2)}}{2^{v/2} \Gamma(v/2)} & (y \geq 0) \\ 0 & \end{cases}$$

This distribution, in which v must be a positive integer, is a special case of the gamma distribution. Its means and variance are equal to v and $2v$ respectively. It is always skewed to the right, but tends to the normal distribution as $v \rightarrow \infty$.

The t-distribution

If X is $N(0,1)$, Y is χ^2 with v.d.f., and X and Y are independent, then

the random variable $t = \frac{X}{\sqrt{\left(\frac{Y}{v}\right)}}$ is said to have a t-distribution with v degrees of freedom.

This distribution is useful in a number of situations, including the following: a random sample, size n , is taken from a normal distribution, mean μ and variance σ^2 . The sample mean, \bar{x} , and sample variance, S^2 , are calculated in the usual way. We know that the

sampling distribution of $\frac{\bar{x} - \mu}{\sigma/\sqrt{n}}$ is $N(0,1)$, and that the sampling distribution of $(n-1)$

s^2/σ^2 is χ^2 with $(n-1)$ d.f. Moreover it can be shown that the random variables s^2/σ^2 and \bar{x} , are independent, even though the values are calculated from the same sample. Thus the statistic

$$t = \frac{\frac{\bar{x} - \mu}{\sigma/\sqrt{n}}}{\sqrt{\frac{(n-1)s^2/\sigma^2}{n-1}}}$$

has a t-distribution with $(n-1)$ d.f.

The p.d.f. of a t-distribution is given by

$$f(t) = \frac{(1+t^2/v)^{-1/2(v+1)} \tau[1/2(v+1)]}{\sqrt{(\pi v) \tau(1/2v)}} \quad (-\infty \leq t \leq +\infty)$$

The distribution is symmetric about $t = 0$. Its means and variance are 0 and $v/(v-2)$ respectively. It tends to the normal standard distribution as $v \rightarrow \infty$.

The F-distribution

If X_1, X_2 are independent χ^2 random variables with v_1, v_2 d.f. respectively. Then the random variable $F = \frac{X_1/v_1}{X_2/v_2}$ is said to have an F-distribution with v_1 and v_2 respectively.

This distribution is useful in a number of situations including the following: two random size samples, size n_1 and n_2 respectively, are taken from a normal distribution, mean μ and variance σ^2 . The two sample variances, S_1^2 , and S_2^2 , are calculated in the usual way.

Then the sampling distribution of $\frac{(n_1-1)S_1^2}{\sigma^2}$ is χ^2 with (n_1-1) d.f., and the sampling distribution of $\frac{(n_2-1)S_2^2}{\sigma^2}$ with (n_2-1) d.f. Thus the statistic

$$F = \frac{\frac{(n_1-1)S_1^2 / \sigma^2}{n_1-1}}{\frac{(n_2-1)S_2^2 / \sigma^2}{n_2-1}} = \frac{S_1^2}{S_2^2}$$

has an F-distribution with (n_1-1) and (n_2-1) d.f.

The mean of the F-distribution is equal to $v_2/(v_2-2)$ for $v_2 > 2$. Thus the mean is very close to one for fairly large values of v_2 , and the distribution is always skewed to the

right. Upper percentage points of the distribution are given in F-table. Lower percentage

points can be found using the equation $F_{1-\alpha, v_1, v_2} = \frac{1}{F_{\alpha, v_2, v_1}}$.

Appendix E

Contingency Tables

The general two-way table will have r rows and c columns. If n observations are taken, let n_{ij} be the number of observations which fall in the i th row and j th column. ¹⁴⁶

Table-E1

$r \times c$ Two-way Table

n_{11}	n_{12}	n_{1c}	$n_{1.}$
n_{21}	n_{22}	n_{2c}	$n_{2.}$
\vdots	\vdots	\vdots	\vdots
n_{r1}	n_{r2}	n_{rc}	$n_{r.}$
$n_{.1}$	$n_{.2}$	$n_{.c}$	n

Let

$$n_{i.} = \sum_j n_{ij} = \text{number of observations in the } i\text{th row,}$$

$$n_{.j} = \sum_i n_{ij} = \text{number of observations in the } j\text{th column.}$$

Thus

$$n = \sum_i n_{i.} = \sum_j n_{.j}.$$

Generally speaking we are interested in testing the independence of the two types of classification. For this reason two-way tables are often called contingency tables because we may ask if the presence of one characteristic is contingent on the presence of another.

We can formalize the null hypothesis as follows. Let p_{ij} be the probability that an item selected at random will be in the i th row and j th column. Let $p_{i.}$ be the probability that an item will be in the

ith row and p_j the probability that an item will be in the jth column. Then the null hypothesis that rows and columns are independent is given by

$$H_0 : p_{ij} = p_i \cdot p_j \quad \text{for all } i, j.$$

It is easy to show that the maximum likelihood estimates of ρ_i and ρ_j

are given by the intuitive estimates n_i / n and n_j / n . Thus if H_0 is true an estimate of the expected frequency in the cell in the ith row and jth column is given by

$$n\rho_{ij} = n\rho_i \cdot n\rho_j = n \frac{n_i}{n} \frac{n_j}{n} = \frac{n_i n_j}{n}$$

This can be compared with the observed value n_{ij} . The test statistic is given by

$$\chi^2 = \sum_{i=1}^r \sum_{j=1}^c \left\{ \frac{(n_{ij} - n_i n_j / n)^2}{n_i n_j / n} \right\}.$$

The number of degrees of freedom is obtained as follows. As the sum of the observed and expected frequencies are equal, this results in the loss of one degree of freedom. In addition the parameters $p_{1.}, p_{2.}, \dots,$

$p_{.1}, p_{.2}, \dots, p_{.c}$ are estimated from the data. However from the first condition we must have $\sum_i \rho_i = 1 = \sum_j \rho_j$, so only $(r + c - 2)$ independent estimates have to be made. Thus the

number of degrees of freedom is given by $rc - 1 - (r + c - 2) = (r - 1)(c - 1)$.

If the value of χ^2 for a two way table is found to be significantly large then the null hypothesis must be rejected. Occasionally we will have a specific alternative hypothesis in mind; but generally a common procedure is simply to look at the data and see where large discrepancies between observed and expected frequencies occur. This may suggest a suitable hypothesis to describe the data.

Appendix F

Response Surface Method (RSM)

Response Surface Methodology consists of a set of techniques used in the empirical study of relationships between one or more measured quality responses such as yield, solder paste thickness. The sequential steps or approach in searching for the settings of the input variables that yield the optimal response value is as follow ¹⁵²:

1. Fitting the simplest form of polynomial, usually a first-degree polynomial, and testing for adequacy of fit.
2. Using the first-degree fitted model to locate higher values of the response along the path of the steepest ascent.
3. In a region where non-planarity in the surface is present, fitting additional terms such as cross product terms and/or pure quadratic terms to produce the second-degree model.
4. Using the second-degree model to map or describe the shape of the response surface in the experimental region. If it is further determined that the optimal or best value of the response is within the boundaries of the region, then we would try to locate the settings of the input variables that yield the optimal value of the response

A. The First Degree Polynomial ^{151, 152}

The first degree polynomial in K coded variables

$$Y_u = \beta_0 + \beta_1 X_{u1} + \beta_2 X_{u2} + \dots + \beta_k X_{uk} + \varepsilon_u \quad [F.1]$$

is the simplest form (lowest-degree) of equation that we would consider using. The model F.1 is appropriate when:

a) The interest is in studying the response behavior only within a limited region of the space of the K factors and where the range of response values can be approximated reasonably well by the hyperplane F.1

b) At the start of the experiment it is not known what the shape of the surface is (that is, what degree polynomial is necessary to adequately model the response) nor where the location of the best response values are. In our search for the region of the best response values, we begin with the simplest form of model in order to try to hold the number of best response required as well as the cost of the experimentation to a minimum.

To estimate the coefficients in F.1, we require data from only $N \geq k + 1$ distinct

experimental trials. Designs used for fitting the first-degree model F.1 are presented in

chapter 3. For present let us assume that data are collected at the 2^k points of a two-level

factorial arrangement in k variables where Y_u represents the observed response for the u^{th}

trial and the two levels of each coded x_i in F.1 are denoted by -1 and $+1$. [The 2^k

factorial arrangement is one of the simplest classes of designs and evolves from the desire

to look only at two levels of each factor.] Then the estimates b_0, b_1, \dots, b_k of the

coefficients in F.1 are calculated using the simple formulas

$$b_0 = \frac{1}{N} \sum_{u=1}^N Y_u = \bar{Y}$$

$$b_i = \frac{\sum_{u=1}^N x_{ui} Y_u}{\sum_{u=1}^N x_{ui}^2} = \frac{1}{N} \sum_{u=1}^N x_{ui} Y_u \quad i=1,2,3,\dots,k \quad \text{F-2}$$

since $\sum_{u=1}^N x_{ui}^2 = N$ is a sum of a series of squared ± 1 's. If only a single observation is collected at each of the 2^k points, then $N = 2^k$; otherwise, if replicates are collected at one or more points, then $N > 2^k$

With each of the k factors having two levels only, the estimates b_i , $i = 1, 2, \dots, k$ are equal to one-half the estimated factorial effects given by the difference between the average responses at the $+1$ and -1 settings of the x_{ui} 's. In other words, in F2 b_i can be expressed as

$$b_i = \frac{1}{2} [Y_{xi=+1} - Y_{xi=-1}]$$

where $Y_{xi=+1}$ and $Y_{xi=-1}$ are the average responses at $x_i = +1$ and $x_i = -1$, respectively.

Furthermore, the variance of b_0 and of the b_i is

$$Var(b_0) = Var(b_i) = \frac{\sigma^2}{\sum_{u=1}^N x_{ui}^2} = \frac{\sigma^2}{N} \quad i=1,2,\dots,k \quad \text{F-3}$$

where σ^2 is the variance of a single observation Y . It is interesting to note at this point that the $k + 1$ coefficient estimates have the same variance. This a property of the 2^k factorial design. We shall discuss these designs more in detail.

Once the estimates in F2 are obtained, they are then substituted into Eq. F1 to produce the fitted model

$$Y = b_0 + b_1x_1 + b_2x_2 + \dots + b_kx_k \quad \text{F-4}$$

Upon ascertaining the fitted model accounts for a significant amount of the variability in the observed response values, the model is then referred to as a prediction equation or a

estimation equation. Predicted values of the response are obtained using F4 by selecting values for X_1, X_2, \dots, X_k , calculating the coded values of x_1, x_2, \dots, x_k , and then by substituting the calculated values of the coded variables into F4.

We shall now work through an example consisting of two independent factors ($k + 2$) to illustrate how to calculate the coefficient estimates and their variances and to estimate the model with the form F4.

B. The Analysis of The Variance Table for Testing the Significance of the Coefficient Estimates in the Fitted Model ^{127, 152}

The results of the analysis of a set of experimental data can be displayed in a format as an analysis of variance table. The entries in the table represent measures of information about the separate sources of variation in the data values.

The total variation in the data values is called the "total sum of squares", SST, and is computed by summing the squares of the observed Y_u 's about their average value $Y = (Y_1 + Y_2 + \dots + Y_N)/N$,

$$SST = \sum_{u=1}^N (Y_u - Y)^2 \quad \text{F-5}$$

The quantity SST has associated with it $N-1$ degrees of freedom.

The total sum of squares is the sum of two quantities; the sum of squares due to regression (or accounted for by the fitted model). The formula for the sum of squares due to the regression of the fitted model containing p terms is

$$SSR = \sum_{u=1}^N (Y_u - \hat{Y})^2 \quad \text{F-6}$$

where the deviation $Y_u - \bar{Y}$ represents a measure of the difference between the value predicted by the fitted model (\hat{Y}_u) for the u^{th} observed value and overall average of the Y_u 's. The degrees of freedom associated with the SSR is the number of terms in the fitted model minus one, $p-1$.

The sum of squares not accounted for by the fitted regression model is

$$SSE = \sum_{u=1}^N (Y_u - \hat{Y}_u)^2 \quad \text{F-7}$$

which is also called the sum of squares of the residuals. The degrees of freedom for the SSE is $N-p$ which is the difference $(N-1) - (p-1) = N-p$.

The analysis of variance table displaying the total, regression, and residual sum of squares (as well as the mean squares) is shown in Table F-1.

Table F-1 The analysis of variance (ANOVA) table

Source	d.f	Sum of Squares	Mean Square
Due to regression	$p-1$	SSR	$SSR/(p-1)$
Residual	$N-p$	SSE	$SSE/(N-p)$
Total	$N-1$	SST	

The usual *test of the significance of the fitted regression equation* is a test of the null hypothesis H_0 : All of the β 's (excluding β_0) are zero against the alternative hypothesis H_A : At least one of the β 's (excluding β_0) is not zero. The test, assuming normality of the errors, involves the F statistic.

$F = \text{Mean Square Regression} / \text{Mean Square Residual}$

$$= \frac{SSR / (p - 1)}{SSE / (N - p)} \quad \text{F-8}$$

If the null hypothesis is true, the F-ratio in F8 follows an F distribution with $p-1$ and $N-p$ degrees of freedom in the numerator and denominator respectively. The value of F in F8 is compared to the table value $F_{(p-1, N-p, \alpha)}$ which is the upper 100α percent point of the F distribution with $p-1$ and $N-p$ degrees of freedom respectively. If the value of F in F8 exceeds $F_{(p-1, N-p, \alpha)}$ then the null hypothesis is rejected at the α level of significance and we infer that the coefficient estimates are not all zero (that is, one or more convey information about the surface) and the variation accounted for by the model (through the b_i 's, $i \neq 0$) is significantly greater than the unexplained variation.

An accompanying statistic to the F statistic of Eq. F8 that is often calculated in the analysis of a fitted model is

$$R^2 = \frac{SSR}{SST}, \quad \text{F-9}$$

The value of R^2 is a measure of the "proportion of total variation of the Y_i 's about the mean Y explained by the fitted regression equation." It is often expressed as a percentage by multiplying the ratio SSR/SST by 100%. One drawback to using R^2 as a criterion of the model adequacy is that as the number of parameters estimated in the model approaches the number of observations in the data set, (that is, when there are no replicate observations), the value of R^2 will approach one even if the model is not appropriate. A related statistic, called the adjusted R^2 statistic is preferred over R^2 by some workers and is

$$R_A^2 = 1 - \frac{SSE / (N / p)}{SST / (N - 1)} = 1 - (1 - R^2) \left(\frac{N - 1}{N - p} \right) \quad \text{F-10}$$

An adjustment to R^2 has been made in F10 by using the degrees of freedom

corresponding to SSE and SST. The R_A^2 statistic is a measure of the drop in the magnitude of the estimate of the error variance achieved by fitting a model other than $Y = \beta_0 + \varepsilon$ relative to the

estimate of the error variance that would be obtained by fitting the model $Y = \beta_0 + \varepsilon$.

C. Test For Lack of Fit of a First-Degree Polynomial 152, 153

Lack of fit of the fitted first degree model

$$Y = b_0 + \sum_{i=1}^k b_i x_i \quad \text{F-11}$$

can stem from the presence of non-planarity in the response surface which goes

undetected owing to the exclusion of pure quadratic (or cubic) terms in F11 such as $b_{ii} x_i^2$

(or $b_{iii} x_i^3$) from the presence of interaction effects among the experimental factors (ξ_i

and ξ_j) which is also undetectable owing to the exclusion of cross-product terms in F11

such as $b_{ij} x_i x_j x_k$. In both cases, fitting a model of the form F11 and in describing the

estimated surface as being a hyperplane, we have understated the complexity of the

response surface and as such have erred in our judgment regarding the effects of the

experimental factors on the behaviour of the response.

The test for lack of fit for the model F11 requires the following two conditions of the experimental design be satisfied:

(i) the number of distinct design points, n , must exceed the number of terms in the fitted model, that is, $n > k + 1$, and

(ii) at least 2 replicate observations must be collected at one or more of the design points unless one has an estimate of the error variance from previous experiments.

In addition, we shall assume the random errors (ϵ_u) are normal and independently distributed with a common variance σ^2 .

When conditions (i) and (ii) hold, the residual sum of squares, SSE of Eq. F7, consists of two sources of variation, The first source is due to the lack of fit of the fitted model

(which is assumed to be due to the exclusion of higher order terms in F11 and the other source is pure error variation. To partition the residual sum of squares into these sources, first the sum of squares due to the replicate observations is calculated from the replicates.

This is called pure sum error of squares (or S.S. Pure Error). The lack of fit sum of squares is obtained by subtracting the pure error sum of squares from the residual sum of squares.

To illustrate the partitioning of the residual sum of squares, let us denote the u th observation at the l th design point by Y_{lu} , where $u = 1, 2, \dots, r_l \geq 1$, and $l = 1, 2, \dots, n$.

Let us define Y_l to be the average of the r_l observations at the l th design point. Then,

$$\text{S.S. Pure Error} = \sum_{l=1}^n \sum_{u=1}^{r_l} (Y_{lu} - Y_l)^2 \quad \text{F-12}$$

and

$$\text{S.S.Lack of fit} = \text{SSE} - \text{S.S.Pure Error} = \sum_{l=1}^n r_l (Y_l - \bar{Y})^2 \quad \text{F-13}$$

where Y_l is the predicted value of the response at the l th design point produced by the fitted model F11. Furthermore, the degrees of freedom associated with the S.S. Pure Error

$$\text{is } \sum_{l=1}^n (r_l - 1) = N - n$$

where N is the total number of observations collected at the n design points, so that the degrees of freedom associated with the S.S. Lack of Fit is obtained by subtraction and is $(N-p) - (N-n) = n-p$, where $p = k + 1$ is the number of terms in F.11. The test of adequacy of the fitted model is

$$F = [\text{S.S.Lack of Fit} / (n-p)] / [\text{S.S.Pure Error} / (N-n)] \quad \text{F-14}$$

The hypothesis of adequacy fit is rejected at the α level of significance when the calculated value of F in F14 is larger than the table value of F . When the calculated value is not larger than the table value, then residual mean square is used as an estimate of σ^2 and is also used to test the significance of the fitted model.

When the hypothesis of adequacy of fit is rejected, the first-degree model is upgraded by the addition of cross-product terms and/or higher degree terms in x_1, x_2, \dots, x_k . If additional design points are required in order to estimate all of the coefficients in the revised model form, these points are added. The data is collected from these points and the analysis is redone.

D. The Path of Steepest Ascent^{127,128}

When one starts at the center of (0,0) of the experimental design, the direction of the path of steepest ascent is to move b_1 ($= +0.2125$) units in the x_1 direction for every b_2 ($= -0.7125$) units in the x_2 direction. The sizes of the step changes in the x_1 and x_2 depends

on the particular units that were used in scaling the original factor levels, X1 and X2, in defining the coded variables, x1 and x2. IN this example, the scaling units were 1/8 and 1/2, for x1 and x2, respectively. different scaling units would have resulted in a different direction for the path. For further reading on what effect the size of the scale units have on the “direction of steepest ascent.” the reader is directed to the discussion of the paper by Box and Wilson (1951).

E. Fitting a second-degree Model in the Neighbourhood of the Optimal Response Value ^{127,128}.

Let us consider the fitting of a second-degree model in K variables of the form

$$Y = \beta_o + \sum_{i=1}^k \beta_i x_i + \sum_{i=1}^k \beta_{ii} x_i^2 + \sum_{i < j}^k \beta_{ij} x_i x_j + \varepsilon \quad \text{F-15}$$

where the β_i are regression coefficients for the first-degree terms, the β_{ii} are coefficients for the pure quadratic terms, the β_{ij} are the coefficients for the cross-product terms and ε is the random error term. The pure quadratic and cross-product terms are of degree 2. The number of terms in the model of Eq.F15 is $p = (k + 1)(k + 2)/2$; for example, when $k = 2$, then $p = 6$.

Designs which are used for collecting observed values of the response for estimating the coefficients in a second-degree model of the form F15 are presented in Chapter 4. For our purposes, let us assume that observed response values are collected at the points of a second-order design and the fitted second-degree polynomial is

$$Y = b_o + \sum_{i=1}^k b_i x_i + \sum_{i=1}^k b_{ii} x_i^2 + \sum_{i < j}^k b_{ij} x_i x_j \quad \text{F-16}$$

After the fitted model of Eq. F16 is checked for adequacy of fit in the region defined by the coordinates of the design and found to be adequate, we shall proceed with the goals of locating the coordinates of the stationary point and of performing a more detailed analysis of the response system.

F. Graphical Method: Mapping the Second-Order Surface¹⁵²

The fitted second-degree model F16 can be used to generate a system of contours of the estimated surface by setting \hat{y} equal to some constant value and mapping the resulting conic in the coordinate system of x_1 and x_2 .

The plotted contours suggest that the response surface inside the experimental region is a hill. The circular nature of the contours within the experimental region of the coded variables, x_1 and x_2 , result of our having forced the experimental region to a circle of radius $\sqrt{2}$. In the system of the original factor levels, X_1 and X_2 , the contours would be ellipses.

The application of the graphical method for studying the shape of the response surface and determining the approximate location of the highest response value requires the use of a contour plotting program. A second approach that can be used to locate the coordinates of the point where the slope of the surface is zero, and which does not use contour plots, is an analytical approach.

References

1. R.Adams, P.Splitz and W.Vahel (Jan,1995), 'Impact of boundary-scan on SMT design, manufacturing, and system test', Journal of SMT, pp14-19.
2. W.E.Bernier, B.T.Ma, P.A.Mesher, A.K.Trivedi and E.J.Vytlacil; "BGA vs QFP: A summary of tradeoff for selection of high I/O components", Proc. Surface Mount Int'l Conf. and Exposition, pp.181-185.
3. R.J.Nieves. "Fine pitch manufacturing meeting the challenge", Circuit Assembly (May,1991), pp.40-48.
4. H,Hirai(1993), " Single point TAB technology for High-Pin-Count, Narrow-Lead-Pitch LSIs", Surface Mount Technology Recent Japanese Developments, Edited by Jan Vardaman, IEEE Press, pp.184-196.
5. Y.Degani, TD.Dudderar, RC. Frye, KL.Tai, Mauree Y.Lau, and Byung J.Han (1996), " Microinterconnect technology: The large-volume fabrication of cost-effective flip-chip MCMs", Flip-Chip technologies, edited by John H.Lau McGraw-Hill, pp.181-221.
6. Chang Hoon Lee(1996), " Anisotropic Conductive Flip Chip- on-Glass technology", Flip Chip Technologies, edited by John H.Lau, McGraw-Hill, pp.317-339.
7. Baba and Carlomagno(1996), "Wire-Bonding Flip Chip Technologies, edited by John H.Lau, Technology, Recent Japanese developments, Edited by Jan Vardaman, IEEE Press pp.184 - 221.
8. Kazuhisa Tsunoi, Toshihiro Kusagaya, and Hidehiko Kira (1996), "Flip Chip Mounting Using Stud Bumps and Adhesive for Evaluation", Flip Chip Technologies, edited by John H.Lau, McGraw-Hill, pp.357-386.
9. D.J.Williams, P.P.Conway and D.C.Whalley (1993), "Making circuits more than once: the manufacturing challenges of electronics intensive products", Proc Instn Mech Engrs Vol 207, pp.83-90.
10. Kenshu Oyama (1993), "Overview of placement and bonding technology for 1005 components and 0.3mm-pitch LSIs: An equipment perspective", Surface Mount Technology Recent Japanese Developments, edited by Jan Vandaman, IEEE Press pp.77-108.
11. J.R Jahn & PP. Conway(1993), " Multichip modules(MCMs): a review of the status quo", Journal of Electronics Manufacturing Vol 3, pp.1-11.

12. Williams D.J, Conway PP, Whalley DC (1992), "Challenges in the manufacture of electronics products", Proc. FAIM 92 Conference, Washington, pp.47-58.
13. Hideyuki Nishida(1993), "The transformation of interconnect technology", Surface Mount Technology Recent Japanese Developments, Edited by Jan Vardaman IEEE Press pp. 52-60.
14. J. Walshak & E.Hashemi(1994), "Current and future trends for plastics, ceramic and tape BGAs," Proceeding of Nepcon West Conference, Calif, pp.456-465.
10. Kenshuu Oyama(1993), " Overview of placement and bonding technology for 1005 components and BGAs", Proceeding of Nepcon West Conference, Calif pp. 456-465.
15. Company Compute Corporation News Letters, 1993.
16. W.E Bernier, B.T. Ma, P.A. Mesher, A.K.Trivedi and E.J Vytlacil (1993), IBM Microelectronics, " BGA Vs QFP: A summary of tradeoffs for Selection of high I/O components," SMT International Conference Proceeding pp.345-403.
17. John Houghten(March, 1994), "Capturing design advantages of BGAs", SMT pp.36-43.
18. Thomas Distefano and Joseph Fjelstand(1996), " A compliant chip-size packaging technology", Flip Chip Technologies, Edited by John Lau, McGraw-Hill pp.387-414.
19. W.Mawen(1993), " Thermal management of BGA packages", Circuit Assembly pp.11-19.
20. Akira Suzuki(1993), " Introducing TAB technology to the production site", Surface Mount Technology Recent Japanese Developments, edited by Jan Vardman, IEEE press pp.255-263.
21. Dave Perry (1991), " Inspection and evaluation of TAB tape", Circuit Assembly pp.23-29.
22. Kenzo Hatada(1993), " Latest technology trends in multichip modules", Surface Mount Technology Recent Japanese Developments, edited by Jan Vardman, IEEE Press pp. 255-263.
23. John M Goward, D.J.Williams and D.C.Whalley (1993), "Properties of anisotropic conductive adhesive pastes for fine-pitch surface mount technology", Journal of Electronics Manufacturing, Vol 3 pp.179-190.

24. ML. Buschbom, WH. Schroen, and ER. Wolfe (1993) "Fine Pitch Packaging for Surface Mount", Handbook of Fine Pitch Surface Mount Technology edited by John H.Lau, Van Nostrand Reinhold, New York pp. 55-80.
25. Puligandla Viswanadham (1993), "Reliability aspects of fine pitch assembly", Handbook of Fine Pitch Surface Mount Technology edited by John H Lau, Van Nostrand Reinhold, New York pp. 598-636.
26. Kazuhisa Tsunoi, Toshihiro Kusagaya, and Hidehiko Kira (1996), "Flip chip mounting using stud bumps and adhesive for encapsulation ". Flip Chip Technologies edited by John Lau, McGraw-Hill pp.357-366.
27. Elke Zakel and Herbert Peichi (1996), "Flip Chip assembly using Gold, Gold-Tin, and Nickel-Gold Metallurgy", Flip Chip Technologies edited by John Lau, McGraw-Hill pp.415-490.
28. Khadpe, S (1993), "A global overview of technology and market trends in TAB/Advanced Packaging", Proceedings of 5th International TAB and Advanced Packaging Symposium, ITAB, San Jose pp.1-8.
29. Zakel E, J.Kloesen, J.Distler. and H.Reichi (1993), "Flip Chip Bonding on Green Tape Ceramic Substrates", Proceedings of the 9th European Hybrid Microelectronics Conference, Nizza pp.339.
30. Totta P and K.Puttlitz (1994), "Flip chip technology, Workshop on Flip Chop (C4), TAB and BGA", Proceeding of International Flip Chip, TAB and Advanced Packaging Symposium , San Jose.
31. Harman. G (1992), "Wire-bonding towards six-sigma yield and fine pitch", Proceeding of 42nd Electronic Components and technology conference (ECTC) San Diego, pp.903.
32. Matsuki. H, M.Yoshikawa, M.Minamizawa, T.Hamano, and K.Muratake.(Sept,1994), "High density and high performance AIN SPGA Package for VLSI", Proceeding of the Technical Conference, International Electronics Packaging Conference, IEPS, Atlanta pp.308.
33. ST Baba and WD. Carlomagno (1996), "Wire-Bonding Flip Chip Technology for Multichip Modules", Flip Chip Technologies, edited by John Lau, McGraw-Hill pp.341-356.
34. Jarada.S and R.Satoh (May, 1990), " Mechanical Characteristics of 96.5 Sn/3.5 Ag Solder in micro-bonding", IEEE 1990 Proceeding of the 40th Electronic Components and Technology Conference, IEEE Press, pp.510-517.

35. Vaynman.S, "Fatigue life prediction of solder material: Effect of ramp time, hold time and temperature", *ibid* (ref. 3) pp.505-509.
36. K.Tsunoi, T.Kusagaya, and H.Kira (1996), "Flip Chip Mounting using Stud bumps and adhesive for encapsulation", *Flip Chip Technologies* edited by John Lau, McGraw-Hill .pp.12-366.
37. Rao RT, and EJ. Rymaszewski (1991), *Microelectronics Packaging Handbook*, Nikkei BP.
38. Lau JH (1993), "A brief introduction to fine pitch surface mount technology", *Handbook of Fine Pitch Surface Mount Technology*, Van Nostrand Reinhold, New York, pp.1-54.
39. Martin.S, D.Gage, T.Powell, and B.Slay (1993), "A practical approach to producing Known-Good-Die", *Proceeding of the 2nd International Conference and Exhibition on Multi-Chip Modules*, pp.139-151.
40. Dr. Mark M Konarski and Jim Heaton (1996), "Electronic Packaging Design Advances Miniaturization", *Circuit Assembly Asia*, Vol. 4, No. 5, pp. 18-23.
41. Dr.K.Gilleo, T.Cinque and A.Silva (1996), "Flip Chip 1,2,3: Bump, Bond and Fill", *Circuits Assembly Asia*, Vol.4, No. 5, pp.34-39.
42. N.E.Brathwaite and M.M.Kuan and Terence Ho (1996), "Implementing COB assembly", *Circuits Assembly*, Vol. 7, No.7, pp.52-59.
43. T.Watari (1993), "Multichip Module Packaging Technology in Computers", *Surface Mount Technology Recent Japanese Developments*, edited by Jan Vardaman, IEEE Press pp.264-275.
44. Y.Degani, TD. Dudderar, RC. Frye, KL Tai, Maureen Y Lau, and Byung J Han (1996), "Microinterconnect Technology : The Large-Volume Fabrication of Cost-Effective Flip Chip MCMS", *Flip Chip Technologies*, edited by John Lau, McGraw-Hill pp.181-222.
45. Doane DA, and PA Franzon (1993), "Multichip Module Technologies and Alternatives", Van Nostrand Reinhold, New York, pp.320-328.
46. Lau. M.Y., KL Tai, RC Frye, M.Saito, and D.D. Bacon (1993), "A versatile IC Process Compatible MCM-D for high performance and low cost applications", *Proceeding of the 1993 International Conference of MCM*, Devan pp.107-112.
47. Ed Zamborsky (1996), "BGAs in the assembly process", *Circuit Assembly Asia*, Vol.4, No.5, pp.30-33.

48. J.Date, Y.Hozumi, H.Tokuhira, M.Usui, E.Horikoshi, and T.Sato (1996), "ACA for fine-pitch flip chip Interconnections", Flip Chip Technologies edited by J.Lau, McGraw-Hill, pp.289-300.
49. Williams DJ, and DC Whalley (1993), "The effects of conducting particle distribution on the behaviour of ACA : Non-uniform Conductivity and Shorting between connections", J.of Electron. Manufact 3: pp. 85-94.
50. Ogunjimi A.O., O.Boyle, D.C. Whalley and D.J.Williams (1992), "A review of the impact of conductive adhesive technology on interconnection," J.of Electronics Manufacturing 2, pp.109-118.
51. Chang Hoon Lee (1996), "Anisotropic Conductive flip chip-on-glass technology", Flip Chip Technologies edited by J.Lau, McGraw-Hill pp.317-339.
52. Masuda.M, K.Sakuma, E.Satoh, Y.Yamasaki, H.Miyasaka, and J.Takeuchi (1989), "Chip on class technology for large capacity and high resolution LCD", IEEE/CHMT International Electronics Manufacturing Technology Symposium, pp.55-58.
53. Shiozawa.N, K.Isaka and T.Ohta (1994), "Electric Properties of Anisotropic Conductive Adhesive Films", Adhesives in Electronics '94, Berlin : VID/VDE.
54. Wong CC (1993), " Flip Chip Connection Technology", in Multichip Module Technologies and Alternatives, Doan.D.A., and P.D.Franzon eds; Van Nostrand Reinhold, New York, pp.429-449.
55. Andoh.H, Y.Yanada, and Y.Fukuda (1993), "Fine connection technology using ACF", Hybrids 8(6) : 19.
56. I.Watanabe, N.Shiozawa, K.Takemura, and T.Ohta (1996), "Flip chip interconnection technology using ACFs", Flip Chip Technologies, edited by J.Lau, McGraw-Hill pp.301-315.
57. Basavanhally.NR, D.D.Chang, B.H.Cranston, and S.G. Seger (1992), "Direct chip interconnect with adhesive connector films", Proceedings of 42nd IEEE Electronic Components and Technology Conference pp.487-491.
58. Shiozawa.N, I.Tsukagoshi, A.Nakajima and I.Itoh (1994), "Anisotropic Conductive Adhesive Film Anisolm AC-2052 for connecting the one metal electrode to another", Hitachi Chemical Technical Report, No.23, pp.23-26.
59. Y.Bessho, etal (1993), "New chip-on-glass mounting technology of LSI", Ceramic Transactions, Vol.33, pp.445-458.

60. Y. Bessho, et al (1993), "A stud-bonding technique for high density multichip-module", Proceedings of 1993 Japan IEMT Symposium, pp.362-365.
61. Y. Kunitomo, et al (1994), "CSP Chip size package", Proceedings of the second VLSI packaging workshop of Japan, IEEE, pp.51-56.
62. Y. Nakamura, et al (1995), "Advanced LSI package using Stud-Bump-Bonding Technology, Chip Size Package", Proceedings of 1995 International Conference on Multichip Modules, Denver, Colorado pp.302-307.
63. George G. Harman (1995), "Wire-Bonding to Multichip Modules and other soft Substrates," Proceedings of 1995, International Conference on MCM, Denver, Colorado. pp.292-301.
64. K. Machida and Y. Nakaoka (1993), "Flat Package Soldering Technology", Surface Mount Technology Recent Japanese Developments, edited by Jan Vardaman, IEEE Press pp.131-143.
65. Frank J de Klein (1993), "Customer experiences with inert reflow soldering soldering", Report to air product Inc/ Soltec Investigation, Netherlands. pp. 1-9.
66. D.C. Whalley, A.O. Ogunjimi, P.P. Conway and D.J. Williams (1992), "The process modelling of the infrared reflow soldering of circuit board assemblies," Journal of Electronics Manufacturing," Vol. 2, pp.23-29.
67. M.T.W de Langen and M.M.F Verguld (1990), "Technical Outline specification and guideline for IR reflow Soldering", Soldering and SMT, No.5, pp. 32-37.
68. Stephen Dow (1993), "Forced connective Solder reflow for fine pitch assembly", Handbook of Fine Pitch SMT edited by J. Lau, Van Nostrand Reinhold, New York, pp.348-375.
69. Dow.S.J (1990), "The use of zone segregated forced convection in SMT mass reflow soldering," Proc. Technical Conf Nepcon West, pp.823-840.
70. Kasturi.S (1990), "Force convection : The key to the versatile reflow process," Proc Technical Conf. Nepcon East, pp. 1015-1024.
71. Sean M.Adam (1993), "Nitrogen-based solder reflow for fine pitch assembly", Handbook of Fine Pitch SMT edited by J.Lau, Van Nostrand Reinhold, New York, pp.376-410.
72. J.Paul Wasielewski (1993), "Vapour phase Solder Reflow for Fine Pitch Assembly," Handbook of Fine Pitch SMT, edited by J.Lau, Van Nostrand Reinhold, New York, pp.308-332.

73. Jan Vardaman(1993), “ Trends in the interconnect equipment industry in the 1990s”, Surface Mount Technology Recent Japanese Development, edited by Jan Vardaman, IEEE Press pp.63-76.
74. K.Machida and Y.Nakaoka(1993), “ Surface Mount Technology Recent Japanese Development, edited by Jan Vardaman, IEEE Press pp. 131-143.
75. Boettinger W.J, Handwerker C.A and Kattenes U.R(1993), “ Reactive Wetting and Intermetallic Formation”, in The Mechanic of Solder Alloy Wetting and Spreading, edited by F.G.Yost et.al, Van Nostrand Reinhold, New York pp.103-140.
76. T.J. Singler(1994), “ Fluid Mechanical Aspects of Soldering Processes”, Electronics Packaging Forum, Multichip Module Technology Issues, edited by J.E. Morris, IEEE Press pp.180-185.
77. P.P. Conway, M.R. Kalantary and D.J. Williams (1995), “ Experimental Investigation of the formation of Surface Mount Solder joints,” Proceeding of the INTERpack’95 Conf, ASME / JSME/ IEEE, Westin Miami, USA, EEP Vol-10, No. 1.pp.95-101.
78. M.R.Kalantary, F. Sarvar, P.P Conway , D.J. Williams and D.C. Whalley(1994), “ Observed phenomenology of the interaction between solder paste and soldering processes,” Soldering & Surface Mount Technology, No. 18, pp.8-11.
79. Kalantary M.R, F.Sarvar, P.P. Conway, D.J. Williams and D.C. Whalley (1994), “ Understanding the interaction between solder pastes and the soldering process,” Proc. Int. Conf. Electronics Technologies, Anugraha, Windsor, U.K, pp.123-130.
80. P.P. Conway, D.J. Williams and D.C. Whalley (1991) “ Joint level thermal modelling of Infra-Red reflow for different termination geometries,” Proc. 1st Int. Conf. Factory Automation and Information Management, Limerick, Ireland, pp.219-228.
81. Conway P.P, Williams D.J, and Whalley.D.C (1991), “Experiments to allow the interpretation of a computer based model of the solder paste reflow process,” Journal of Processing of Advanced Materials, Vol.1, No. 3/4 pp.175-180.
82. P.P. Conway, A.O. Ogunjimi, P.M. Sargent, A.C.T Tang, D.C. Whalley and D.J. Williams(1991), “ SMD reflow soldering: A thermal Process Model,” Annals of the C.I.R.P, Vol 40/1/1991. pp.21-24.
83. F.Sarvar and P.P Conway (1996), “ Effective transient process modelling of the reflow soldering of printed circuit assemblies”, Proceeding of INTERpack’96, IEEE, Miami ,USA.

84. P.P Conway and D.J. Williams (1995), " Experiments to improve the understanding of defects occurring in reflow soldering of soldering of solder paste materials," VDR/ADB, Productronic'95, pp.53-60.
85. M.R.Kalantary, P.P. Conway , F. Sarvar, and D.J.Williams (1995), " Towards a standard for Differential Scanning Calorimetry (DSC) measurement of solder paste products," 17th IEEE IEMTS, pp. 337-343.
86. Ehrhard.P and S,H. Davis (1991), " Non-Isothermal spreading of liquid drops on horizontal plates", J. of fluid mechanic pp.365-388.
87. Colin Lea(1988), " A Scientific Guide to Surface Mount Technology", Electrochemical Publications Limited, pp.309-361.
88. R.J.KLein Wassink (1984), " Soldering in Electronics", Electrochemical Publications Limited, Ayr Scotland pp.14-52.
89. M.Nylen and S.Norgen(1990), " Temperature variations in soldering and their influence on microstructure and strength of solder joints", Soldering and SMT, No.5, pp. 15-20.
90. T.J.Ennis, N.Brandy, B.Keane and A. Donnelly (1992), " A study of the effects on IR reflow profile on solder joint strength and structure", Soldering & SMT, No.12, pp.12-15.
91. W.J.Boettinger, C.A. Handwarker and L.C. Smith (1992), NIST, Metallurgy Division," On the wetting of the intermetallic Cu_6Sn_5 and Cu_3Sn by Pb-Sn Alloys," The Metal Science of Joining, edited by M.J. Cieslak, J.H.Perepezko, S.Kang and M.E. Glicksman, The Minerals, Metals & Materials Society pp.183-189.
92. C.Y. Huang & K.Srihari, Ph.D.(1995), " Flux activity evaluation using the wetting balance," IEEE/ CPMT Int'l Electronics Manufacturing Technology Symposium, pp.344-350.
93. Hanae Shimokawa, C.Lee, K.Yamamoto and T.Soga(1995), Proceeding of 1995 Japan IEMT Symposium, IEEE Components, Packaging, and Manufacturing Technology Society(CPMT), "New estimation method of wetting and surface tension by measuring area of spreading solder in flux atmosphere based on ellipse approximation of Sessile drop configurations", pp.421-424.
94. C.Lee, K.Yamamoto, H.Shimokawa, and T.Soga (1995), " The analysis on bridge between leads of Quad Flat Package in Reflow soldering on Printed Circuit Boards", Proceeding of 1995 Japan IEMT Symposium pp.411-414.

95. P.G. de Gennes(1985), "Wetting: statics and dynamics," reviews of Modern Physics, Vol. 57, No. 3, Part 1, pp.828-861.
96. K.Sherman and C.A.Mackay(1990)," A thermoanalytical study of the components and formulation of a rosin based flux", soldering and SMT, No. 6 pp.28-31.
97. R.R. Rye, J.A. Mann, and F.G. Yost(1996), " the flow of liquids in Surface grooves", Langmuir, Vol.12 No.2 .pp.555-565.
98. F.G.Yost, J.R. Michael and E.T. Esienmann (1995), " Extensive wetting due to roughness", Acta metal mater, Vol.43, No.1. pp. 299-305.
99. Young.T(1805), " An essay on the cohesion of fluids," Trans. Roy.Soc. (Philosophical), Vol.95. pp.65-87.
100. Bondi.A(1953), " The spreading of liquid metals on solid surfaces", Chem. Rev, 52,(2) pp.417-457.
101. Tabelev.V.D, Rossoshinskii A.A, Ivanova L.R (1981), " The connection between oxidation and flow of Pos-61 solder," Automatic Welding (Avt. Svarka), 34, (5), pp. 37-38.
102. K. Yamamoto, C.Lee, et al (1995), " Separation property under melting and simulation of soldering on fine pitch LSI package," Journal of Japan Institute for Interconnecting and Packaging Electronic Circuits, 10(6), pp. 408-415.
103. Rayleigh. Lord(1892-1902), " Intensity of light reflected from water and mercury," Collected Scientific Paper IV, pp.13-14.
104. C.Lee, K.Yamamoto, H.Shimokawa, and T.Soga (1995), "The analysis and mercury," collected Scientific Papers IV, pp.13-14.on bridge leads of quad-flat-package in reflow soldering on printed circuit boards," Proceeding of 1995 Japan IEMT Symposium pp.411-414.
105. Brakke.K (1992), " The Surface Evolvers", Experimental Mathematics Vol.1 No.2 pp.141-165.
106. Livia Racz and Julian Szekely(1993), " Estimation of Solder Volume ", Handbook of Fine Pitch Surface Mount Technology, edited by John Lau, Van Nostrand Reinhold, New York. pp.267-307.
107. D.C.Whalley(1996), " A model to explain SMT open circuit joints associated with adjacent solder bridges", Journal of Electronics Manufacturing, Vol. No.1 pp. 39-44.

108. D.C. Whalley, P.P. Conway, F.Sarvar and D.J. Williams quality and reliability”, Soldering and Surface Mount Technology, No. 21, pp.10-12.
109. Racz L.M, Szekely.J, and Brakke. K.A (1993), “ A general statement of the problem and description of a proposed method of calculation for some Meniscus problems in Material processing,” ISIJ International, Vol.33, No.3 pp.328.
110. E.E. de Kluizenaar(1990), “ Reliability of solder joints: A description of the state of the art, Part 1”, Soldering & Surface Mount Technology, No. 4 pp.27-38.
111. E.E. de Kluizenaar(1990), “ Reliability of solder joints: A description of the state of the art Part 2,” Soldering & SMT, No.5. pp.56-66.
112. E.E. de Kluizenaar(1990), “ Reliability of solder joints: A description of the state of the art, Part 3, “ Soldering & SMT, No. 6, pp.18-27.
113. B.Brox and PE.Tegehall(1995), “Reliability of electronics in harsh environments”, Journal of the SMART(Surface Mount & Related Technologies) Group No.21, pp.13-16.
114. Hakan Ugur and Jim Adriance(1994), “ Mass reflow experiments/ six solder pastes Assembly yield Experiment”, CD- ROM, Ultra Fine Pitch Consortium Universal Instruments Corporation, edited by LM Westby.
115. Hakan Ugur and Jim Adriance(1994), “ Mass reflow experiments / UFP # II Assembly yield improvement (Attachment pad length),” Ultra Fine Pitch Consortium, Universal Instruments Corporation, CD-ROM, edited by L.M .Westby.
116. C.Y. Huang, K.Srihari, A.J. McLenaghan and G.R.Westby (1995) , “Flux activity evaluation using the wetting balance”, Proceeding of IEEE/ CPMT, Int’l Electronics Manufacturing Technology Symposium, pp.344-350.
117. De Vore J.A(1991), “ Good Soldering Performance ,” Circuits Assembly, pp.28-37.
118. Elkins M.A.(1994), “ Component solder ability test/ criteria evaluation,” Proceeding of the 1994 International Electronics Packaging Conference, Atlanta Georgia, pp.525-533.
119. Denny. D (1994), “ Consideration for qualifying a no-clean solder paste,” Proceeding-Nepcon West 1994, Volume I, Anaheim, C.A. pp.732-742.
120. C.Lea(1995), “ Qualitative Solderability measurement of electronic components, part 1: The Wetting Balance,” Journal of the SMART (Surface Mount & Related Technology) Group, No. 4 pp.8-13.

121. S.H. Mannan, N.N Ekere, I.Ismail and M.A. Currie (1994), " Computer Simulation of Solder Paste flow Part 1: Dense suspension theory", *Journal of electronics Manufacturing* , Vol. 4, pp.141-147.
122. S.H.Mannan, N.N.Ekere, I.Ismail and M.A. Currie (1994), " Computer Simulation of solder paste flow Part 2: Flow out of a stencil aperture", *Journal of Electronics Manufacturing*, Vol.4 pp. 149-154.
123. Dr. Williams E Coleman and Kimberly A Aeschliman(1994), " Application and stencil design guide," *Surface Mount International Conference & Exposition, Technical Proceedings*, San Jose California pp. 220-226.
124. Dr. M. Warwick & P.Hedges(Aug. 1994), " Solder paste design & consideration", *Circuit Assembly*, pp.36-42.
125. T.J.Singler and J.J Curran (1994), " Mass Reflow Experiments: An experiment investigation solder bridging", *Universal Instruments Corporation, Ultra Fine Pitch Consortium Report*, edited by LM.Westby CD-ROM.
126. G.Taguchi, *System of Experimented Design-Engineering Methods to Optimize Quality and Minimize Costs*, Vols. 1 and 2, American Supplier Institute, Dearborn, MI, 1987.
127. G.E.P.Box and K.B. Wilson(1951), " On the experimental attainment of optimal conditions", *J. of the Royal Statistical Society*, pp.1-45.
128. S.Hall, M.P.M. Corp (1993), " Developing a low DPPM defect level ultra-fine pitch printing process", *MPM Users Guide*, pp.21-33.
129. G.E.P Box, W.G. Hunter, and J.S. Hunter (1978), *Statistics for Experiments*, John Wiley, New York.
130. N.N.Ekere and E.K.Lo(1991), " New challenges in solder paste printing", *Journal of Electronics Manufacturing*, pp.289-40.
131. M.D.Osterman(1991), " Component placement strengthening the link," *Circuit Assembly*, pp.47-53.
132. E.A.Kress and K.Wickers (1985), *Solder Pad Geometry Studies for Surface Mount of Chip Capacitors*, AVX Corporation, Corporate Research Lab(US), ECC, pp.21-32.

133. K.Oyama (1993), "The trend towards higher pin-counts and narrower pitch," Surface Mount Technology, Recent Japanese Developments, Ed. Jan Vardaman, IEEE Press, pp.77-108.
134. K.C.Teo(1996), " The origin and prevention of post reflow defects in surface mount assembly," Journal of Electronics Manufacturing, Vol. 6, No. 1, pp.1-12.
135. T.N.Goh(1987), " An active approach to quality improvement", Journal of Industrial Engineering, Singapore 27, pp.29-34.
137. K.C.Teo and D.J.Williams(1996), " Insufficient solder and solder bridge: An experimental study of the interrelations between assembly process faults," Journal of Electronics Manufacturing, Vol 6, No. 2, pp.93-99.
138. J.R.Ellis and G.Y.Masada(1990), " Dynamic behavior of SMT chip capacitors during solder reflow," IEEE Trans.Components, Hybrids, and Manufacturing Technology, Vol. 13, No. 3 pp.545-552.
139. The Institute of Interconnecting and Packaging Electronic Circuits, IPC-SM-728 Surface Mount design and Land Pattern Standard (Aug.1993).
140. Paul Walter(March 1996), " Bond testing enters mainstream PCB assembly," Circuit Assembly, Vol 3, pp.34-36.
141. J.Paul Wasielewski(1992), " Vapour phase solder reflow for fine pitch assembly", Handbook of Fine Pitch Surface Mount Technology, Eds John.H.Lau, Van Nostrand Reinhold, New York pp.308-332.
142. D.C.Whalley, P.P.Conway and M.Kalantang(1995), "Simulation and interpretation of wetting balance tests using the Surface Evolver," Proc. Interpack 95 Conf. pp.1-12.
143. Philip Zarrow(1991), " Fine-pitch Soldering," Circuit Assembly, pp.46-55.
144. Duncan Zarrow(1955), " Multiple Rang and Multiple F-Tests", Biometrics, Vol 11, pp.1-42.
145. Keengan, Bradaigh, Kearney and Monaghan(1993), " Thermal fatigue life prediction for a middle gull-wing joint using finite element analysis," EEP-Vol 4-1 Advances in Electronic Package ASME pp.499-506.
146. Christopher Chatfield(1970), " Statistic for Technology", Penguin Books pp.264-268.

147. Daniel.C(1959), " Use of half-normal plots in interpreting factorial two-level experiments," *Technometrics* 1, pp.311-341.
148. Daniel. C(1976), " Applications of Statistics to Industrial Experimentation," New York: Wiley.
149. Yates.F(1937), *The design and analysis of factorial experiments*, London: Imperial Bureau of Soil Science.
150. D.C.Montgomery(1991), *Design and Analysis of Experiments*, 3rd Edition, John Wiley & Sons, New York. pp.479-487.
151. Box G.E.P and N.R.Draper(1975), " Robust Designs," *Biometrika*, 62, pp.347-352.
152. John.A.Cornell(1984), " Volume 8: How to apply response surface methodology," American Society for Quality Control, edited by J.A. Cornell and Samuel.S.Shapiro, pp.1-41.
153. I.Okamoto, A.Omori, and H.Kihadra(1973), " Studies on Flux action of Soldering(Report 2)- Amine hydrochloride," *Transactions of JWRI* 2.
154. DC.Whalley and PP.Conway (1996), "Simulation and interpretation of wetting balance tests using the Surface Evolver", *The American Society of Mechanical Engineers*, Vol 118, Number 3, pp.134-141.
155. T.J.Singler, Xu Zhang and K.A.Brakke (1996), "Computer simulation of solder bridging phenomena," *The American Society of Mechanical Engineers*, Vol 118, Number 3, pp.122-126.
156. K.W.Moon, W.J.Boettinger, M.E.Williams, D.Josell, BT.Murray, W.C.Carter and C.A.Handwerker (1996), "Dynamic Aspects of Wetting Balance Tests," *The American Society of Mechanical Engineers*, Vol.118, Number 3, pp.174-183.